Macromolecules, Dendrimers, and Nanomaterials in Magnetic Resonance Imaging: The Interplay between Size, Function, and Pharmacokinetics

Aaron Joseph L. Villaraza, Ambika Bumb, and Martin W. Brechbiel*

Radiation Oncology Branch, National Cancer Institute, National Institutes of Health, Bethesda, Maryland 20892

Received June 30, 2009

Contents

* Address for correspondence: Martin W. Brechbiel, Ph.D., Radioimmune & Inorganic Chemistry Section, Radiation Oncology Branch, NCI, NIH, Building 10, Room 1B53, 10 Center Drive, Bethesda, MD 20892. Telephone: +1 301-496-0591. Fax: +1 301-402-1923. E-mail: martinwb@mail.nih.gov.

1. Introduction

Magnetism in medicine has had a long and interesting history. In the 10th century A.D., Egyptian physician and philosopher Avicenna prescribed a grain of magnetite dissolved in milk for the accidental swallowing of rust, reasoning that magnetite would render the poisonous iron inert by attracting it and accelerating its excretion through the intestine.[1] A thousand years later, on July 3, 1977, "Indomitable", the little machine that could, labored for 5 h to produce one image, an event that used magnetism to change the landscape of modern medicine.[2] Looking at the homemade superconducting magnet constructed from 30 miles of niobium−titanium wire that now resides in its rightful place at the Smithsonian Institution, it is incredible to comprehend how in a mere 30 years magnetic resonance imaging (MRI) has gone from its crude, almost ugly, human scan to where physicians can now regularly order MRIs off their menu of diagnostic tools because of its exquisite anatomical resolution, routinely down to 0.5−1 mm.

When the field was first reviewed in this journal in 1987,[3] only 39 papers were found in Medline with the keywords "gado-" and "MRI".[4] Today, this same search on PubMed pulls out over 250,000 records, of which a significant component has been development of MR contrast agents. The human body is essentially a supersized water bottle, with about two-thirds of its weight consisting of water. Water's hydrogen atoms are able to act as microscopic compass

10.1021/cr900232t
Published on Web 01/12/2010

Aaron Joseph L. Villaraza was born 1979 in Manila, Philippines. He received his B.S. in Chemistry from the University of the Philippines—Diliman in 2001 and taught at the same university until 2004. In 2008 he obtained his doctorate from Manchester University, U.K., working under the supervision of Prof. Stephen Faulkner (currently at Oxford University) on the synthesis of heteropolymetallic luminescent lanthanide complexes. At present, he is on a visiting scholar fellowship at the National Cancer Institute, working in the group of Dr. Brechbiel on the synthesis of polymer−protein bioconjugates for cancer imaging and therapy.

Ambika Bumb was born in 1984 in Rajasthan, India. She studied biomedical engineering in Atlanta, GA, at the Georgia Institute of Technology and obtained her doctorate in 2008 from Oxford University, U.K., while on the Marshall Scholarship. For her graduate research, she focused on synthesizing and characterizing multimodal imaging nanoparticles and exploring their diagnostic applications in animal models. The work was conducted through the National Institutes of Health−Oxford Graduate Partnership Program under the collaborative guidance of Prof. Peter Dobson, Dr. Martin Brechbiel, Dr. Peter Choyke, and Prof. Lars Fugger. She is currently at the National Cancer Institute on a postdoctoral fellowship, further pursuing her interests in developing imaging contrast agents and expanding their applications for drug delivery and hyperthermia treatment.

needles that stand "at attention" when placed in a strong magnetic field. When submitted to pulses of radio waves, their magnetic alignment is disrupted and the differences in how they relax to the previous state are used to generate images. Contrast agents can act to catalyze the process of the return to the ground relaxed state. Now commonplace in the clinic, paramagnetic or superparamagnetic metal ions are administered in 40−50% of the 7−10 million MR examinations per year.[5] These image-enhancing contrast agents add significant morphological and functional information to unenhanced MR images, allowing for enhanced tissue contrast, characterization of lesions, and evaluation of perfusion and flow-related abnormalities. In this review, we will introduce small molecule agents, but we focus primarily on macromolecular MR contrast agents, particularly those

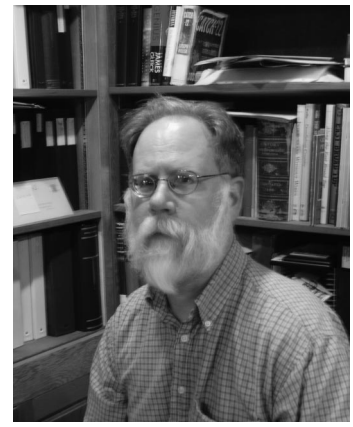

Martin W. Brechbiel received his B.A. in 1979 from Gettysburg College and a M.S. in 1982 from the University of Delaware under the guidance of Professor Harold Kwart. After working for FMC Corp, he joined the National Cancer Institute in 1984. Thereafter, he worked to develop novel bifunctional chelating agents for sequestering radionuclides and their conjugation to immunoproteins under the direction of Dr. Otto A. Gansow while simultaneously obtaining a Ph.D. from American University in 1988 with Professor Thomas Cantrell. He remained with the NCI and in 1997 was appointed Acting Section Chief of the Radioimmune & Inorganic Chemistry Section and was tenured as the Section Chief in 2001. His research group's activities span the range of continuing development of novel chelating agents for radionuclides, the development of contrast media for MRI, Electron Paramagnetic Resonance, and CT imaging, and the medicinal chemistry of novel metal complexes.

containing gadolinium (Gd^{3+}) that are assembled or based in part on these same small molecules. A brief discussion on iron oxide and manganese (Mn^{2+}) agents is also provided.

2. Relaxation Theory and Mechanisms

While a detailed explanation of relaxation theory can be found in a number of excellent articles,[6−8] we will reintroduce the essentials because of their importance in understanding how contrast agents work. The signal-to-noise ratios in MRI depend on the density of protons present in the region of interest and the degree of polarization of the nuclear spin states. When placed in a magnetic field, a slight majority of protons will orient in the direction of the magnetic field and precess at a Larmor resonance frequency related to the strength of the magnetic field. Relaxation is measured in two directions, longitudinal and transverse. Longitudinal or spin−lattice relaxation is defined by the time constant T_1 and occurs in the direction of the main magnetic field. Signals related to T_1 relaxation are obtained after excitation by an RF pulse at the Larmor frequency as the proton's dipole moment vector begins to realign or relax back to its ground state of alignment with the main magnetic field. Transverse or spin−spin relaxation corresponds to vector dephasing in the plane perpendicular to the main magnetic field and is characterized by T_2. T_1 represents the time required for the magnetization vector to be restored to 63% of its original magnitude, and T_2 represents a 37% decrease in net signal. T_2 is always equal to or shorter than T_1. Inhomogeneity in the static magnetic field and spin−spin relaxation have an effect on the transverse magnetization and are characterized by

$$\frac{1}{T_2^*} = \frac{1}{T_2} + \frac{1}{T_2'} \quad (1)$$

where T_2' is a time constant arising from magnetic field inhomogeneity and T_2^* is the spin−spin time constant that

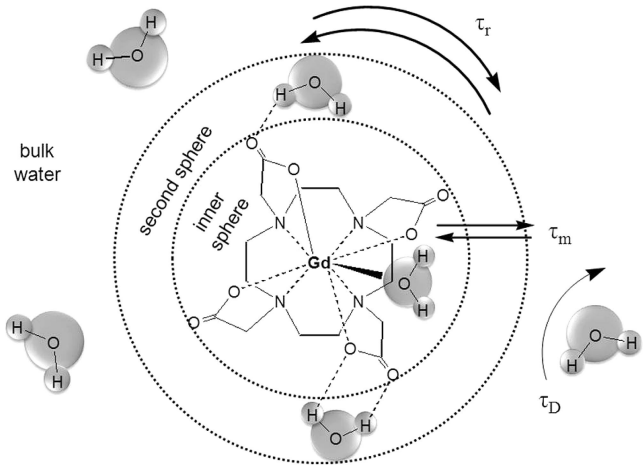

Figure 1. Relaxation coordination spheres of water: inner-sphere, secondary-sphere, and bulk water.

takes into account these issues. T_2* is always less than T_2. Signals received from spin vectors are used to produce images by the superimposition of magnetic gradients which define the spatial location of the signal. Tissue types vary in their relaxation properties, and thus MRI is used to reconstruct images of structures such as organs and lesions and to evaluate perfusion and flow-related abnormalities.

Though it is possible to obtain images distinguishing tissues types by manipulation of pulse sequences alone, MRI is best optimized by use of contrast agents that dramatically highlight anatomic and pathologic features of interest. Paramagnetic ions decrease the proton relaxation time of bound water molecules. Thus, unlike other diagnostic media such as radionuclide, optical, and X-ray agents, MR contrast agents are themselves not a source of a signal and are not directly visualized but rather affect the surrounding water molecules, that in turn directly influence the signal. Paramagnetic species decrease T_1 and T_2, increasing longitudinal (spin−lattice) and transverse (spin−spin) relaxation of solvent nuclei. The observed solvent relaxation, $(1/T_i)_{obs}$, is the sum of the intrinsic diamagnetic solvent relaxation rate in the absence of the paramagnetic species, $(1/T_i)_d$, and the additional paramagnetic contribution, $(1/T_i)_p$.

$$\frac{1}{(T_i)_{obs}} = \frac{1}{(T_i)_d} + \frac{1}{(T_i)_p} \qquad i = 1,2 \qquad (2)$$

In the absence of solute−solute interactions, the solvent relaxation rate is linearly dependent on the concentration of the paramagnetic ion, c_{agent}:

$$\frac{1}{(T_i)_{obs}} = \frac{1}{(T_i)_d} + (R_i)_{agent} c_{agent} \qquad i = 1,2 \qquad (3)$$

where $(R_i)_{agent}$ is the relaxivity of the paramagnetic agent, typically defined in units of $mM^{-1}\ s^{-1}$. The effect of the agent is dependent on the distance from the ion and the diffusion of solvent molecules. Water interaction with the metal ion is classified into three types: (1) primary coordination sphere, (2) hydrogen-bonded molecules in the secondary coordination sphere, and (3) bulk water that translationally diffuses past the metal (Figure 1).[3]

Inner-sphere relaxation is the enhancement found in the first coordination sphere. If the time of interaction is long compared to the time of diffusion, second coordination sphere water molecules demonstrate similar relaxation to the first sphere. However, typically enhancement in the second coordination sphere and bulk water is grouped together as outer-sphere relaxation. Thus, the total paramagnetic relaxation enhancement is

$$\frac{1}{(T_i)_p} = \frac{1}{(T_i)_{inner\text{-}sphere}} + \frac{1}{(T_i)_{outer\text{-}sphere}} \qquad i = 1,2 \qquad (4)$$

2.1. Inner-Sphere Relaxation: Solomon−Bloembergen−Morgan (SBM) Equations

The inner-sphere contributions to longitudinal and transverse relaxation are a function of the mole fraction of metal ion per solvent molecule (P_m), the number of bound water (or solvent) nuclei per metal ion or the hydration number (q), and the average residence time of the solvent molecule in the complex (τ_m or $1/k_{ex}$, the reciprocal of the solvent exchange rate).[3,4,9,10]

$$\frac{1}{(T_1)_{inner\text{-}sphere}} = \frac{P_m q}{T_{1m} + \tau_m} \qquad (5)$$

$$\frac{1}{(T_2)_{inner\text{-}sphere}} = q P_m \frac{1}{\tau_m}\left[\frac{T_{2m}^{-1}(\tau_m^{-1} + T_{2m}^{-1}) + \Delta\omega_m^2}{(\tau_m^{-1} + T_{2m}^{-1})^2 + \Delta\omega_m^2}\right] \qquad (6)$$

The "m" subscript refers to the solvent molecule in the inner-sphere, and $\Delta\omega_m$ is the difference in Larmor frequencies between the inner coordination sphere and the bulk solvent reference. The relaxation times of the bound water molecules ($T_{1,2m}$) are further defined by the Solomon−Bloembergen−Morgan (SBM) equations[4,8,11] which represent the sum of dipole−dipole ("through-space") and scalar (contact or "through-bonds") contributions:

$$\frac{1}{(T_i)_m} = \frac{1}{T_i^{DD}} + \frac{1}{T_i^{SC}} \qquad i = 1,2 \qquad (7)$$

$$\frac{1}{T_1^{DD}} = \frac{2}{15}\frac{\gamma_I^2 g^2 \mu_B^2 S(S+1)}{r^6}\left[\frac{3\tau_{c1}}{1+\omega_I^2\tau_{c1}^2} + \frac{7\tau_{c2}}{1+\omega_S^2\tau_{c2}^2}\right] \qquad (8)$$

$$\frac{1}{T_1^{SC}} = \frac{2}{3}S(S+1)\left(\frac{A}{\hbar}\right)^2\left[\frac{\tau_{e2}}{1+\omega_S^2\tau_{e2}^2}\right] \qquad (9)$$

$$\frac{1}{T_2^{DD}} = \frac{1}{15}\frac{\gamma_I^2 g^2 \mu_B^2 S(S+1)}{r^6} \times \left[\frac{3\tau_{c1}}{1+\omega_I^2\tau_{c1}^2} + \frac{13\tau_{c2}}{1+\omega_S^2\tau_{c2}^2} + 4\tau_{c1}\right] \qquad (10)$$

$$\frac{1}{T_2^{SC}} = \frac{1}{3}S(S+1)\left(\frac{A}{\hbar}\right)^2\left[\frac{\tau_{e2}}{1+\omega_S^2\tau_{e2}^2} + \tau_{e1}\right] \qquad (11)$$

Here, γ_I is the nuclear gyromagnetic ratio, g is the electronic g-factor, μ_B is the Bohr magneton, r is the proton−metal ion distance, ω_I and ω_s are the proton and electron Larmor precession frequencies, respectively, $A/\hbar$ is the electron−nuclear hyperfine coupling constant, and S is the total electron spin of the metal ion. The dipole−dipole and scalar correlation times, τ_{ci} and τ_{ei}, that modulate relaxation are defined by

$$\frac{1}{\tau_{ci}} = \frac{1}{T_{ie}} + \frac{1}{\tau_m} + \frac{1}{\tau_R} \qquad i = 1,2 \qquad (12)$$

$$\frac{1}{\tau_{ei}} = \frac{1}{T_{ie}} + \frac{1}{\tau_m} \qquad i = 1,2 \qquad (13)$$

T_{1e} and T_{2e} are the electronic longitudinal and transverse relaxation times of the metal ion, τ_m is the water residence time, and τ_R is the rotational tumbling or correlation time of the entire metal−water complex.

The nuclear or electron Larmor frequency is directly related to the magnetic field, B, by the gyromagnetic ratio, γ:

$$\omega = \gamma B \qquad (14)$$

Thus, all these equations describe relaxation as a function of magnetic field. The same is also true for the electronic relaxation rates. Equations 8−11 are only valid for ions with electronic spin $S > {}^1/_2$, where inner-sphere collisions lead to zero field splitting (ZFS) of the electron spin levels. This ZFS modulates electronic relaxation rates by the following functions:

$$\frac{1}{T_{1e}} = B\left[\frac{1}{1 + \omega_S^2\tau_v^2} + \frac{4}{1 + 4\omega_S^2\tau_v^2}\right] \qquad (15)$$

$$\frac{1}{T_{2e}} = \frac{B}{2}\left[\frac{5}{1 + \omega_S^2\tau_v^2} + \frac{2}{1 + 4\omega_S^2\tau_v^2} + 3\right] \qquad (16)$$

$$B = \frac{1}{5\tau_{s0}} = \frac{\tau_v}{25}\Delta^2[4S(S + 1) - 3] \qquad (17)$$

where the constant B is related to the magnitude of the transient ZFS, τ_{s0} is the electronic relaxation time at zero field, τ_v is a correlation time for the modulation of this transient ZFS, and Δ is the trace of the ZFS tensor.

2.2. Limitations to the SBM Equations

The Solomon−Bloembergen−Morgan (SBM) equations are the most commonly used approach to describe relaxation theory; however, there are a few points about the SBM methods to consider with caution. T_{1e} and T_{2e} are difficult parameters to determine independently because of their field dependence. Equations 15 and 16 are only valid as a monoexponential electronic relaxation process under the limit of extreme narrowing, where $\omega_s^2\tau_v^2 \ll 1$.[6] Outside the extreme narrowing condition, electronic relaxation becomes multiexponential for an $S = {}^7/_2$ ion such as Gd^{3+}.[12] A number of groups[6,7,13−20] have shown that the SBM equations are invalid in the "low-field" region when the energy of the ZFS interaction is larger than that of the Zeeman energy of the interaction between the magnetic moment of the molecule and the applied magnetic field. In the Zeeman or SBM limit, the electron spin precesses about the axis of the external magnetic field. In the ZFS limit, the electron spin precesses about the principal axis of the ZFS tensor and the nuclear relaxation is strongly dependent upon the angle between the electron spin−nuclear spin vector and the ZFS tensor axis. The symmetry of the molecule also plays a role; that is, rhombicity in the ZFS can greatly reduce nuclear relaxation. Qualitatively, the magnetic field dispersion profiles of nuclear relaxation generated using low-field theories look similar to those generated using SBM.

Another point of discussion is that of anisotropic rotation. Strategies to increase the rotational correlation time τ_R include incorporation of a metal chelate onto a macromolecule such as a polymer or a dendrimer. In these cases, relaxation is a function of both the overall motion of the macromolecule and its fast internal motion, i.e. side chain rotations. Lipari and Szabo[21] have derived expressions that account for the fast motion by a second spectral density term.

2.3. Outer-Sphere Relaxation

The SBM theory can also be applied to describe second coordination sphere relaxation enhancement. Protons that are hydrogen-bonded to the contrast agent relax via a dipole−dipole interaction with the paramagnetic species, and consequently, their relaxation can be described by eqs 5, 6, 8, and 10 with the relevant parameters denoted with a prime (*e.g.*, q', r', τ_m'). However, because the number of second-sphere water molecules and the ion−H distances are unknown, second coordination relaxation is difficult to quantify. Furthermore, τ_m is very short and the likely limiting parameter in determining T_{1m}.

Outer-sphere relaxation is most often described by translational diffusion of the water molecules past the metal complex. This contribution to relaxation is approached based upon a rigid-sphere model (Hwang and Freed model)[4,22−24] where the water molecules and metal complex are treated as hard spheres.

$$\frac{1}{(T_1)_{\text{outer-sphere}}} = C[3j(\omega_I) + 7j(\omega_S)] \qquad (18)$$

$$\frac{1}{(T_2)_{\text{outer-sphere}}} = C[2 + 1.5j(\omega_I) + 6.5j(\omega_S)] \qquad (19)$$

$$C = \left(\frac{32\pi}{405}\right)\gamma_I^2\gamma_S^2\hbar^2 S(S + 1)\frac{N_A M}{1000aD} \qquad (20)$$

$$j(\omega) = \mathrm{Re}\left\{\frac{1 + \frac{1}{4}\left(i\omega\tau_D + \frac{\tau_D}{T_{ie}}\right)^{1/2}}{1 + \left(i\omega\tau_D + \frac{\tau_D}{T_{ie}}\right)^{1/2} + \frac{4}{9}\left(i\omega\tau_D + \frac{\tau_D}{T_{ie}}\right) + \frac{1}{9}\left(i\omega\tau_D + \frac{\tau_D}{T_{ie}}\right)^{3/2}}\right\} \qquad i = 1,2 \qquad (21)$$

$$\tau_D = \frac{a^2}{D} \qquad (22)$$

where γ_I and γ_S are the nuclear and electron gyromagnetic ratios, N_A is Avogadro's number, M is the concentration of the metal ion, a is the distance of closest approach between the protons and the paramagnetic complex, D is the sum of the diffusion constants of water and the complex, ω_I and ω_S are the proton and electron Larmor angular velocities, and τ_D is a diffusional correlation time. In the spectral density function, $j(\omega)$, Re stands for "the real part of".

The second coordination sphere relaxation contribution is difficult to measure, and the separation of the two contributions in a $q = 0$ chelate has not been observed, where q is the number of water molecules bound to the paramagnetic center. In fact, the inner-sphere relaxivity is often determined by subtracting the relaxivity of a $q = 0$ complex such as $[Gd^{3+}(TTHA)]^{3-}$ from the observed r_1 with the assumption that it is a reasonable estimation of outer-sphere plus second-sphere relaxivity.[25,26]

Detailed discussions about outer-sphere relaxation are in the cited references. Second sphere relaxivity is not well characterized, and outer sphere relaxivity can vary from paramagnetic complex to complex. As with inner-sphere models, SBM equations have limitations with regard to describing electronic relaxation in the low-field limit. Suffice it to say that outer-sphere relaxivity is complex and typically the focus is placed on inner-sphere relaxation when developing Gd^{3+}-based MR contrast agents.

2.4. Relaxation Theory—Lessons Learned

Overall, relaxivity is a weighted average of relaxation rates from three local proton environments, with the principal contribution from within the inner hydration sphere of the ion. From the equations listed previously, it is evident that relaxation enhancement by paramagnetic ions on their surrounding protons is a compound effect of a number of factors. The most commonly used MR agents are Gd^{3+} based, wherein, due to the nature of its ionic bonding, the hyperfine coupling constant, $A/\hbar$, is quite small. This coupling makes scalar relaxation ($1/T_1^{SC}$, eq 9) inefficient and inner-sphere relaxation more dependent on dipole−dipole relaxation ($1/T_1^{DD}$, eq 8). The key variables, thus, are τ_m, τ_R, q, r, T_{1e}, and T_{2e}. Increasing the hydration number, q, increases the inner-sphere relaxivity (eq 5), but it is often accompanied by a decrease in thermodynamic stability and/or kinetic inertness of chelated Gd^{3+} associated with toxicity issues (*vide infra*) and may lead to the formation of ternary complexes with endogenous ligands such as phosphates and carbonates. Decreasing the distance between the water proton and the unpaired electron spin, r, has a large effect on relaxivity because of the $1/r^6$ dependence noted in eq 8. Gd^{3+}−water oxygen distances range from 2.41 to 2.50 Å for monomeric complexes in the solid state (*vide supra*), and even a decrease of 0.2 Å would result in a 60% increase in relaxivity. The challenge with this distance r, however, is that it is a difficult parameter to both measure and control. The difficulties of modeling and determining electronic relaxation times T_{1e} and T_{2e} were described in the previous sections, and so that leaves τ_m and τ_R.

Water residence time, τ_m, is the term used to describe the fast exchange between metal-coordinated water molecules and water in the bulk solvent. If exchange among protons in the shells is rapid, they all exhibit similar relaxation behavior. Studies have been conducted to improve the rate of water exchange,[4] but the vast majority of efforts have been directed at lengthening the rotational correlation time, τ_R. Increased steric hindrance and hydrodynamic size slows the rotation of larger molecules and increases τ_R. Thus, relaxivity is improved, and there is more enhancement per unit dose of the paramagnetic ion. While rotational correlation times can be estimated in a number of ways,[4] if there is a good estimate of the viscosity, η, the Debye−Stokes theory can be used for a spherical molecule of radius a:

$$\tau_r = \frac{4\pi a^3 \eta}{3kT} \tag{23}$$

where k is the Boltzmann constant and T the absolute temperature. It is important to note that, in microheterogeneous solutions, macroscopic translational viscosity may differ from rotational microviscosity, which is a parameter that is not well understood. Additionally, for molecules with a long τ_R and in high magnetic fields, the Curie spin relaxation mechanism may contribute to the normal dipole−dipole mechanism, but it is negligible at the low fields used in MRI (typically at 1.5−3 T; however, higher field instruments, e.g. 8 T, are becoming available).[4,27]

3. Some "Gado" Please

Because of its seven unpaired 4f electrons, the lanthanide ion Gd^{3+} (atomic number = 64, standard atomic weight = 157.25) is by far the most frequently chosen paramagnetic ion for MRI. Advances in MRI for faster scans and higher resolution have required more rapid pulsing and thus have favored T_1-weighted imaging and use of contrast enhancers such as Gd^{3+}. Two other lanthanide ions, dysprosium (Dy^{3+}) and holmium (Ho^{3+}), have larger magnetic moments than Gd^{3+} because they have orbital contributions to electron angular momentum. However, their asymmetric electronic ground state shifts solute resonance frequencies without line broadening.[28] The 9f-electrons of Dy^{3+}, for instance, distribute themselves among the 7f-orbitals, leaving the ground state highly anisotropic, the net moment part spin/part orbital, and the spin−orbit interactions large. This reduces the electronic relaxation time (increases relaxation rate) 100-fold and has a large effect on the proton resonance frequency. Meanwhile, the symmetry of the electronic S-state of Gd^{3+} makes it a broadening "relaxer" whose major effect is to increase the longitudinal and transverse relaxation rates of the solute without shifting proton resonance frequencies. With its seven electrons forming a half-filled f-shell, Gd^{3+} has an isotropic S-ground state with no net orbital momentum and little spin−orbit interaction.[28] This configuration leads to long electronic relaxation times or slower relaxation rates.

What prevents Gd^{3+} from being directly administered is its high toxicity in free form. Gd^{3+} is chemically similar to Ca^{2+} in size (Gd^{3+} radius = 1.05−1.11 Å, Ca^{2+} radius = 1.00−1.06 Å), bonding, coordination, and donor atom preference.[29] Acutely, neuromuscular transmission arrest can occur by Gd^{3+} ions interfering with calcium-ion passage through muscle cells and calcium flow in bone epiphyses and nerve tissue cells.[30] Chronically, accumulation can be found in bone and liver with a biological half-life of several weeks.[31] Further complications can occur by transmetalation, where Gd^{3+} also can replace endogenous metals, such as zinc.[30]

To sequester and render the ion nontoxic, a number of chelating agents have been developed. These highly stable complexation cages have a greater affinity for Gd^{3+} than other metals commonly present *in vivo* such as Zn^{2+}, Ca^{2+}, or Cu^{2+}. Furthermore, after chelation, renal excretion increases ~550-fold as compared with the case of free Gd^{3+}.[32]

4. Chelating Agents

There are currently eight clinically approved gadolinium-based contrast agents (Table 1, Figure 2): Magnevist (gadopentetate dimeglumine, Gd-DTPA), Dotarem (gadoterate, Gd-DOTA), ProHance (gadoteridol, Gd-HP-DO3A), Gadovist (gadobutrol, Gd-BT-DO3A), Omniscan (gadodiamide, Gd-DTPA-BMA), OptiMARK (gadoversetamide, Gd-DTPA-BMEA), MultiHance (gadobenate dimeglumine, Gd-BOPTA), and Eovist/Primovist (Gd-EOB-DTPA). The chelates fall into two classes: cyclic and acyclic. The macrocyclic chelates, e.g. Dotarem and ProHance, are derivatives of 1,4,7,10-tetraazacyclododecane (cyclen).[4] The cyclen-based tetraacetic acid derivative complex with gadolinium, Gd^{3+}-DOTA, is formulated as its *N*-methylglucamine salt. Two neutral

Table 1. Clinical Gadolinium Agents[30,35−40]

	Gd-DTPA	Gd-DTPA-BMA	Gd-DOTA	Gd-HP-DO3A	Gd-DO3A-butrol	Gd-BOPTA	Gd-DTBA-BMEA	Gd-EOB-DTPA**
generic name	Gadopentetate dimeglumine	Gadodiamide	Gadoterate meglumine	Gadoteridol	Gadobutrol	Gadobenate dimeglumine	Gadoversetamide	
trademark	Magnevist	Omniscan	Dotarem	ProHance	Gadovist	MultiHance	OptiMARK	Primovist (Europe), Eovist (USA)
cyclic/acyclic	acyclic	acyclic	cyclic	cyclic	cyclic	acyclic	acyclic	acyclic
molecular weight	547	573	558	558	604	711	661	682
r_1/r_1* (mM^{-1} s^{-1}) (20 MHz, 310 K)	3.8/3.9	3.8/4.8	3.5/4.3	3.7/5.6	3.7/5.6	4.8/9.7	4.1 (308 K)	5.5
τ_m (ns) (310 K)	143	967	122	176	176	140	1320 (308 K)	82
τ_R (ps) (310 K)	54	65	217		57	89	71 (308 K)	86
thermodynamic stability constant ($\log K_{eq}$) (0.5 mol/L)	22.1	16.9	25.8	23.8	21.8 (1 mol/L)	22.6	16.6	23.46 (0.25 mol/L)
osmolality (Osm/kg)	1.96	0.65	1.35	0.63	1.6	1.97	1.11	0.688
viscosity (mPa s at 37 °C)	2.9	1.4	2.0	1.3	4.96	5.3	2.0	1.19
approval	USA, EU, Japan	USA, EU, Japan	EU	USA, EU, Japan	EU, Canada	USA, EU	USA	USA, EU
approved doses (mmol/kg) for body imaging	0.1	0.1−0.3	0.1	0.1−0.3	not approved	liver: 0.05	0.1	25 μmol/kg or 0.1 mL/kg
approved doses (mmol/kg) for CNS[a] imaging	0.1−0.2	0.1−0.3	0.1−0.3	0.1−0.3	0.1−0.3	0.1	0.1	not approved
approved doses (mmol/kg) for MR angiography	0.1−0.3[b]	0.1−0.3	0.2	not approved	0.1−0.15 (imaging of 1 field of view); 0.2−0.3 (imaging of >1 field of view)	not approved	not approved	not approved
approved doses (mmol/kg) for children	0.1	from 6 months: 0.1	0.1	from 2 years and above: 0.1; 6 months−2 years: caution; <6 months: contraindicated	not approved <18 years	not approved <18 years	not approved <18 years	not approved <18 years

[a] CNS: central nervous system. [b] Approved for whole body imaging and for doses of 0.1−0.3 mmol/kg but does not have a trial-based approval for MR angiography.

macrocyclic derivatives of 1,4,7-tricarboxymethyl-1,4,7,10-tetraazacyclododecane (DO3A) are gadoteridol and gadobutrol. They are characterized by substitution of one carboxylate with a hydroxyl donor group. The second class of acyclic chelates is comprised of derivatives of polyaminocarboxylic acids such as diethylenetriaminepentaacetic acid (DTPA). Gd^{3+}-DPTA was approved for clinical use in adult patients in 1988 and has since become the most commonly used MR contrast agent. Two diamide derivatives of DTPA were also approved for human use: Gd^{3+}-DTPA-BMA and Gd^{3+}-DTPA-BMEA. By reacting the dianhydride of DTPA with an amine (methyl amine or methoxyethyl amine, respectively), two carboxylates were replaced with two amide oxygen donors. This reaction strategy resulted in neutrally charged chelates that remain highly water-soluble. They were developed in part to lower the osmolality of aqueous solutions.[33] Chelating agents do reduce the number of coordinated water molecules in comparison to the case of free metal ion. For example, Gd^{3+}- and Gd^{3+}-DTPA have approximately 8−9 and 1 coordinated water molecules, respectively, and the corresponding relaxivities are 7.0 and 2.0 at 37 °C, 20 MHz, and 0.5 T.[34] However, other factors also determine the *in vivo* efficacy of an agent in obtaining quality images, namely clearance rate and route of excretion.

Clearance is dependent on a number of properties such as size, shape, surface charge, and chemical makeup of the agent. Gd^{3+} chelates are generally excreted unchanged by passive glomerular filtration. They are typically hydrophilic, extracellular-fluid markers with low molecular masses of ~500 Da. These agents are rapidly cleared from the intravascular space through capillaries and into the interstitial space, but they do not cross an intact blood−brain barrier. The biological elimination half-life is approximately 1.5 h[41] with no detectable biotransformation, decomposition, or serum protein binding. When observed in mice and rats after 14 days, residual whole body Gd^{3+} for acyclic agents was found to be higher than that for macrocyclic agent, with the order from least to most being as follows: Gd^{3+}-HP-DO3A ≈ Gd^{3+}-DOTA = Gd^{3+}-DTPA < Gd^{3+}-DTPA-BMA.[42] For Gd^{3+}-DPTA, 90% of the injected dose is cleared by renal filtration and vessel leakage in less than an hour.[43] For patients with normal renal function, rapid clearance improves the safety profile. The converse of that same rapid clearance is that it can pose a challenge for conducting time-dependent imaging studies or obtaining highly resolved images.

Two Gd^{3+} chelates with almost double the relaxivity of the above-mentioned chelates are also available: Gd^{3+}-BOPTA and Gd^{3+}-EOB-DTPA. These agents are eliminated through both the renal and hepatobiliary pathways with 2−4% hepatic uptake of the injected dose for Gd^{3+}-BOPTA and 50% for Gd^{3+}-EOB-DTPA.[30] Thus, they can be used both as conventional extracellular contrast agents within minutes after injection and also to enhance normal liver parenchyma in a later, delayed phase (40−120 min postadministration). Tumor nodules typically lack functional hepatocytes and remain unenhanced in these MR images, allowing for increased sensitivity and specificity in the detection and characterization of liver tumors.[44] Additionally, Gd^{3+}-BOPTA may have potential for MR angiography (MRA) due to weak and transient protein binding.[30]

While these agents are the approved and most commonly used chelates, the contents of Table 1 are by no means a complete list. Since 1995, a body of work has also been published based off the structure of Gd^{3+}(TREN-1-Me-3,2-

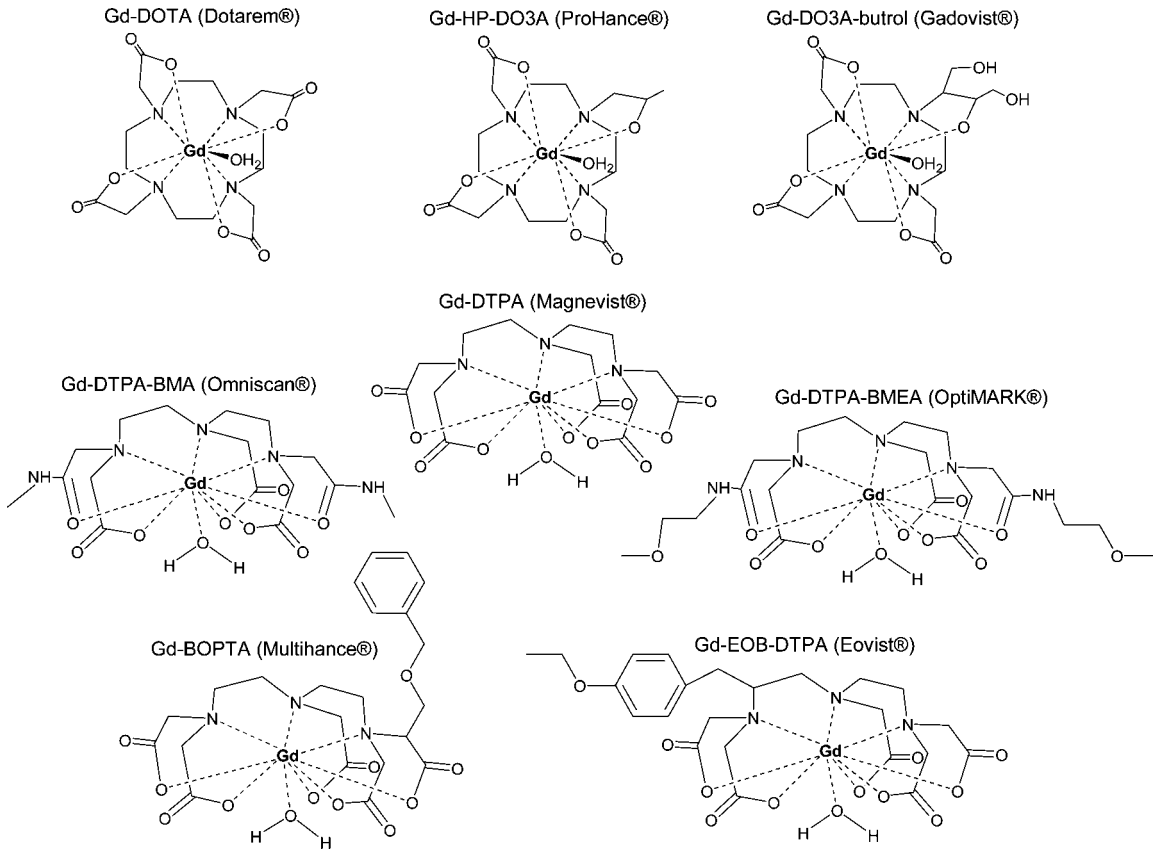

Figure 2. Commercially available Gd^{3+} chelate MR agents.

HOPO)$(H_2O)_2$ (Figure 3).[45] Hexadentate hydroxypyridinone (HOPO) based chelates bind high numbers of water molecules, at least doubling relaxivity, while also maintaining high stability. TREN-bis-HOPO-terephthalamide (TAM) chelates demonstrated the best relaxometric and solubility properties,[46] and when their biodistribution in mice was evaluated at 1 h after IV injection, accumulation was found in the liver.[47] To make their synthesis more straightforward, the TREN (tris-(2-aminoethyl)amine) scaffold was replaced with a triazacyclononane (TACN) derivative.[46] This TACN ligand cap allowed for a hydration number of 3, compared to the $q = 1$ of commercial agents. Given that it is difficult to introduce new functionalities in the heterocyclic pyridinone ring of HOPO, a recent modification has been the use of 2-hydroxy-2H-isoquinolin-1-one (1,2-HOIQO) 3-carboxylic acid instead of the cyclic hydroxamic acid units. The TREN-1,2-HOIQO chelate forms mononuclear complexes with Fe^{3+} and one-dimensional coordination polymers with lanthanide(III) cations, including Gd^{3+}.[48]

Numerous analogues of these chelates have been synthesized, but reviewing their synthesis and characterization is beyond the scope of this review. For the following sections, our discussion focuses on those agents currently in use in humans.

4.1. Dosage

Because clearance is rapid, quick T_1-weighted imaging is typically required with these agents to maximize enhancement. The recommended dosage of gadolinium chelates for visualization of lesions with abnormal vascularity in body tissue (excluding the heart) and in the central nervous system (brain, spine, and associated tissues) is 0.1−0.3 mmol/kg. Larger doses allow for better enhancement and discrimination of lesions from healthy tissue. The agents that have been approved for MRA can be administered at larger dosages (Table 1).[30] For hepatic imaging, Gd^{3+}-BOPTA and Gd^{3+}-EOB-DTPA have been approved at lower dosages of 50 and 25 μmol/kg, respectively, though Gd^{3+}-BOPTA can be used for CNS imaging at 0.1 mmol/kg (0.2 mL/kg of a 0.5 M solution). Four of these agents have been approved for administration in children, as no significant adverse clinical events or vital sign trends have been observed. In Europe, from day one after birth, Gd^{3+}-DTPA and Gd^{3+}-DOTA can be given in doses up to 0.2 mmol/kg for CNS studies. Gd^{3+}-DTPA-BMA is approved in Europe for infants from 6 months of age at a dose of 0.1 mmol/kg, and 0.1 mmol/kg Gd^{3+}-HP-DO3A can be injected in children of 2 years and above.

In 2005, the Contrast Media Safety Committee of the European Society of Urogenital Radiology (ESUR) evaluated the use of gadolinium-based agents in pregnant and lactating women.[49] The recommendation was that when MR was deemed necessary, gadolinium media could be given to pregnant women with no need for follow up neonatal tests. Further studies demonstrated that minimal amounts (<0.04% of the injected dose) of gadolinium were found in human breast milk 24 h after administration in the mother.[50] The amount in the gut of a nursing child after intravenous administration of a Gd^{3+} contrast agent to the mother is 100-fold less than the permitted dose for the infant.[50] Furthermore, very small amounts of Gd^{3+} contrast agents are absorbed when they enter through the gut. Although instructions for use state to delay breast-feeding for 24−72 h after agent administrations, the Committee's recommendation was to continue normally.[49]

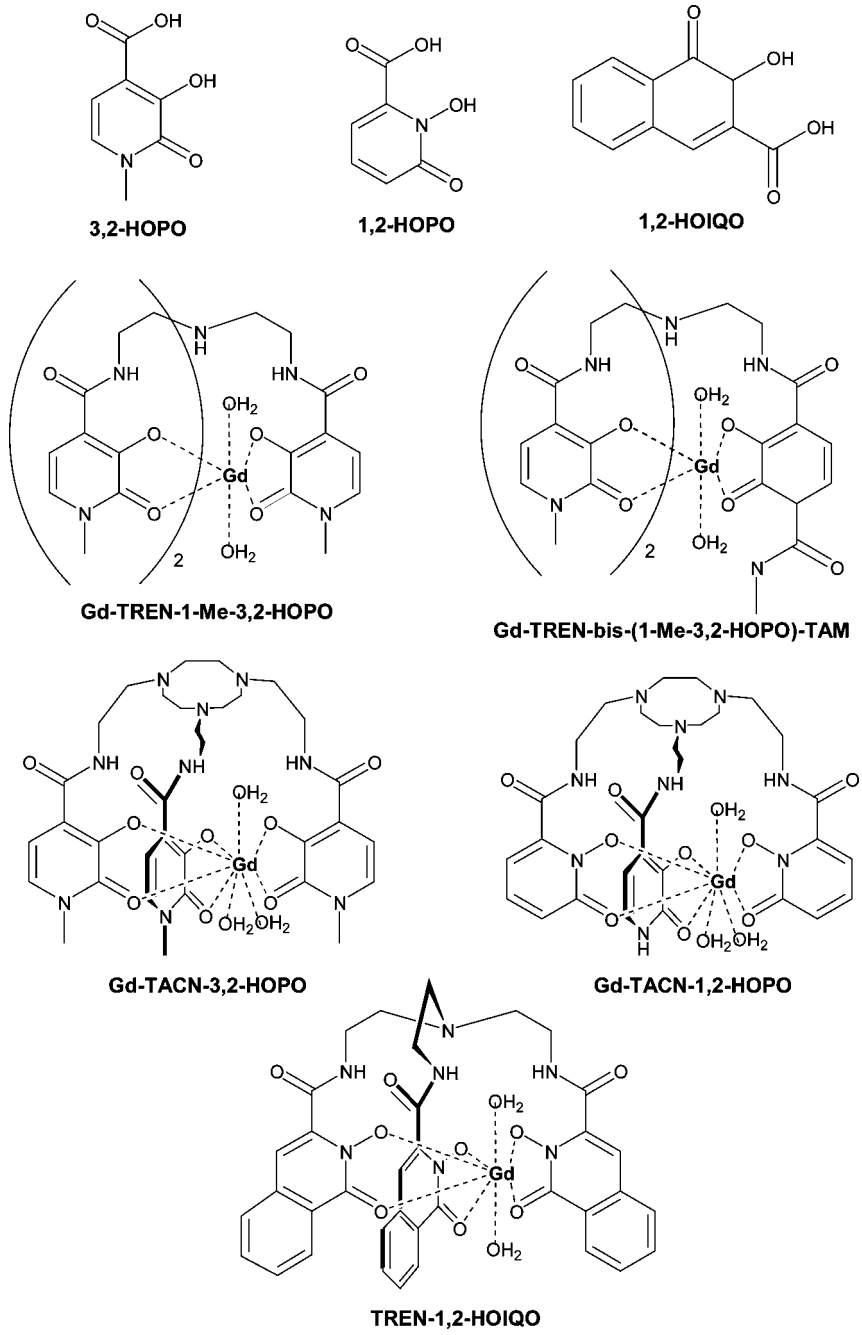

Figure 3. HOPO- and HOIQO-based chelating agents.

4.2. Adverse Reactions and Toxicity

Gd^{3+} chelates are tolerated well at both standard and high doses, with no clinically relevant difference among these agents. Adverse events, mostly mild and transient, are observed with an incidence of less than 2%.[30] These may include nausea, headache, vomiting and pain, warmth, and localized edema at the injection site. Anaphylactic reactions have been reported with a prevalence of 0.0002−0.001%,[5] but mostly in patients with a history of respiratory difficulties or respiratory allergic disease. The major concern is for patients with compromised kidney function who may develop nephrogenic systemic fibrosis (NSF).

NSF, first described in 2000,[51] is a systemic disorder characterized by widespread tissue fibrosis that can develop rapidly, confining patients to a wheelchair within a few weeks. Increased tissue deposition of collagen is observed with thickening and hardening of the skin of extremities. Involvement of other tissues such as lung, skeletal muscle, heart, diaphragm, and esophagus can occur,[52] and while the disease sometimes stabilizes, it rarely spontaneously remits. No effective treatment exists, and so prevention is currently the only approach.[53]

Of the more than 200 cases identified in the past decade, NSF is almost exclusively found among patients with advanced kidney disease.[54] Since it was first proposed that gadolinium agents might be associated with NSF,[55] much literature has been published supporting this relationship. It is theorized that lowered renal clearance of gadolinium increases tissue exposure to the metal and its dissociation from the chelate.[56] Though the actual mechanism remains unclear, the result is an inflammatory reaction and fibrosis.[57−59] A meta-analysis of the controlled studies examining gadolinium agents and the development of NSF suggests a causal relationship.[56]

The FDA and American College of Radiology (ACR)'s recommendation is to withhold all gadolinium-based agents from patients with Stage 4−5 chronic kidney disease (CKD). If patients with severe CKD need gadolinium contrast media, the FDA recommends prompt hemodialysis following contrast administration,[60] while the ACR only feels this is warranted in patients who are already on dialysis. For patients not already on hemodialysis, the recommendation is to consider the risks of initiating hemodialysis against that of developing NSF.[61] For Stage 3 or moderate CKD patients, the data was not sufficient to make any recommendations. Both the FDA and ACR have given their recommendation across the board for all Gd^{3+} based agents assuming that NSF is not linked to one specific agent. While there are suggestions that Gd^{3+}-DTPA-BMA administration may lead to a greater risk of NSF, currently there is no solid evidence to compare it relatively with the other gadolinium agents.

4.3. Motexafin Gadolinium

In the context of Gd^{3+} agents, motexafin gadolinium (MGd) deserves mention. MGd is an amphiphilic texaphyrin, a class of synthetic, aromatic macrocycles that resemble expanded porphryins, first prepared in 1988 by Sessler et al.[62] The macrocyclic skeleton of this agent surrounds the Gd^{3+} that is coordinated by 5 pyrrole- and imine-derived nitrogens. In the presence of oxygen, MGd is reduced by various metabolites and forms reactive oxygen species by redox cycling.[63] It selectively localizes in tumors and targets oxidative stress proteins such as metallothioneins and thioredoxin reductase. Oxidative stress impairs metabolism, alters metal ion homeostasis, and makes the cell more vulnerable to apoptosis. Why both texaphyrins and porphryins demonstrate tumor selectivity is not well understood, but *in vitro* uptake of the agent is temperature dependent, increases at lower pH, and is inhibited by serum proteins.[64] Tumor response to radiation and chemotherapy is enhanced by MGd, and it may intrinsically be cytotoxic. International randomized studies in brain metastasis patients reported that, in combination with MGd, radiation therapy improves time to neurological progression (15.4 months with and 10.0 months without MGd).[65] MGd is being evaluated in a number of clinical trials for monotherapy and in combination with radiation and/or chemotherapy and monoclonal antibodies for various carcinomas, including lymphomas, leukemia, lung cancer, renal cell cancer, and glioblastoma.[63] Based off a phase I trial, the maximum tolerated single dose is 22.3 mg/kg, with dose-limiting reversible renal toxicity at 29.6 mg/kg.[66] The noted adverse effects were diarrhea, nausea, vomiting, albuminuria, and reversible discoloration of skin, urine, and sclera.

5. From Small Molecule to Macromolecular Agents

Low molecular weight agents have been the pioneers in improving MR contrast. They do have limits *in vivo*, though, particularly with rapid elimination restricting timing for studies and extravasation out of the vasculature reducing contrast from surrounding tissue. Macromolecular metal−chelate complexes, sometimes known as blood pool agents or macromolecular contrast media (MMCM), are larger agents with a molecular weight greater than 30 kDa that were originally designed to address these issues. Their size limits extravasation through healthy vascular endothelium but favors enhanced permeability and retention (EPR) in leaky vasculature that may be present where there is a pathology such as cancer[67] or arthritic inflammatory response.[68] Furthermore, because of increased steric hindrance, these agents have greater relaxivity than low molecular weight agents such as Magnevist and Dotarem. As was previously described, slower molecular tumbling increases rotational correlation time, τ_R, resulting in more enhancement per unit dose of the paramagnetic ion. Additionally, multiple chelates and metal ions can be appended to a macromolecular platform, thereby also increasing enhancement and reducing the dose of agent needed for satisfactory image acquisition.

In order to attach paramagnetic ions to larger structures, a class of chelates known as bifunctional chelates have been developed based on DTPA and DOTA. These chelating agents are typically modified to have an electrophilic group that is available for conjugation to nucleophile groups on biomolecules. For example, these functional groups include anhydride, bromo- or iodoacetamide, isothiocyanate, *N*-hydroxysuccinimide (NHS) ester, and maleimide. In cases where the biomolecules contain only electrophilic functionality, such as a carboxylic acid group, the common strategy is to use cross-linking agents that provide a link between the two moieties or introduce functionality that makes conjugation more amenable.

A plethora of MR macromolecular contrast agents have been reported over the last 30 years, ranging from protein- to polymer- to dendrimer-based molecules. As reviewed by Venditto et al.[69] and references therein, these agents *typically* have diameters greater than 1−2 nm to reduce renal excretion, as compared to low molecular weight agents such as Magnevist. At 8 nm, observations have been made that hepatic uptake begins to dominate clearance routes, and by 10−12 nm the reticuloendothelial excretion route becomes the dominant route for clearance. Increased retention times and limited extravasations affect the biodistribution profile of such agents.

6. Dendrimers in MRI

6.1. Synthesis and Structure

The use of dendrimers as scaffolds for MR contrast agents has generated a tremendous amount of interest, and several reviews[69−72] have been written describing their synthesis and applications since the first dendrimer-based contrast agents were reported in 1994.[43] The principle behind the massive potential of this class of molecules in the development of diagnostic agents lies in that the synthetic chemistry used to construct them permits the "controlled occupation of space in three-dimensions as a function of size, shape and disposition of desired organic functionality".[73] The use of simple starting reagents, reaction conditions of high yields, and relatively easy purification procedures allows the precise size determination of monodisperse products based on generation number *G*; for example, generation 3 is termed G3. Furthermore, the multivalent surface of the final product allows one to tailor the molecule for specific applications (Table 2).

A dendrimer consists of a "core" from which subunits emanate in a branchlike fashion. Two general strategies are employed in the synthesis of dendrimers—a *convergent* approach, in which branches of desired generation are linked to a central core, and a *divergent* approach, in which subsequent branches originate and emanate from a central core—the chemistries of which are reviewed in thorough

Table 2. Dendrimer Generation (*G*) and Terminal Amines (*Z*)

	Z			
G	Am	EDA	DAB	CYS
0	3	4	4	4
1	6	8	8	8
2	12	16	16	16
3	24	32	32	32
4	48	64	64	64
5	96	128	128	128
6	192	256	256	256

detail elsewhere.[74−76] The convergent approach was first demonstrated by Hawker and co-workers in the synthesis of a series of dendritic polyether macromolecules based on the monomer 3,5-dihydroxybenzyl alcohol grafted onto a multifunctional core.[77] Size-exclusion chromatography experiments demonstrated that the G5 member of this series exhibited a polydispersity index (PDI) less than 1.03. PDI, the ratio of the weight average molecular weight to the number average molecular weight, is a measure of the distribution of molecular mass in a sample. Jayaraman and co-workers used this same approach in the development of a new family of dendrimers with an aliphatic polyether backbone exhibiting PDIs less than 1.01.[78] These examples demonstrate that the convergent approach permits a high degree of control in producing dendrimers of a very narrow molecular weight distribution.

The divergent approach was made possible by Buhleier and co-workers when they first demonstrated the synthesis of unidirectional branched polyamines in a "cascade-like" manner.[79] Using a monoamine or diamine as a starting point, generations were produced by repetitive reaction with acrylonitrile to form "branches" with terminal nitrile groups, followed by reduction to the amine, permitting the "growth" of succeeding generations. In an analogous manner, Newkome demonstrated the unidirectional synthesis of branched polyalcohols known as "arborols".[80] The ability to grow branches in a "cascade-like" manner was used by Tomalia and co-workers to produce dendrimers possessing three-dimensional, radial symmetry, a class of molecules since called "Starburst" dendrimers.[81] Generations were produced by the repeated reaction of either an ammonia (Am) or ethylenediamine (EDA) initiator core with an acrylate ester *via* Michael addition, followed by amidation of the resulting ester with alkylene diamine. Hence, these dendrimers also came to be known as poly(amidoamine) or PAMAM dendrimers. As a result of the three-dimensional growth of these structures, the number of terminal amines increases exponentially with generation number. However, the monodispersity of the final products was slightly affected detrimentally by unwanted side reactions caused by dendrimer fragmentation, bridging, or incomplete removal of unreacted reagents at each generation sequence. Nevertheless, the PAMAM dendrimers have enjoyed an almost monopolistic usage in the development of dendrimer-based MR contrast agents, as described below. Systematic investigations of the atomistic structure of EDA-core PAMAM dendrimers up to G11 have also been performed to determine theoretical limits for uniform growth of successive generations.[82] Poly(propylene imine) (or PPI) dendrimers based on a diaminobutane (DAB) core have also been synthesized,[83,84] the first five generations of which were found to have a polydispersity index of 1.002.[85] More recently, a family of PAMAM dendrimers with a cystamine (CYS) core was synthesized, which provides a versatile platform for producing novel shapes and terminal functionalities through redox chemistry at the disulfide core.[86]

Owing to the structural complexity of dendrimers, a system of nomenclature for this class of molecules should clearly express what the core, repeat, and terminal units are. For cascade polymers having the same repeat unit throughout the structure (such as PAMAM dendrimers), Newkome et al. suggest[75] that these may be represented by the formula

$$[\text{core unit}](\text{repeat unit})_{N_b}^{G}(\text{terminal unit})_{N_c} \qquad (24)$$

where G is the generation number, N_b the branch multiplicity of the repeat unit, and N_c the branch multiplicity from the core. From this, the number of terminal groups Z can be calculated using $Z = N_c N_b^G$. A name can then be assigned using the general formula

$$Z - \text{cascade:core}[N_c](\text{internal units})^n\text{:terminal unit} \qquad (25)$$

where n denotes the number of repetitions of that unit. Applying these rules, a second generation Am-core PAMAM dendrimer is then represented by the formula

$$[N][CH_2CH_2CONHCH_2CH_2N]_2^2[(CH_2CH_2CONHCH_2CH_2NH_2)]_3$$

and its name written as

12-cascade:ammonia[3]:(ethylamidoethylamine)^2:ethylamidoethylamine

Though this system of nomenclature is articulate, for brevity in this review we will use, where appropriate, a shorthand nomenclature which involves stating in sequence the kind of dendrimer (PAMAM vs PPI), core, generation number, and terminal chelate. For example, a second generation Am-core PAMAM dendrimer with terminal amines functionalized with the chelating ligand DOTA will be written simply as "PAMAM-Am-G2-DOTA".

Furthermore, some confusion in the literature exists regarding the assignment of G to PPI dendrimers, and as a result, the formula for Z may not apply. *For the purpose of this review, we define G0 of the PAMAM and PPI dendrimers not as the initiator core, but as the functionalized core possessing terminal amines* (Figure 4). It is important to stress this point, as any meaningful comparison between increasing generations of PAMAM and PPI dendrimers in their use as contrast agents depends on the number of terminal amines (Z) available for functionalization with a paramagnetic chelate.

6.2. Solution Studies

The first report of dendrimer-based MR contrast agents described the conjugation of G2 and G6 PAMAM-Am dendrimers with Gd^{3+}-1B4M.[43] Due to their large molecular weight (and hence, a large molecular tumbling rate, τ_R), these agents exhibited very high longitudinal relaxivities. In terms of molar relaxivity, the G6 dendrimer was found be ~6 times that of Gd^{3+}-DTPA alone. Owing to the potential usefulness of these compounds, an improved synthesis was reported more recently involving nonaqueous conjugation chemistry.[87] Langereis and co-workers reported the synthesis of a series of G0, G2, and G4 PPI dendrimers conjugated with Gd^{3+}-DTPA and found that both molecular and ionic relaxivities also increased as a function of generation number.[88] Analogously, Margerum reported that the measured relaxivities of PAMAM-Am-DO3A dendrimers, ranging from G2 to G5,

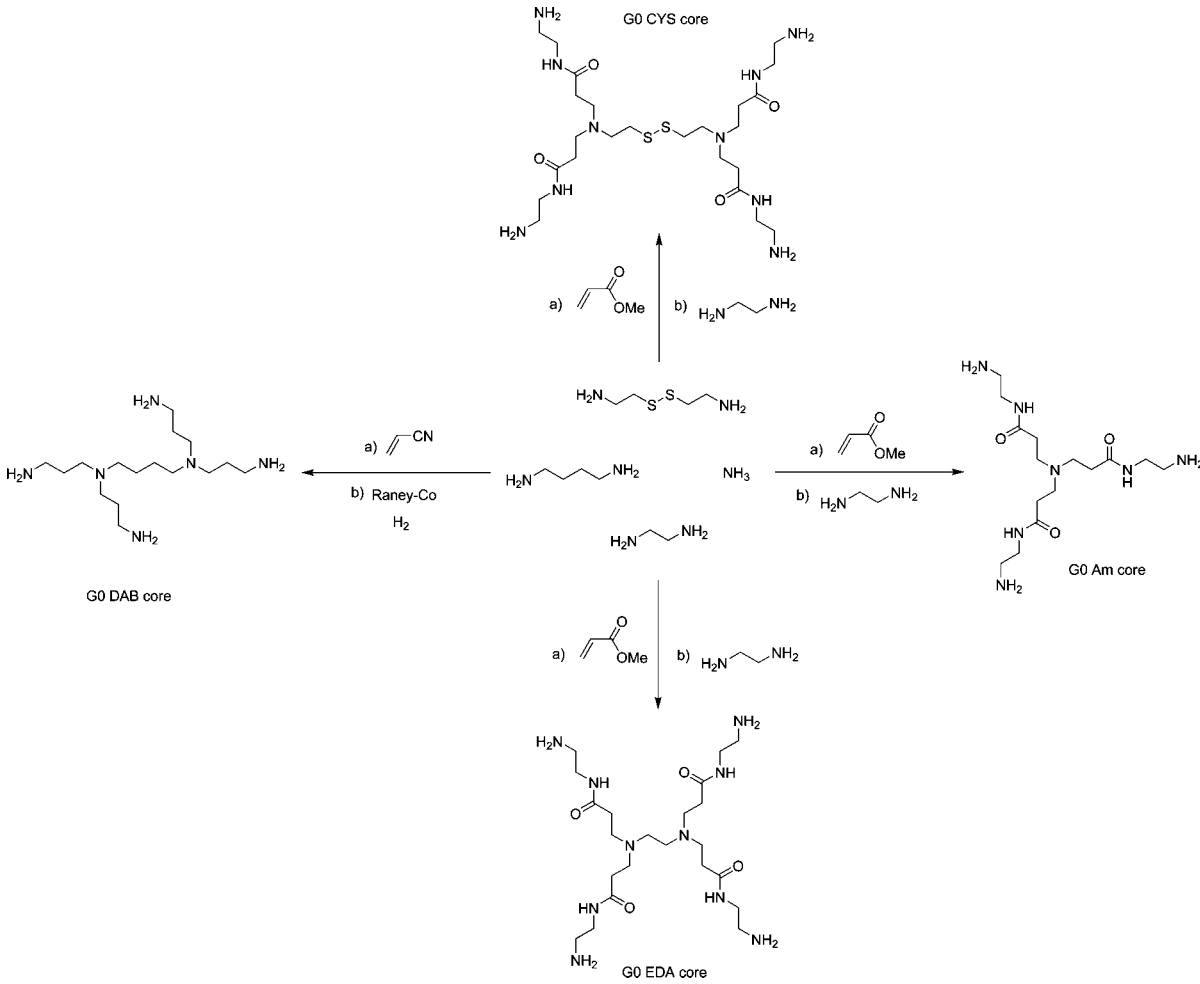

Figure 4. Synthesis of G0 Am-, EDA-, DBA-, and CYS-core dendrimers.

and those of higher generations of PAMAM-EDA dendrimers conjugated with Gd^{3+}-DOTA, ranging from G5 to G10, synthesized by Bryant and co-workers, increased with increasing molecular weight.[89,90] However, Bryant observed that molar relaxivities achieved a saturation limit beyond G7. Toth and co-workers performed a series of variable temperature and pressure ^{17}O NMR experiments on Gd^{3+}-DO3A labeled PAMAM-Am dendrimers of lower generation (specifically, G3 to G5), to study the effects of water exchange and rotational dynamics on the relaxivity of these agents.[91] Their measurements showed that while τ_R increases approximately by a fourth with each increase in generation, the water exchange rate constants k_{ex} remain the same for all the systems studied, sacrificing any theoretical increase in molar relaxivity. They concluded by stating that these systems possess rotational correlation times long enough for the rate of water exchange to affect the overall relaxivity of the dendrimer and that further improvements would entail not just increasing molecular weight but designing chelate systems which promote the dissociation step of water molecules bound to the paramagnetic Gd^{3+} ion. Furthermore, their results demonstrated that conjugation of the macrocyclic chelate to the large dendrimer did not affect the rate of water exchange at the metal center, suggesting that the k_{ex} value determined for any monomeric chelate should apply to any future dendrimeric conjugate.

To this effect, Laus and co-workers synthesized a series of higher generation (G5 to G9) PAMAM-EDA dendrimers conjugated with a novel ligand, ethylenepropylenetriamine pentaacetic acid (EPTPA).[92] ^{17}O NMR experiments have shown that Gd^{3+}-EPTPA possesses a water exchange rate 10-fold greater than that of Gd^{3+}-DTPA.[93] This is attributed to steric crowding around the Gd^{3+}, thereby accelerating the dissociation of bound solvent molecules. The relaxivities of the systems measured increased from G5 to G7 (37 °C, 30 MHz), demonstrating the beneficial effect of using chelates with faster water exchange rates. However, the trend was found to decrease upon reaching G9. Relaxivity measurements at different pH values suggest that protonation of the tertiary amines of the dendrimer results in a more rigid and open structure, thereby improving relaxivity. Hence, it was rationalized that, even with faster water exchange kinetics, the overall relaxivity of higher generation dendrimers is affected also by internal motion. Similarly, Rudovsky and co-workers reported a series of PAMAM-EDA dendrimers ranging from G1 to G4 conjugated with a Gd^{3+}-DO3A derivative, 1,4,7,10-tetraazacyclododecane-4,7,10-triacetic-(methyl(4-aminophenylmethyl)phosphinic acid), (DO3A-P^{ABn}).[94,95] ^1H nuclear magnetic resonance dispersion (NMRD) and VT-^{17}O NMR measurements have shown that Gd^{3+}-DO3A-P^{ABn} possesses an optimally short water residence time and a higher than expected relaxivity, due to steric crowding and the formation of a secondary hydration sphere by the bulky phosphinate group.[96] As expected, the measured relaxivities of these systems increased with generation number, and protonation of the tertiary amines of the dendrimer backbone resulted in a further increase in relaxivity. Furthermore, it was also demonstrated that formation

Table 3. Relaxivites of Various Paramagnetically-Labeled PAMAM Dendrimers

dendrimer	core	ionic r_1 (mM^{-1} s^{-1})	molec r_1 (mM^{-1} s^{-1})	field strength	temp (°C)	pH	ref
PAMAM-G2-DTPA	Am	21.3 ± 0.3	234	25 MHz	20	7.4	43
PAMAM-G3-DO3A	Am	14.8 ± 0.4		25 MHz	37		89
PAMAM-G4-DO3A	Am	16.9 ± 0.4		20 MHz	37		89
PAMAM-G5-DO3A	Am	18.8 ± 0.2		25 MHz	37		89
PAMAM-G6-DTPA	Am	34 ± 4	5800	25 MHz	20	7.4	43
PPI-G0-DTPA	DAB	14.4 ± 0.2	45.6	1.5 T	20	5.8	116
PPI-G2-DTPA	DAB	15.2 ± 0.2	243	1.5 T	20	5.8	116
PPI-G4-DTPA	DAB	19.3 ± 0.2	1234	1.5 T	20	5.8	116
PAMAM-G5-DOTA	EDA	30	2880	20 MHz	23	7.4	90
PAMAM-G7-DOTA	EDA	35	13300	20 MHz	23	7.4	90
PAMAM-G9-DOTA	EDA	36	47520	20 MHz	23	7.4	90
PAMAM-G10-DOTA	EDA	36	66960	20 MHz	23	7.4	90
PAMAM-G1-DO3A-P^{ABn}	EDA	14.8		20 MHz	25	7.5	94
		10.1		20 MHz	37	7.5	94
PAMAM-G2-DO3A-P^{ABn}	EDA	19.7		20 MHz	25	7.5	94
		14.1		20 MHz	37	7.5	94
PAMAM-G4-DO3A-P^{ABn}	EDA	25.8		20 MHz	25	7.5	94
		18.6		20 MHz	37	7.5	94
PAMAM-G5-DTTAP	EDA	26.8		20 MHz	37	6.25	97
PAMAM-G5-EPTPA	EDA	25.1		20 MHz	20	6.0	92
		17.1		20 MHz	37	6.0	92
PAMAM-G7-EPTPA	EDA	35.8		20 MHz	25	6.0	92
		25.6		20 MHz	37	6.0	92
PAMAM-G9-EPTPA	EDA	29.2		20 MHz	25	6.0	92
		24.2		20 MHz	37	6.0	92

of adducts with positively charged polycations, such as poly(Arg) and poly(Lys), increased relaxivity by reducing the internal motion in these dendrimers, which are negatively charged. The formation of adducts did not affect the water exchange rate, and relaxivities remained stable up to pH 9.5 for the poly(Lys) adduct and pH 12 for the poly(Arg) adduct. A further report by Lebduskova and co-workers described the enhanced relaxivity of a PAMAM-EDA-G5 dendrimer conjugated with a DTPA-based chelate containing one phosphinate group, DTTAP, which also cited the benefits of faster water exchange and the role of the secondary hydration sphere.[97] More recently, Ali and co-workers described a PAMAM-EDA-G5 dendrimer conjugated with a DOTA-like tetraphosphonate ligand, DOTA-4AmP, sensitive to pH changes, whose relaxivity more than doubles when pH is changed from pH 9 to pH 6.[98] A comparison of the relaxometric properties of these dendrimers is summarized (Table 3).

Novel ideas include the synthesis of G0 and G2 PPI dendrimers functionalized with Yb^{3+}-DOTAM as a pH sensitive paramagnetic chemical exchange saturation transfer (PARACEST) agent, in which the maximum effect was observed with decreasing pH from the mononuclear chelate to the G2 dendrimer.[99] PARACEST agents (see section 10.1.4) have been gaining more interest in molecular imaging since paramagnetic ions induce large shifts in the resonances of neighboring nuclei which can be visualized at will by the proper choice of irradiation frequency.[100] The different chelates used to functionalize dendrimers are summarized (Figure 5).

Lastly, a series of Gd^{3+}-chelate-core branched-alcohol dendrimers was synthesized via a convergent approach.[101] Unidirectional amino-substituted arborols of increasing length and branching were conjugated to a Gd^{3+} chelate possessing a DOTA-like ligand with peripheral carboxylate groups. Placing the Gd^{3+} ion at the center of a macromolecular structure was proposed to effectively couple the local motion of the $Gd^{3+}-OH_2$ vector with the rotation of the entire assembly, resulting in an increased relaxivity (Table 3, Figure 6).[102] ^{17}O NMR measurements indeed show that a greater length and degree of arborol branching of the complex in comparison with the case of the parent compound correlate with a slower rotational correlation time, τ_R. However, the largest of these complexes, having the largest number of methyl and methylene groups, exhibited the slowest water exchange rate k_{ex}, thereby compromising any further theoretical gain in relaxivity.

6.3. Biodistribution

6.3.1. Passive Distribution

The most important property which determines the biodistribution of dendrimer-based MR agents is their size, which in turn is determined by (a) the nature of the central core and the interior architecture and (b) the generation number, *G*.

PAMAM-Am-G2-DTPA and PAMAM-Am-G6-DTPA were the first dendrimer-based MR contrast agents evaluated for use in magnetic resonance angiography (MRA).[43] These agents possessed enhancement half-lives double and ten-times longer than that of Gd^{3+}-DTPA, respectively, as measured in mice. An early dose−response study described the use of PAMAM-Am-G5-DO3A in visualizing vasculature in rabbits, reporting a minimum effective dose of 0.02 mmol/kg and a maximal contrast enhancement produced at a dose of 0.03 mmol/kg.[103] In MRA experiments involving a series of PAMAM-Am-DO3A (G2 to G5), the blood clearance half-lives of these agents were observed to increase with increasing generation number.[89] Gadomer-17 (Schering AG, Berlin, Germany), also known as the Gd^{3+}-DTPA-24-cascade polymer,[104] in comparison with Gd^{3+}-DTPA, polyLys-DTPA, and Gd^{3+}-DTPA-albumin,[105−107] was shown to visualize intratumoral vasculature, exhibiting high vascular permeability[108] and acute myocardial ischemia,[109] and a dose of 0.033 mmol/kg of PAMAM-Am-G6-1B4 M in mice was sufficient to visualize intratumoral vasculature as small as 100-μm in diameter.[110] Furthermore, Gadomer-17, which is a dendrimer consisting of a trimesoyl triamide core with branched lysine amino acids,[104] was used to image vascu-

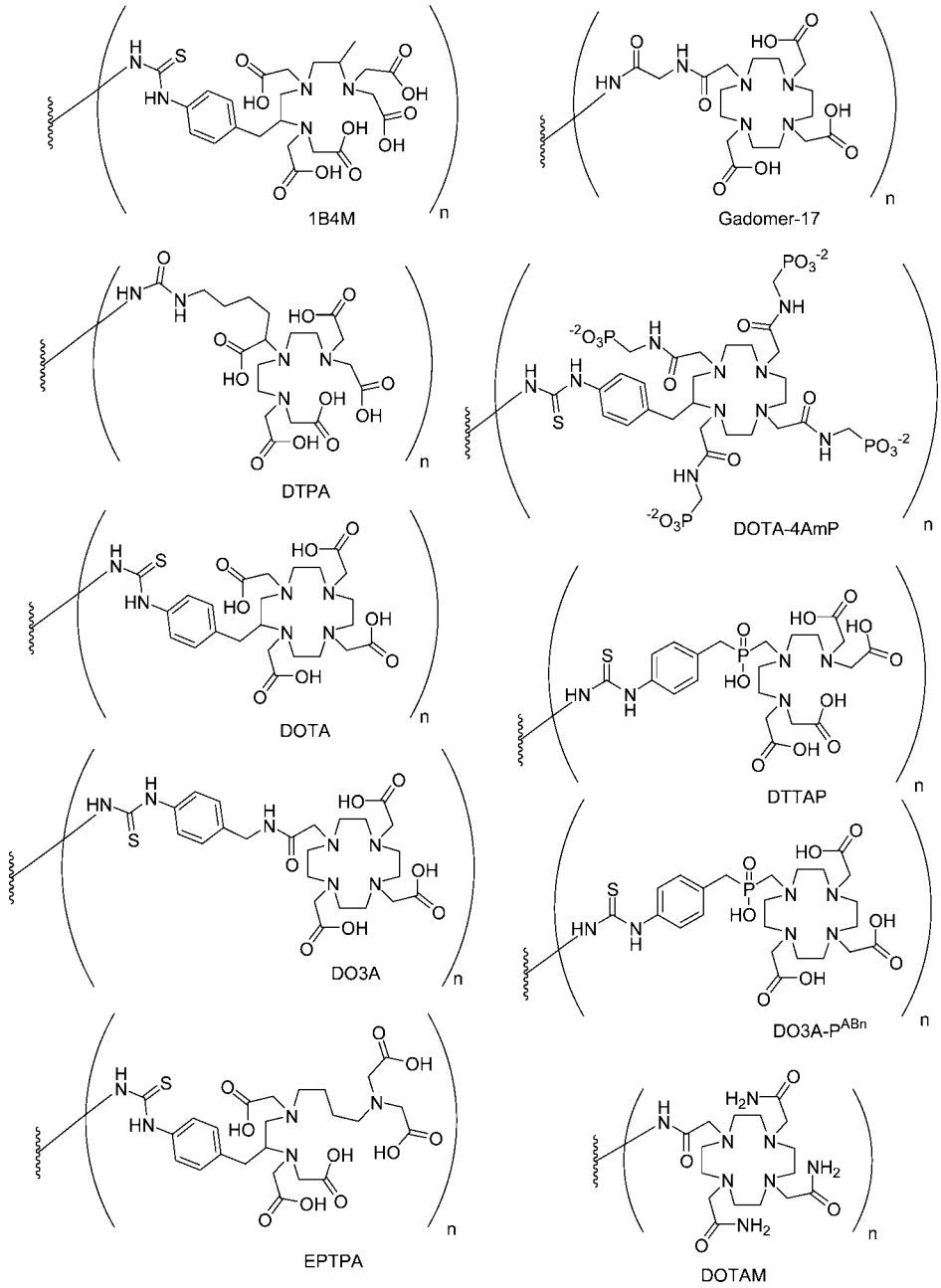

Figure 5. BFCAs conjugated to dendrimers.

lature in dogs; MRA images showed that a 0.1 mmol/kg of Gadomer-17, with 24 Gd^{3+}-DOTA units, produced more enhanced contrast than a 0.3 mmol/kg dose of Gd^{3+}-DTPA.[111]

Sato,[112] Kobayashi,[113,114] and Yordanov[115] and co-workers embarked on systematic studies of the biodistribution of PAMAM-EDA-1B4 M chelating Gd^{3+}dendrimers, ranging from G3 to G10, for use in MRA studies for the visualization of both normal and tumoral vasculature. Their results show that smaller generations (G3 to G5) exhibit rapid clearance from the body and a high glomerular filtration rate, though G5 and G6 were retained long enough to visualize normal fine vasculature up to a 200 μm limit. Higher-generation dendrimers G7 to G9 were found to have less renal uptake than G6, with G8 and G9 exhibiting a much higher hepatic accumulation. Furthermore, G8 was found to visualize intratumoral vessels in a more stable manner over time than G6, due to the increased vascular permeability of fast-growing cancer cells. In summary, the authors indicated G7 as the best candidate for visualizing intratumoral vasculature, since it was retained in blood circulation the longest; the low liver uptake and slow glomerular filtration may permit longer image acquisition times. The highest generation dendrimer studied, G10, was found to precipitate at physiological pH.

In a similar fashion, Langereis and co-workers studied the biodistribution of a range of lower to intermediate generation PPI-DTPA dendrimers (from core to G4).[116] All the agents studied exhibited renal clearance, though higher generations prolonged blood retention. Furthermore, G2 and G4 exhibited a lesser tendency to leak from tumoral vasculature into the tumor, whereas core and G0 were found to do so rapidly. Lastly, the largest dendrimer studied, G4, was found to have a lowest detectable concentration around 80 nM, more than 2 orders of magnitude lower than that of Gd^{3+}-DTPA.

Kobayashi and co-workers also embarked on systematic comparisons of biodistribution based on the nature of the PAMAM core. Results show that between PAMAM-Am-

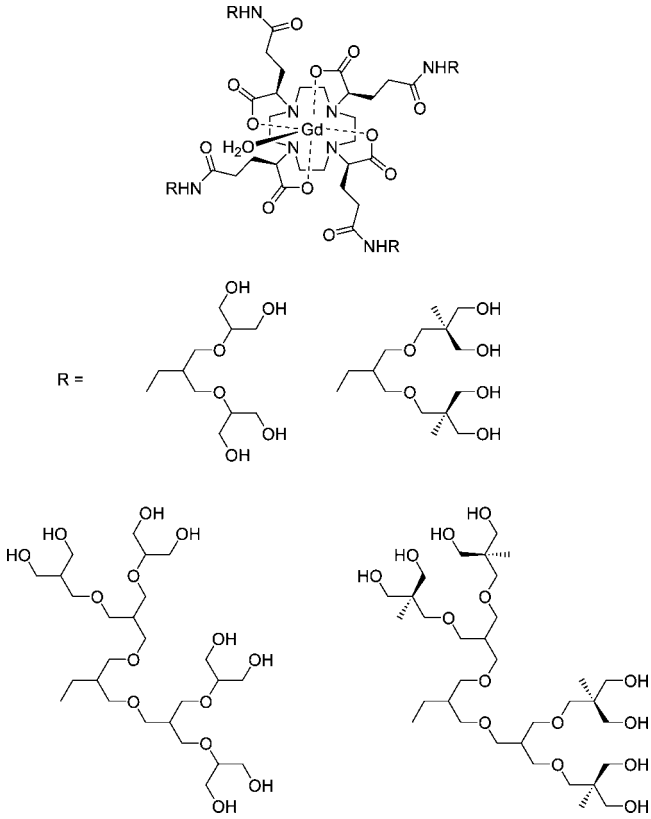

Figure 6. Gd^{3+} chelate at the barycenter of the dendrimer.

G6-1B4M and PAMAM-EDA-G6-1B4M, the latter exhibited longer blood retention and slower renal uptake, making it a better blood pool agent.[117] In addition, PPI-G4-1B4M was found to exhibit a significant amount of hepatic uptake in comparison with PAMAM-EDA-G4-1B4 M due to its relatively higher hydrophobicity,[118] and it has been demonstrated to visualize both normal liver parenchyma and micrometastatic tumors of 0.03-mm diameter in mice.[119] Due to problems of prolonged retention in blood and poor clearance, a comparison study between dendrimers of different cores and sizes was performed to determine which possessed the best renal excretion properties, citing PAMAM-EDA-G2-1B4M, PPI-G3-1BM, and PPI-G2-1B4M as the best candidates for clinical studies,[120] with PPI-G2-1B4M found to be the best agent for functional kidney imaging and early diagnosis of renal damage.[121] Furthermore, control over circulation and excretion properties was demonstrated with conjugation of the dendrimers with polyethylene glycol (PEG),[122] coinjection with lysine,[123] or biotinylation of the dendrimer followed by an avidin chase.[124]

Higher generation dendrimers were found to be more suitable for MR lymphangiography applications. For example, PAMAM-EDA-G8-1B4M, with its large size and therefore low vascular permeation, was found to be retained inside lymphatic compartments, permitting discrimination between infection and proliferative or neoplastic swelling.[114] A comparison between dendrimers of different cores showed this same dendrimer-based agent was more suitable for imaging lymphatic vessels while PPI-G5-DTPA better visualized lymph nodes.[125] Lastly, advances in bioconjugation chemistry permitted the synthesis of a dendrimer-based fluorescent-MRI multimodal probe capable of visualizing sentinel lymph nodes in mice.[126,127] More recently, PAMAM-EDA-G8-1B4M was also evaluated as a CT-MR probe administered in conjunction with convection-enhanced delivery (CED) of therapy to the brain, though the effect of dendrimer size and core in this area of use has yet to be determined.[128]

6.3.2. Targeted Agents

Several attempts have been made to improve the selectivity of dendrimer-based MR agents by synthesizing targeted bioconjugates. Wu and co-workers were among the first to describe the synthesis of a set of antibody-labeled (mAb 2E4) dendrimers, PAMAM-Am-G2-DOTA and PAMAM-Am-G2-CHXB, which were efficiently labeled with ^{90}Y, ^{111}In, ^{212}Bi, and Gd^{3+}, without loss of immunoreactivity, as potential tools for either directed radiotherapy or MR imaging.[129] Kobayashi and co-workers also demonstrated that conjugation of PAMAM-EDA-G4-1B4M with OST7, a murine monoclonal IgG1, did not compromise immunoreactivity. Furthermore, in addition to specific accumulation in tumor sites, the antibody-dendrimer construct had better blood clearance behavior than the simple 1B4M-labeled antibody.[130] PAMAM-Am-G4-DTPA conjugated with folic acid has been successfully shown to selectively label ovarian cancer tumors overexpressing the high-affinity folate receptor (hFR).[131−134] PAMAM-EDA-G3 was consecutively conjugated with cyclic-RGD, a fluorescent dye, and Gd^{3+}-1B4M to selectively visualize integrin $\alpha_V\beta_3$, a marker for angiogenesis.[135] Though *in vitro* results were initially promising, the approach met with limited success *in vivo*.

6.3.3. Cell Transfection

Lastly, several efforts have been made to develop strategies for the intracellular delivery of contrast agents. Solution studies of dendrimer- and nondendrimer-based contrast agents in combination with commercially available cell transfection agents found that adduct formation reduced the relaxivity of the Gd^{3+}-based agents (by blocking water coordination sites), but that adduct dissociation was a function of pH, suggesting a further capability of these systems as a pH switch.[136] Successful cell delivery was reported by Kobayashi and co-workers using a bioconjugate construct composed of PAMAM-EDA-G6 labeled with biotin, Gd^{3+}-1B4M, and, lastly, avidin, which was found to accumulate in SHIN3 tumor cells (human ovarian cancer) 50 times more than mononuclear Gd^{3+}-DTPA.[137] Zhu and co-workers employed a three-step pretargeting approach to visualize Her-2/*neu* xenografts in mice: biotinylated trastuzumab was first administered to label the tumors, followed by an avidin chase and, lastly, a biotinylated PAMAM-G4-DTPA dendrimer. Though only limited selective MR enhancement was observed in the tumor xenografts, the bioconjugate construct was retained in tumors due to the EPR effect.[138] Also, Xu and co-workers described the use of a cysteamine-core dendrimer to produce a multimodal dendrimer-based agent, employing rather clever chemistry. PAMAM-CYS-G2 was first conjugated with 1B4M-DTPA[Gd^{3+}], after which the disulfide core of the dendrimer was cleaved to allow for site-specific conjugation with biotin. Up to four of these bioconjugate constructs formed an adduct with fluorescently labeled avidin, and multimodal imaging techniques confirmed the accumulation of this supramolecular construct in mice bearing ovarian cancer tumors.[139]

7. Linear Polymers in MR Imaging

Synthetic linear polymers have also been studied and tested as potential core platforms for creating macromolecular MR contrast media, citing characteristic advantages similar to those of dendrimers, namely, that polymer chemistry is certainly established enough to exercise control over polydispersity and molecular weight, a wide enough variety of monomers exist to produce polymers of minimal or no immunogenicity, and polymers can be made to respond to environmental changes which are diagnostic of physiological phenomena.

7.1. Poly-L-lysine

By far, the most studied linear polymer in MRI imaging is poly-L-lysine. Poly-L-lysine is commercially available in a wide variety of molecular weights, and conjugation with DTPA takes place on the ε-amino group of lysine. Two labeling methods have been described, using either DTPA dianhydride or DTPA-OSu ester, with the latter method displaying better conjugation efficiencies up to 100% on poly-L-lysine (38.5 kDa).[140] DOTA has also been conjugated to polylysine via a mixed anhydride method.[141] Complexation with Gd^{3+} resulted in polymers possessing a longitudinal relaxivity r_1 three times greater than that of the monomeric chelate,[142] independent of polymer chain length.[140] Pharmacokinetic studies have shown it to be well-tolerated *in vivo*, as reflected by a high LD_{50}, and that clearance occurs primarily through the kidney, requiring at least a day to clear completely in rat and rabbit models.[142,143] However, it was also shown that Gd^{3+}-DTPA-polylysine formulations of higher molecular weight clear slower from the blood in comparison with smaller polymers, resulting in prolonged and constant tissue enhancement over a 1 h period.[144]

These positive characteristics have since led to a series of *in vivo* studies employing Gd^{3+}-DTPA-polylysine. As a possible blood pool agent, it was tested in MRA in rabbits to monitor blood flow in the extremities[145] and to distinguish normal myocardium from peripheral ischemic zones in cats.[146] Gd^{3+}-DTPA-polylysine has also been conjugated to human serum albumin to improve its blood pool behavior, based on other efforts to develop Gd^{3+}-labeled albumin as an MR contrast agent (section 4.1).[141] Gd^{3+}-DTPA-polylysine has also been used to visualize pulmonary disease states exhibiting abnormal blood flow[147−149] and has also been shown to accumulate in tumors, resulting in tumor tissue enhancement lasting for several days in a rat model.[150]

7.2. Polyethyleneglycol (PEG)

Polyethyleneglycol (PEG) was a most likely candidate for use as a platform for macromolecular MR contrast agents, since it has for many years been used to covalently modify biomolecules and small-molecule drugs in order to prevent their recognition by the immune system and facilitate solubility and clearance.[151] For example, PEGylated bovine serum albumin was observed to possess virtually no immunogenicity when injected into rabbits, thereby prolonging its blood circulation time.[152] ^{17}O NMR studies of Gd^{3+}-DTPA-labeled PEG showed that the water exchange rate k_{ex} between bulk and bound water molecules on the paramagnetic center is identical between the polymer and the monomeric chelate, indicating a large degree of flexibility in the polymer chain.[153] Functionalized PEG for conjugation chemistry is also available in a wide range of molecular weights, and Gd^{3+}-DTPA-PEG of molecular weights greater than 20 kD has been shown to exhibit good blood pool enhancement dynamics while smaller conjugates demonstrate faster tumor enhancement in rabbits.[154]

Gd^{3+}-labeled conjugates based on combinations of both polylysine and PEG have also been reported in the literature (Figure 7), as a strategy to improve solubility in blood and reduce the immunogenicity of polylysine. A prototype was reported by Bogdanov and co-workers, which exhibited a blood half-life of 14 h and constant vascular enhancement for 2 h.[155] This concept was developed more thoroughly by Fu and co-workers, who described the synthesis and characterization of a series of Gd^{3+}-labeled polylysine dendrimers of different generations linked by PEG cores of varying length.[156] These compounds exhibited good water solubility, good stability in both buffer and plasma, narrow size dispersity, and longitudinal relaxivities approximately three times that of the monomeric chelate. These polylysine-based agents have recently been used as contrast agents in MRI to visualize and distinguish cancerous from normal soft tissue in rat models.[157]

7.3. Other Linear Polymers

The wide variety of monomers and resulting polymers either commercially available or easily synthesized permits the evaluation of many other possible polymer-based macromolecular contrast agents. Cavagna and co-workers reported that the synthetic polypeptide polyaspartate containing ~220 monomers was capable of chelating as many as 40 mol Gd^{3+} per mole of polyaspartate, though no comment was made about the stability of the resulting polychelate.[158] Allen and co-workers described the use of ring-opening metathesis polymerization (ROMP) to produce a polymer incorporating the ligand hydroxypyridonate (HOPO) in its backbone, capable of chelating Gd^{3+} with high stability.[159] Indeed, DTPA dianhydride itself has been used in copolymerization with different kinds of α,ω-diamines, to form polymers with Gd^{3+} chelating units along the polymer backbone (Figure 8). For example, DTPA has been copolymerized with tartaric acid to produce a polymer with increased hydrophilicity and reduced toxicity.[160] In contrast, DTPA has been copolymerized with alkyldiamines of different alkyl chain lengths, resulting in macromolecular structures exhibiting relaxivities similar to those of dendrimers.[161] It was hypothesized that intramolecular hydrophobic interactions between the alkyl chains resulted in the formation of rigid structures; indeed, variable-temperature, multiple-field ^{17}O NMR and electron paramagnetic resonance studies have shown that the relaxivity behavior of these polymers is more characteristic of rigid globular micellar structures rather than of a linear system.[162] Another report described the synthesis of polysuccinimide derivates containing PEG, as a hydrophilic component, and hexadecylamine, as a hydrophobic component, copolymerized with DTPA, toward the development of biocompatible micellar MR agents with improved *in vivo* stability.[163] Ladd and co-workers also reported a systematic study of DTPA copolymers which relate molecular weight, polymer rigidity, metal content, viscosity, and chelate stability in the design of polymer-based blood pool agents.[164]

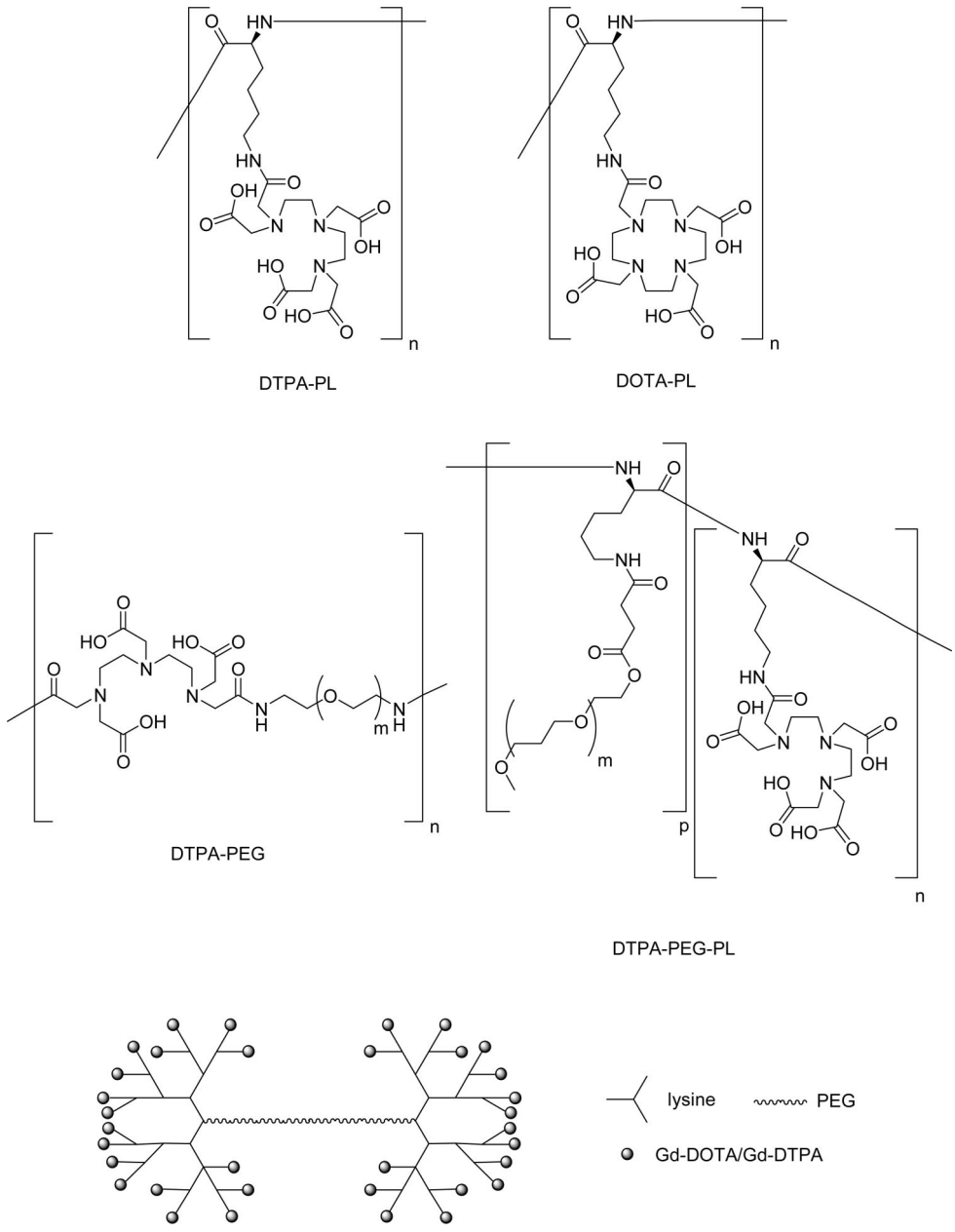

Figure 7. DTPA- and DOTA-conjugated polylysine (PL), polyethylene glycol (PEG), and mixed PL-PEG species.

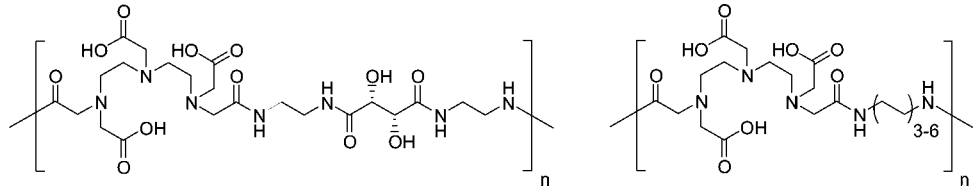

Figure 8. Examples of DTPA copolymers of α,ω-diamines.

7.4. Targeted and Functional Polymers

Furthermore, by careful selection of copolymer, the nature of the polymer bond, or even the metal chelate itself, polymer macromolecular contrast agents can be designed either with an intrinsic controlled biodistribution or to reflect particular physiological phenomena. For example, DTPA and sulfadiazine were incorporated into polyaspartamide and then labeled with Gd^{3+} to produce a tumor specific polymer contrast agent, exhibiting preferential uptake in and significant MR enhancement of hepatoma in a mouse model.[165] Similarly, *N*-(2-hydroxypropyl)methacrylamide was copolymerized with mannosamine and then labeled with Gd^{3+}-DOTA to produce a contrast agent specific for mannose receptors overexpressed in activated macrophages.[166] More recently, polydiamidopropanoyl dendrimer was labeled with multiple Gd^{3+} chelates and then conjugated with a peptide nucleic acid as a MR hybridization probe capable of hybridizing with specific mRNA.[167]

Bogdanov and co-workers described the novel strategy called MR signal amplification, or MRamp, which is based on enzyme-mediated polymerization of a paramagnetic monomer into oligomers exhibiting high relaxivity (Figure

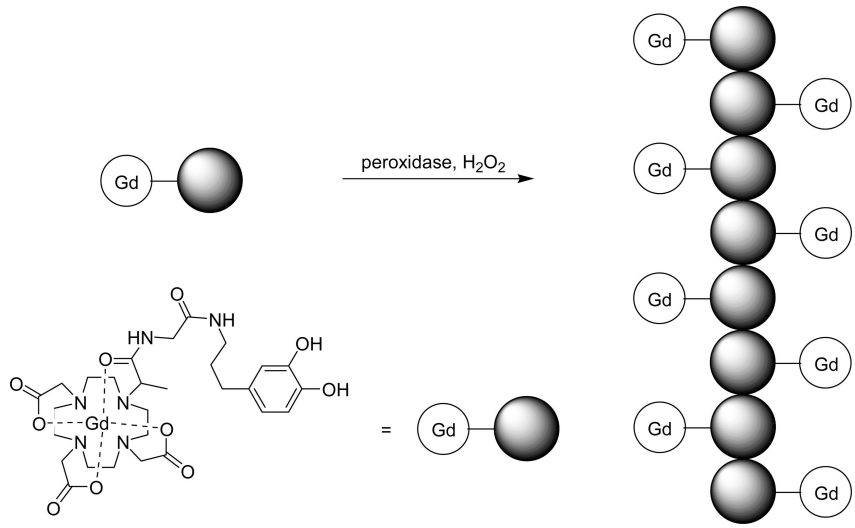

Figure 9. MRamp polymerization of paramagnetic chelates.

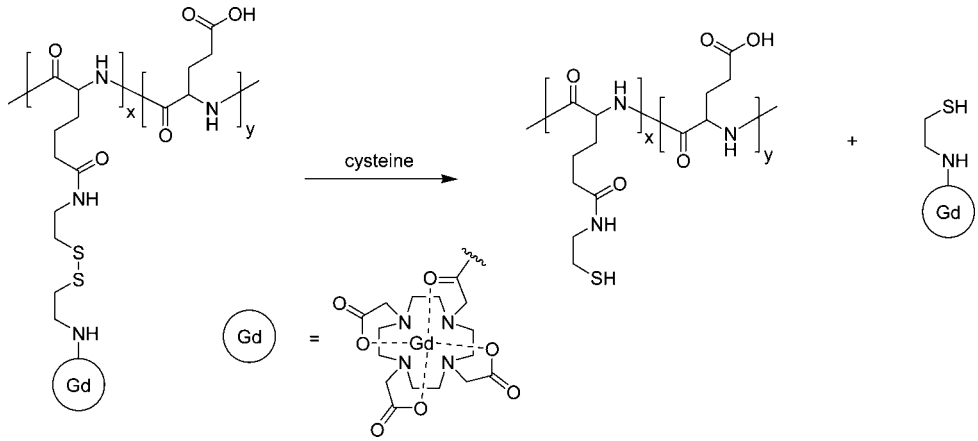

Figure 10. Paramagnetic polymer with biodegradable spacer.

9).[168] This strategy was demonstrated by labeling E-selectin expressed on endothelial cells with an anti-E-selectin antibody conjugated with peroxidase. Subsequent administration of phenol-functionalized Gd^{3+}-chelates resulted in the formation of polymetallic oligomeric species of high molecular weight and increased relaxivity. While the method was sensitive enough to detect nanomolar amounts of peroxidase, clearance of the resulting oligomers was not discussed. A reverse strategy was reported by Lu and co-workers in which Gd^{3+}-labeled polyglutamic acid with a biodegradable disulfide spacer is broken down in the presence of endogenous blood plasma thiols, to facilitate clearance from the blood via renal filtration (Figure 10).[169] Similarly, Wen and co-workers reported a polyglutamic acid based MR contrast agent which degrades in the presence of cathepsin B, a lysosomal enzyme.[170] Gd^{3+}-labeled polyglutamic acid has been tested for visualization of human breast cancer xenografts in mice, with the larger molecular weight polymer construct exhibiting better accumulation in tumors.[171] Mohs and co-workers also reported Gd^{3+}-labeled PEG-L-cystine copolymers which are also broken down in the presence of endogenous thiols,[172] and they reported that variations in PEG length had little effect on the relaxivity of the polymer.[173]

A pH sensitive polymer MR contrast agent was also reported by Mikawa and co-workers,[174] composed of Gd^{3+}-DTPA conjugated to a polycation, poly[2-(diethylamino)ethyl methacrylate], which exhibited an increase in relaxivity when the pH is decreased from 7.2 to 5. Pathological states present different microenvironments in comparison with normal states, such as lowered pH in a lesion, and therefore, a pH sensitive MR contrast agent would be useful in detecting these physiological states in a noninvasive manner. Lastly, a Eu^{3+}-labeled small polymeric CEST agent has been described in the literature, which makes use of the paramagnetic chemical exchange saturation transfer (CEST) mechanism conferred by the presence of the lanthanide. Though small in size, the authors suggest that the CEST effect will permit detection of the agent even at low concentrations; furthermore, the small size of the polymer will facilitate its clearance via the kidney.[175]

8. Protein-Based MR Agents

8.1. Albumin Covalently Bound to Gd^{3+}-DTPA

Paramagnetically labeled albumin has received significant attention over the past few years, and much has been done toward its development as an intravascular probe. Initial biodistribution experiments involving the monomeric chelate Gd^{3+}-DTPA showed that, after 5 min postinjection, as much as 80% of administered contrast agent had been cleared from intravascular space, an effect directly related to low molecular weight.[176] In a comparison study, the enhancement due to paramagnetically labeled albumin persists for an hour, while that of Gd^{3+}-DTPA completely disappears within that same time frame.[177] As stated earlier, longer blood retention times

are desirable, as they permit both sufficient accumulation of contrast agent in sites of interest and longer acquisition times.

After Lauffer and co-workers reported a protocol for the direct reaction of DTPA-dianhydride with a variety of proteins and subsequent labeling with Gd^{3+},[178] the method was soon applied to human serum albumin and procedures were determined to control the number of paramagnetic chelates, ranging from 9 to 19 chelates per albumin.[179,180] Solution studies showed that albumin-$(Gd^{3+}$-DTPA$)_{19}$ possesses a longitudinal relaxivity r_1 of 14.8 mM^{-1} s^{-1}, a value three times that of the monomeric chelate when measured under the same conditions, a result of the larger molecular weight of the contrast agent and hence its higher rotational correlation time τ_R.[180] However, a study by Paajanen and co-workers in which Gd^{3+}-labeled albumin was compared with the larger molecular weight conjugates Gd^{3+}-labeled IgG and fibrinogen found that not only was a wide range of chelate numbers possible for all proteins studied but also the measured relaxivities for all three were relatively the same.[181] Furthermore, since conjugation of the protein with DTPA via this method requires amide bond formation with one of the acetates of DTPA, Sherry and co-workers raised a caveat early on citing thermodynamic measurements which indicate a compromise of chelate stability.[182]

In addition to long blood retention times, initial biodistribution studies of Gd^{3+}-labeled albumin reported enhancement intensity increases over 100%, as observed in myocardium and liver with albumin-Gd^{3+}-DTPA at concentrations one-third that of Gd^{3+}-DTPA, which produced enhancement increases much less than 100%.[177] These results lead to a series of *in vivo* tests to evaluate the performance of paramagnetically labeled albumin as a contrast agent in tissue exhibiting a high degree of vascularization. In addition to using albumin-Gd^{3+}-DTPA to determine blood plasma volume by MRI techniques,[183] it was also used to measure capillary permeability by monitoring the leakage rate of contrast agent from plasma to interstitial water or tissue plasma under normal conditions[184] or when pharmacologically induced.[185] A similar concept was employed in measuring CO_2-induced changes in cerebral blood volume[186] and monitoring inflammation in arthritis.[187] Disease states characterized by regions of reduced blood pool, such as ischemia of the kidney[188] and myocardium,[189−192] have also been visualized, as well as their reperfusion.

Albumin-Gd^{3+}-DTPA has also been used in contrast-enhanced imaging of cancerous tissue, having a different histological profile from normal tissue and abnormal capillary permeability.[193] Indeed, Daldrup and co-workers performed a series of imaging studies to correlate histologic tumor grade, ranging from benign to highly malignant, with MR enhancement. Their results show that correlation was possible only when albumin-Gd^{3+}-DTPA was used, in comparison with the case of monomeric chelate, which fails to distinguish between tumor grades.[194] Similar techniques were used to determine histologic tumor grade in prostate[195] and breast[196,197] cancer models. Furthermore, albumin-Gd^{3+}-DTPA was also demonstrated to be an effective probe for measuring increases in capillary density, thereby suggesting its use in estimating angiogenic activity.[198] Monitoring changes in tumor capillary permeability under pharmacological stress[199] or irradiation[200] have also been reported, as well as the use of albumin-Gd^{3+}-DTPA as a surrogate imaging tracer for convection-enhanced delivery of tumor-targeted toxins into rat brain.[201]

8.2. MS-325

In spite of its initial success, covalently labeled albumin suffers from several undesirable traits. Elimination of the agent is slow and incomplete, and it has been shown to remain in circulation for more than a week, eventually accumulating in liver and bone. In addition, albumin is also potentially immunogenic, and the combined risk of poor elimination and *in vivo* degradation has confined its use as a model prototype MR contrast agent in animal studies.[202]

MS-325 is a blood pool contrast agent which reversibly binds to albumin in a noncovalent fashion. The monomeric chelate is composed of a C-functionalized Gd^{3+}-DTPA derivative conjugated to a cyclohexyl diphenyl group via a phosphodiester linkage. Its solution properties and structure have been studied extensively,[203] demonstrating superior stability in comparison with Gd^{3+}-DTPA at physiological pH.[204] Binding with human serum albumin is close to 100% with a constant of about 6100 ± 2130 M^{-1},[205] and upon binding with HSA, this agent exhibits a 6- to 10-fold increase in relaxivity due to a large increase in rotational correlation time,[206,207] although the relaxivity enhancement has recently been found to be dependent on the species of albumin used.[208] This phenomenon has since been referred to as receptor-induced magnetization enhancement (RIME). While the hydrophobic group provides its affinity for albumin, the phosphodiester linkage is essential for preventing its accumulation in liver and increasing its plasma half-life to 155 min (versus 36 min for monomeric Gd^{3+}-DTPA).[209] Furthermore, biodistribution studies in cynomologous monkeys have demonstrated its efficient clearance via the renal pathway with up to 90% of an administered dose eliminated after 24 h postinjection and complete elimination by 72 h.[210] However, a study by Corot and co-workers compared the bolus and steady state phases of MS-325 with two other contrast agents, namely, an ultrasmall superparamagnetic iron oxide and P792 (a macromolecular derivative of Gd^{3+}-DOTA). They report that, in the bolus phase, tissue distribution of MS-325 is characteristic of a monomeric chelate, which extravagates into the surrounding tissue and is cleared by the kidney. The high concentrations of contrast agent in the bolus exceed that of available albumin. But after 1 min postinjection, the steady-phase is achieved and 75% of MS-325 exists in the albumin bound form.[211]

MS-325 advanced into clinical studies. After preliminary concentration studies in comparison with monomeric chelates and iron particles,[212] MS-325 was first evaluated as a contrast agent for the imaging of peripheral and carotid vasculature in humans and to establish patient tolerance. The study reported that the long-circulation time of the agent permitted the imaging of different zones of interest. The dose required to produce an enhanced MR image was less than half that required to produce the same quality of image using simple monomeric Gd^{3+}-DTPA. In addition, vessels as small as 1 mm in diameter were visualized.[213] The success of this first study led to its clinical evaluation as a contrast agent in carotid imaging[214] and the diagnosis aortoiliac occlusive disease,[215−217] and it was reported as safe and effective in these applications.

The use of MS-325 has also been evaluated in the detection of proteinuria in rat kidney[218] and in the determination of capillary permeability in rat breast tumor.[219]

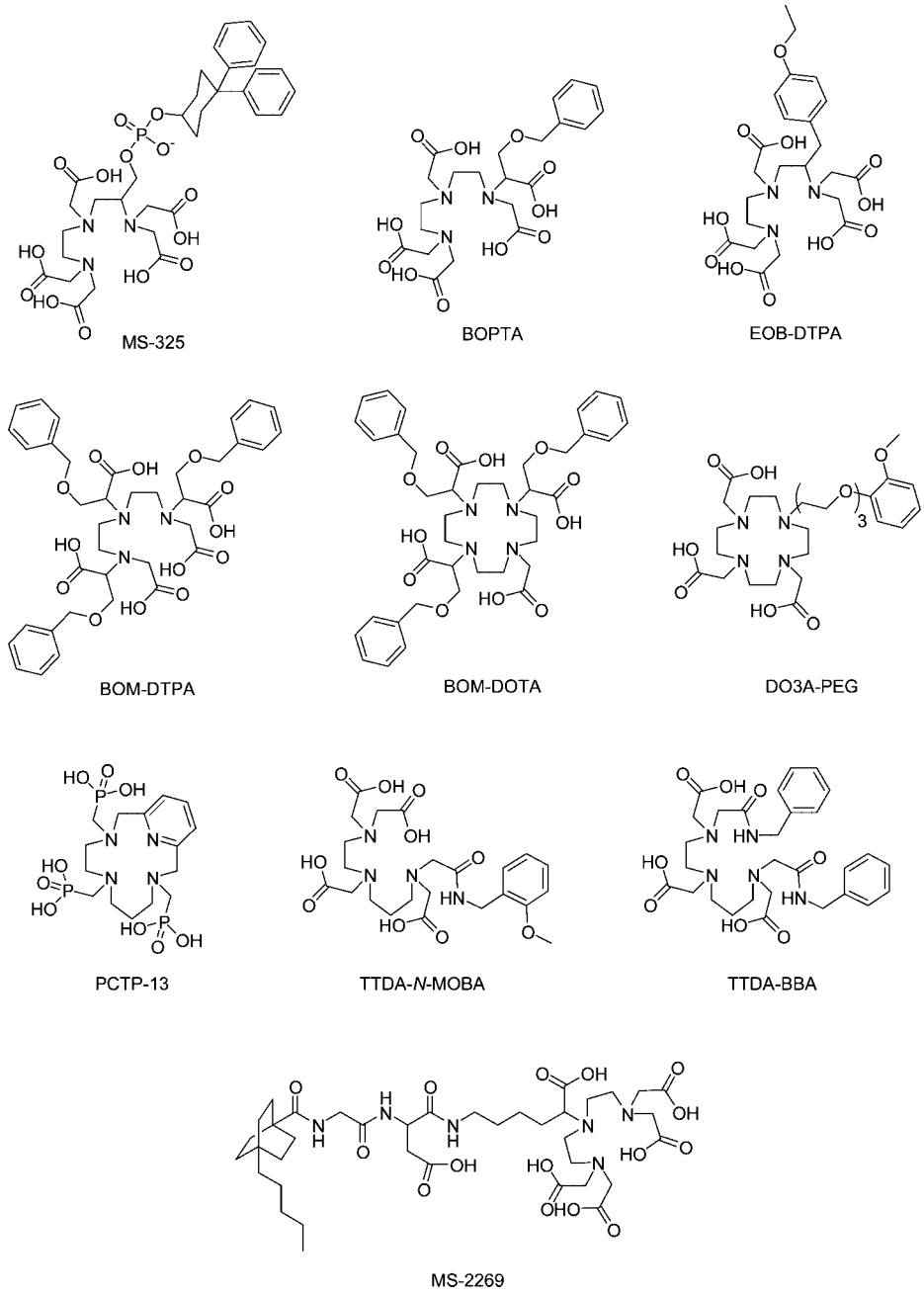

Figure 11. Ligands used for albumin-affinity MR agents.

8.3. Other Albumin-Affinity Agents

The success of MS-325 has prompted further investigation into developing other lipophilic RIME Gd^{3+} chelates (Figure 11). These include the use of the acyclic ligand 4-carboxy-5,8,11-tris(carboxymethyl)-1-phenyl-2-oxa-5,8,11-triazatridecan-13-oic acid (BOPTA)[220−222] and the macrocyclic and acyclic analogues of benzyloxymethyl substituted DOTA/DTPA (DOTA/DTPA-BOM).[223,224] The stability constants of Gd^{3+}-chelates based on these ligands show that the presence of the aromatic group does little to affect the stability of the chelate. Furthermore, increasing the number of these substituents also increases the affinity to human serum albumin, with the cyclic Gd^{3+}-BOM chelate of three substituents exhibiting a relaxivity of 53.2 ± 0.7 mM^{-1} s^{-1}. However, the theoretical maximum of enhancement is not achieved due to a reduction in the exchange rate of the coordinated water molecule upon adduct formation with HSA. Another Gd^{3+} chelate employing the macrocyclic ligand 3,6,10,16-tetraazabicyclo[10.3.1]hexadecane-3,6,10-tris(methanephosphonic) acid (PCTP-[13]) has an aromatic group as part of the carbon backbone of the ligand, providing the chelate with sufficient lipophilic character for HSA binding.[225] Furthermore, enhancement is due not only to adduct formation but also to the formation of a secondary hydration sphere around the chelate, caused by the methylene phosphonate arms of the ligand, resulting in outer-sphere relaxation effects. In other examples, PEG was introduced as a spacer between the chelate and the aromatic group, in order to increase the solubility of the complexes and exploit the beneficial effects of a large molecular weight. Though these demonstrated strong binding with HSA, the expected enhancement was not achieved,[226] perhaps due to the flexibility of the PEG linker and the displacement of water coordinated to the paramagnetic center upon protein adduct formation. The synthesis of a Gd^{3+}-chelate based on a DTPA derivative with no aromatic substituents, 4-pentylbicyclo[2.2.2]octane-1-carboxyldiaspartyllysine-derived-DTPA (MP-2269), has

also been described.[227] Preliminary animal studies have demonstrated its use in the visualization of vasculature and a 70% clearance after 24 h via the hepatobiliary pathway. In contrast with the PEGylated complexes described earlier, ^{17}O NMR studies of this chelate show that neither the presence of the hydrophobic chain nor adduct formation with albumin significantly affect the water exchange rate between bound and bulk solvent molecules.[228] Acyclic ligands based on 3,6,10-tri(carboxymethyl)-3,6,10-triazadodecanedioic acid (TTDA) and its derivatives have also been described in which the aromatic groups are covalently linked via amide bonds.[229] In addition to possessing affinity to HSA, Gd^{3+} chelates based on these ligands also exhibit decreased water exchange rates, a function of reduced steric crowding around the coordination site, and a reduced charge effect, since the chelates are neutral. The Gd^{3+} complex of (4*S*)-4-(4-ethoxybenzyl)-3,6,9-tris(carboxylatomethyl)-3,6,9-triazaundecandioic acid (EOB), constituted of a DTPA derivative covalently linked with a lipophilic ethoxybenzyl moiety, was initially developed as a contrast agent for hepatobiliary imaging.[230−232] However, comprehensive MR studies have shown it also possesses affinity for serum proteins,[232] with the *S* isomer possessing a higher affinity for HSA than the *R* isomer.[233] Also, multimetallic complexes with affinity for albumin have been reported[234,235] which deliver a higher payload of paramagnetic ions per protein molecule, thereby reducing the minimal dose required for the observation of significant enhancement. Finally, enzyme-activatable pro-RIME agents have also been described in the literature. Nivorozhkin and co-workers report the use of a DTPA derivative functionalized with aromatic moieties for HSA binding, but which are masked by lysine residues which inhibit protein binding.[236] Upon exposure to the enzyme thrombin-activatable fibrinolysis inhibitor (TAFI), the lysine residues are cleaved, resulting in a 100% increase in relaxivity at 37 °C in the presence of HSA. The authors propose this as a strategy to detect disease states associated with certain protease activities. More recently, Hanaoka and co-workers reported a similar Gd^{3+}-DTPA-based reporter agent employing galactopyranose as a masking group.[237] Exposure to β-galactosidase, commonly used to monitor gene expression, cleaves the masking group, resulting in a 57% increase in relaxivity in the presence of HSA.

8.4. Other Protein-Binding Agents

Indeed there are many examples in the literature of Gd^{3+}-based MR contrast agents which form adducts with proteins and which have been shown to visualize specific tissues of interest or dynamic physiological phenomena. Anelli and co-workers described the synthesis of a Gd^{3+}-DTPA derivative covalently linked to sulfonamide and possessing a strong affinity for carbonic anhydrase (K_A of 15,000 ± 5,000 M^{-1}); the resulting adduct was measured to have a relaxivity of 25.8 mM^{-1} s^{-1}.[238] Since carbonic anhydrase is ubiquitously expressed in various tissues, the authors proposed use of this agent to visualize compartments outside the blood pool. Similarly, Tomaselli and co-workers described a Gd^{3+}-DTPA derivative covalently linked to cholanoic acid, and its adduct with liver bile acid binding protein characterized by multidimensional NMR techniques.[239] Work by De Leon-Rodriguez and co-workers described a Gd^{3+}-DOTA derivative conjugated with a 20 amino acid peptide sequence that binds to the yeast transcription repressor protein Gal80 with high affinity ($K_A = 5 \times 10^5$ M^{-1}) and specificity, resulting in a 10-fold increase in image enhancement.[240] Other peptide-functionalized Gd^{3+} contrast agents, EP-1873 (a DTPA derivative)[241] and EP-2104R (a DOTA derivative),[242] were designed to bind strongly to fibrin, a protein abundant in arterial thrombi and associated with a variety of pulmonary disease states. EP-1873 has been shown to visualize thrombus formation in rabbits, and EP-2104R to possess affinity over a wide range of fibrins and excellent specificity over fibrinogen and serum albumin. An area with much potential in its own right, the synthesis and application of DOTA-peptide conjugates have recently been reviewed elsewhere.[243]

Larger constructs involve labeling of proteins with paramagnetic reporters. Aime and co-workers described the encapsulation of about 10 neutral Gd^{3+} complexes within an apoferritin cavity. As with similarly constructed ensomes, the assembly was measured to have a much higher relaxivity in comparison with the free monomeric chelate; in this particular example, the value increased as much as 20-fold.[244] Molecular biological techniques have also been used to rationally design a multivalent protein containing evenly spaced lysine residues along the protein backbone and capable of conjugating an average of 8 to 9 Gd^{3+}-chelates.[245] Similar techniques were employed in the creation of a series of proteins designed with Gd^{3+} binding sites using amino acid residues and water molecules as coordinating ligands and which exhibit a 20-fold increase in relaxivity in comparison with small-molecule contrast agents.[246]

More sophisticated strategies take advantage of known strong protein−protein interactions to visualize physiological phenomena. For example, Gustafsson and co-workers describe the conjugation of bovine serum albumin modified with maleic acid (mal-BSA) with as many as 22 Gd^{3+}-DOTA chelates via a thioether linkage, which forms an adduct with a scavenger receptor class A (SR-A) protein, present in high numbers on macrophages and therefore a convenient diagnostic marker for vascular lesion formation.[247] Langereis,[248] Dirksen[249] and co-workers have developed a target-specific multivalent contrast agent based on the strong interaction between biotin and avidin. The authors conjugated a cyclic NGR peptide sequence, a specific ligand for aminopeptidase CD 13 overexpressed by angiogenic endothelial cells, with Gd^{3+}-DTPA and biotin, which then forms an adduct with avidin in a 4:1 fashion. Again, adduct formation was accompanied by a dramatic increase in relaxivity. In a similar fashion, Jung,[250] Neves,[251] and co-workers employed this strategy in the biotinylation of the C2A domain of the protein synaptotagmin I, known to bind to phosphatidyl serine expressed on the surface of apoptotic cells, followed by an administration of Gd^{3+}-labeled avidin. This supramolecular aggregate has since been used to successfully visualize by MR the dynamic apoptotic response of tumors in mice when treated with etoposide.[252]

8.5. Antibody-Based Agents

Efforts in producing antibody-based MR agents have been met with only modest success. Employing facile antibody-labeling methods first described by Hnatowich toward the development of radiolabeled probes,[253] Paik and co-workers reported a study which investigated the factors influencing DTPA conjugation of monoclonal antibodies with DTPA-dianhydride. Labeling experiments with $^{111}In^{3+}$ demonstrated that increasing the number of metal ions on the antibody results in a loss of immunoreactivity.[254] However, bovine IgG labeled with an average of four Gd^{3+} ions was measured

to have a longitudinal relaxivity r_1 of 26 mM^{-1} s^{-1}, roughly six times that of monomeric Gd^{3+}-DTPA.[178] Unfortunately, imaging of animals injected with Gd^{3+}-labeled monoclonal antibodies resulted in virtually none or only modest enhancement of tumor sites.[255,256] Indeed, this result suggests that the potential of labeled monoclonal antibodies in tumor imaging lies in γ-camera and PET imaging, rather than in MRI, which has relatively low sensitivity. Local tissue concentrations greater than 5×10^{-7} M Gd^{3+} would have to be achieved for significant enhancement to occur,[256] implying the needfor the use of either higher field strengths in MR imaging or higher Gd^{3+} loading of antibodies without compromising immunoreactivity. In contrast, melanoma[257] and human rectal carcinoma[258] were successfully visualized with antibodies directly labeled with Gd^{3+}-DTPA, suggesting that the detrimental effects of direct conjugation of DTPA onto an antibody apply on a case-to-case basis.

Interestingly, Curtet and co-workers reported the labeling of monoclonal antibody 19-9, specific for human gastrointestinal cancer, with as many as 16−25 Gd^{3+} ions with only a slight loss of immunoreactivity,[259,260] confirming that different antibodies react differently when conjugated with DTPA. Though this agent demonstrated good visualization of tumor, it unfortunately suffered from poor clearance characteristics and was shown to accumulate in liver at high levels even at five days postinjection.

Even higher numbers of Gd^{3+}-loading were achieved with the synthesis of Gd^{3+}-labeled poly-L-lysine-antibody conjugates. Work by Shreve described a conjugate of this type incorporating as many as 30 Gd^{3+} chelates. Unfortunately, not only did this construct present only a modest improvement in relaxivity (5.6 mM^{-1} s^{-1}), indicating a high degree of rotational movement in the polymer, it was found to have an immunoreactivity reduced by as much as 70%.[261] Manabe and co-workers achieved a poly-L-lysine-IgG_1 conjugate containing up to 42.5 mol of DTPA per mol of antibody, with only a 10% loss of immunoreactivity.[262] Göhr-Rosenthal and co-workers reported even higher numbers of Gd^{3+} in a poly-L-lysine-mAb (RA96) conjugate incorporating an average of 65 Gd^{3+} chelates, exhibiting a relaxivity of 15.86 mM^{-1} s^{-1}, but with a 30% loss of immunoreactivity. Though MR enhancement of tumor was achieved, this bioconjugate also suffered from poor clearance characteristics and was found to accumulate not only in tumor but also in the liver, spleen, kidney, and bone.[263] To further circumvent the undesirable effects produced by direct labeling of antibodies, Artemov and co-workers reported the use of a pretargeting strategy involving the primary administration of biotinylated anti-HER-2/*neu* antibody followed by the administration of Gd^{3+}-labeled avidin.[264] *In vivo* studies in mice demonstrated selective enhancement of breast cancer tumors for those samples pretreated with biotinylated antibody, and a complete clearance of contrast after 48 h. Furthermore, the relatively small size of these modular components permitted extravasation into the interstitia of the tumors, as confirmed by an analogous fluorescence-based experiment.

9. Carbohydrate-Based MR Contrast Agents

The potential of dextran as a platform for MR contrast agents was suggested by its use as plasma volume expander for over 50 years, an indication of its low toxicity. Similar to PEG, conjugation of antibodies with low molecular weight dextran has been shown to reduce the protein's natural immunogenicity in addition to prolonging blood circulation.[265,266] Indeed, many dextran-based therapeutics exist in the literature and have been reviewed elsewhere.[267] Furthermore, the metabolic function of sugars and their roles in cell-signaling have also suggested their use as targeted drug delivery agents.

9.1. Dextran, Starch, and Inulin

9.1.1. Synthesis and Solution Properties

Initial attempts to conjugate dextran with DTPA involved reaction of DTPA dianhydride with hydroxyl groups along the sugar polymer backbone to form ester linkages. However, a study by Gibby and co-workers in which a series of dextrans of increasing molecular weights ranging from 17 kDa to 150 kDa were evaluated found this method resulted in cross-linking producing polydisperse products.[268] Similar chemistry could be applied to carboxymethyl dextran, inulin, and hydropropyl starch.[269,270] The ester bond was found to be relatively robust against hydrolysis, possessing a half-life of 21 h (37 °C, pH 7.4),[269] although concerns were raised as to the stability of the resulting Gd^{3+} chelates, since in the cross-linked polymer, carboxylates of the DTPA moiety were used for ester bond formation. To circumvent this, strategies were employed which involved conjugating the carbohydrate backbone with DTPA through a diamine linker which serves as a "tether" for amide, thioester, or thiourea bond formation[270−273] and serves to reduce the degree of cross-linking (Figure 12). The relaxivities of the resulting Gd^{3+}-DTPA-labeled dextrans were invariably found to be more than twice that of the monomeric chelate, though it was also found that differences in the length of the "tether" or increasing the molecular weight of the dextran had no bearing on the relaxivity of the conjugate.[274−276] It was suggested that any theoretical increase in relaxivity as a result of an increase in molecular weight is offset by the rapid internal motion of the glucose units of the polymer.[274] On the other hand, Gd^{3+}-DO3A-labeled hydroxyethyl starch and inulin were found to have relaxivities greater than four and five times that of monomeric Gd^{3+}-DTPA, respectively.[277−279]

9.1.2. Biodistribution

In a study by Gibby and co-workers involving cross-linked Gd^{3+}-labeled dextrans of different molecular weights, bioconjugates larger than 100 kDa were found to exhibit enhancement of the intravascular space and kidney and only moderate enhancement of the liver in rats. Furthermore, the polymer was found to accumulate in the bladder within 70 min, where it was metabolized and excreted completely with urine within 24 h.[280] A 75 kDa Gd^{3+}-DTPA-dextran conjugate bearing 15 Gd^{3+} atoms was then tested as an intravascular MR contrast agent in rats, and the agent was similarly found to enhance imaging of vasculature in rats for a period of 1 h postinjection.[281] However, when tested for imaging acute myocardial infarction in pigs, the same agent failed to visualize the areas of infarction *in vivo*; discrimination between healthy and diseased tissue was possible only in *ex vivo* MR exams.[282] More recently, a 165 kDa dextran conjugate labeled with as many as 187 Gd^{3+}-DTPA chelates was synthesized and evaluated as a blood pool agent and used for tumor delineation in rabbits.[283]

Gd^{3+}-labeled carboxymethyl dextran (CMD) has also been tested *in vivo*. A 40 kDa CMD was found to enhance vasculature in a stable and prolonged manner in rabbit

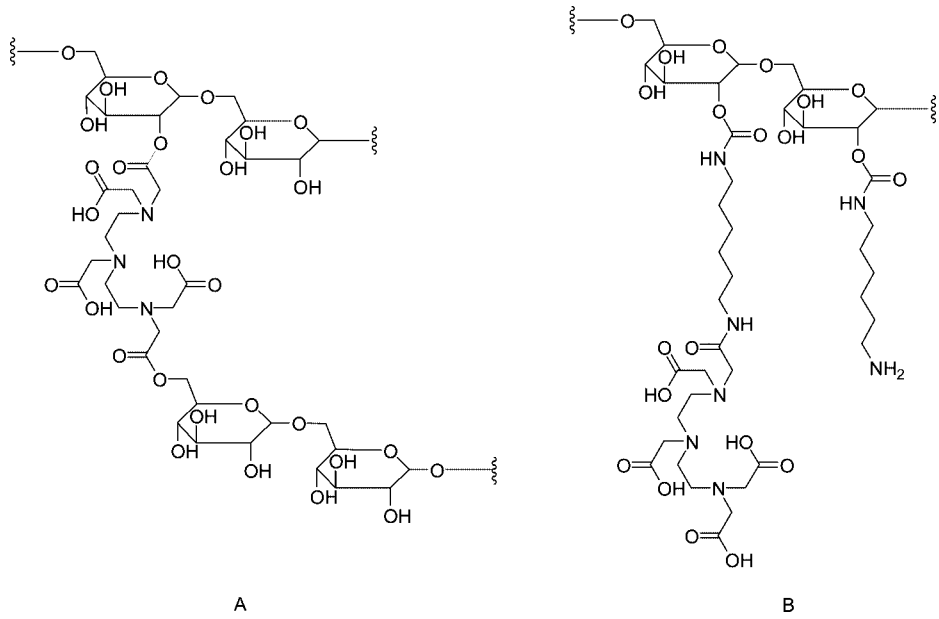

Figure 12. (A) Cross-linked and (B) amide-linked DTPA-dextran.

models, including the distal part of the aorta and renal arteries.[274,284] Similarly, a 52 kDa CMD-Gd^{3+}-DOTA conjugate was demonstrated to be an effective agent for visualizing myocardial perfusion, the aortic arch, and abdominal vasculature of pigs.[285,286] Gd^{3+}-labeled carboxymethyl hydroxyethyl starch, bearing 35 Gd^{3+}-DO3A units (72 kDa) was also employed as an MRA contrast agent in rats, capable of visualizing the leaky vasculature of tumors.[277]

Furthermore, Gd^{3+}-labeled dextran has found a unique function in embryology, as a contrast agent for MR microscopy. Indeed, a developing frog embryo was injected with Gd^{3+}-dextran at the 16-cell stage, and cell movements during the gastrulation and neurulation stages were visualized over a period of several days.[287] This idea was extended by colabeling dextran with both Gd^{3+}-DTPA and rhodamine, and cell movements were correlated by both MR and fluorescence microscopy.[288] This same multimodal imaging agent was also used to successfully track the movements and distribution of neural stem cell transplants in rats.[289]

9.2. Other Carbohydrate-Based Agents

Other carbohydrate-based agents have been reported which make use of the inherent chemical and biochemical properties of glycoconjugates in general, employing novel and clever synthetic strategies, which may prove useful in an MRI setting. Convergent synthetic strategies have been employed to produce dendritic MR contrast agents by conjugating branched carbohydrate branches onto a paramagnetic core. For example, Takahashi and co-workers produced branched amino glycoside wedges of four and twelve glucose moieties which were reacted with DTPA dianhydride to form a glycodendrimer.[290] Similarly, Fulton and co-workers reported C-4 symmetric glycoconjugates in which four branched carbohydrate wedges, with twelve terminal glucose or galactose resides, were grafted onto a DOTA core (Figure 13).[291] As in the case with similarly constructed paramagnetic arborols,[101] the resulting Gd^{3+}-chelate exhibited a high relaxivity which was a result not only of the secondary hydration sphere effect, but also of enhanced motional coupling due to the Gd^{3+} ion residing at the barycenter of the macromolecular structure.

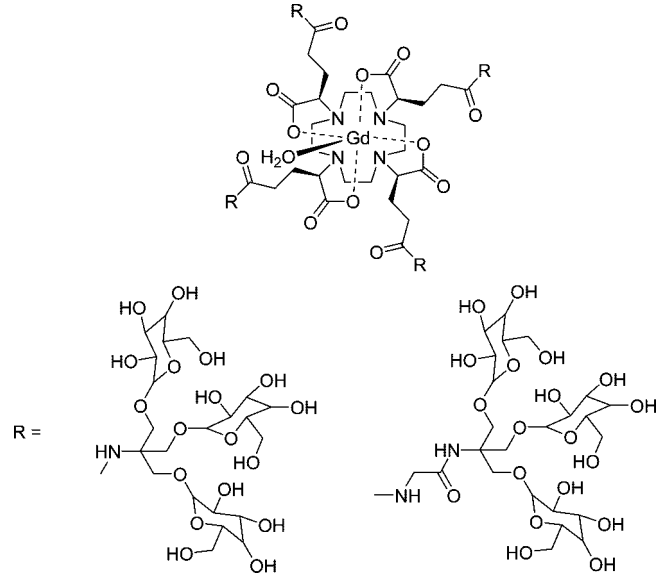

Figure 13. Glycodendrimers.

Gd^{3+}-labeled oligosaccharides have also been reported which show some promise in MRI applications. NMS60 is an agent composed of chitotriitol conjugated to three Gd^{3+}-DTPA moieties. The synthesis and characterization and NMS60 and analogues have been described in detail.[292] Though small by macromolecular standards (2.1 kDa), NMS60 is still large enough to avoid fast diffusion from vascular to interstitial space and be useful as a blood pool agent; it has been used to visualize arterial vasculature in a canine model[293] and to delineate tumors implanted in rabbits[294] even an hour postinjection.

Finally, targeted carbohydrate-based MR contrast agents have been synthesized and characterized. These take advantage of the strong carbohydrate−protein interactions which occur *in vivo* and serve as markers for either particular tissues or specific physiological phenomena. For example, a bioconjugate composed of a polylysine backbone cofunctionalized with Gd^{3+}-DTPA and galactose residues has been demonstrated as a multivalent probe with strong affinity for the lectin asialoglycoprotein receptor (ASGPR) expressed

specifically on liver hepatocytes.[295] In tests with rats implanted with liver-implanted mammary adenocarcinoma, tumor regions were distinguished from healthy tissue. Similar multivalent glycoconjugates specific for ASPGR were synthesized, and the structures of the resulting lanthanide chelates, based on either macrocyclic DOTA[296] or acyclic DTPA[297] ligands, were described in detail. Furthermore, the macrocyclic analogue has been shown to accumulate in rat liver implanted with human hepatocyte carcinoma cell line Hep G2, and that ASPGR is highly selective for the galactosyl analogue over the glycosyl analogue.[298]

10. Liposomes and Micelles in MR Imaging

10.1. Supramolecular Assembly and Solution Properties

Liposomes have long been used in drug delivery applications, and the idea of using these structures to deliver MR contrast media was not long in coming. The ease of preparation, the use of simple reagents, and the ability to control the size of these supramolecular assemblies and their membrane permeabilities all contributed in producing a vast wealth of literature, which not only explores the intrinsic properties of these systems but also introduces novel functions such as sensitivity to the pH, the temperature, and the design of the targeted agents. Over the last 20 years, several reviews have been published which provide an account of the development of liposomes in MR imaging.[299−304] In-depth calculations performed very early on provide a theoretical understanding of their behavior, both verifying established experiments and prompting the investigation of improved systems.[305,306] To date, the examples which exist in the literature can roughly be classified into the following groups: ensomes, memsomes, micelles, and, more recently, lipoCEST agents (Figure 14).

10.1.1. Ensomes

Initial attempts at producing liposome-based MR contrast agents involved the encapsulation of water-soluble paramagnetic species within the aqueous interior of the liposome; the resulting systems were hence referred to as "ensomes". Encapsulated species included $MnCl_2$[307] or Mn^{2+} complexed with either DTPA[308] or albumin,[309] and small-molecule Gd^{3+} complexes.[310−312] Although these agents shortened the T_1 relaxation times of bulk water solvent, it was observed that the relaxivities of these liposomes were greatly reduced in comparison with that of free metal chelate; encapsulation of these agents within the interior of the liposome effectively "shields" bulk solvent water molecules from the inner-sphere coordination with the metal centers. Liposome size, membrane composition, and water-membrane permeability all influence the relaxivity of an ensome, as these affect the rate of water exchange across the lipid membrane, the mechanisms of which were described in detail by Pütz and coworkers.[306] Indeed, relaxivity was found to be linearly dependent on the surface-area-to-volume ratio of a vesicle; the smaller the ensome, the higher the relaxivity.[310] Other systems have been found to respond to pH, although the mechanisms of these have not been described in detail.[311−313] Also, increasing temperature also increased the permeability of the liposome membrane, resulting in an increase in relaxivity.[314]

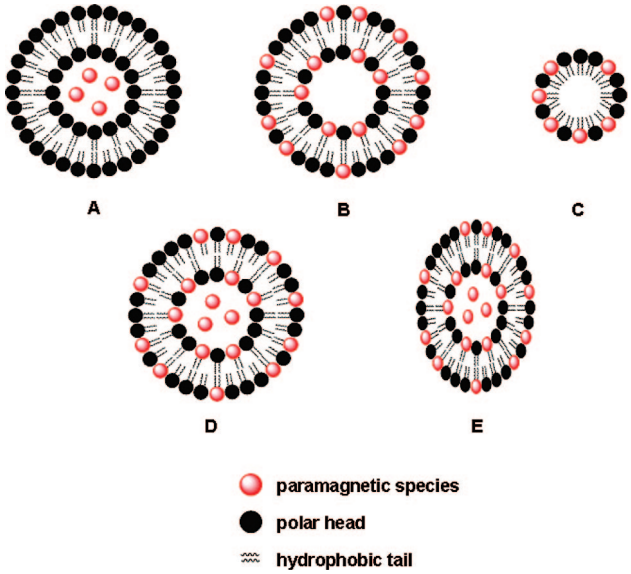

Figure 14. Schematic representations of (A) ensome, (B) memsome, (C) micelle, (D) combined ensome−memsome, and (E) shrunken lipoCEST agent.

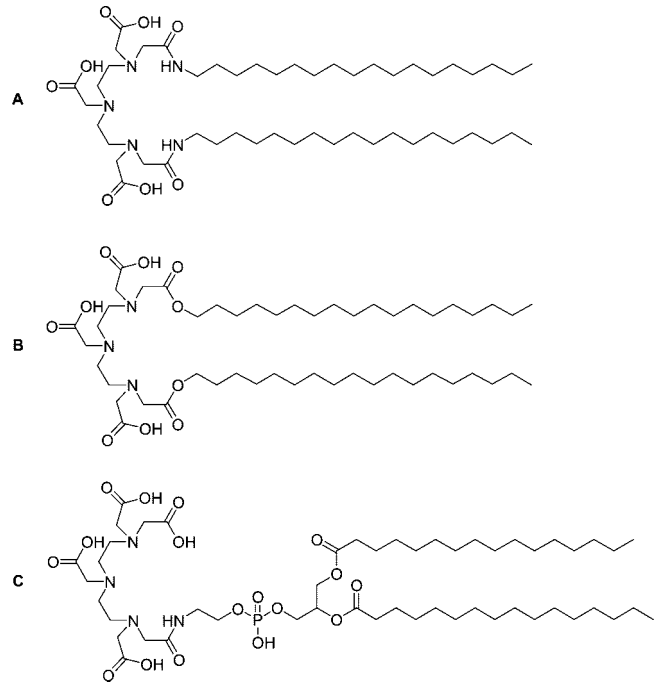

Figure 15. DTPA-derivatives (A) stearylamide, (B) stearylester, and (C) phosphatidylethanolamine.

10.1.2. Memsomes

The limitation of water exchange across the lipid membrane is circumvented by incorporating the metal chelate into the membrane itself by conjugating the metal-binding site to the hydrophilic heads of the membrane molecules (Figure 15), thereby providing solvent water molecules direct access to the inner-sphere coordination with the metal centers; these systems, in turn, are referred to as "memsomes". The first examples include Gd^{3+}-DTPA derivatives which contain hydrophobic alkyl chains linked by either an amide or an ester bond.[315−318] Incorporation of metal chelates into a large supramolecular assembly increases its effective molecular size and hence its rotational correlation time in solution (i.e., large τ_R). Indeed, when Gd^{3+}-DTPA-stearylamide and Gd^{3+}-DTPA-stearylester were incorporated into the lipid membrane

of a liposome, the resulting memsomes were found to exhibit relaxivities two to five times that of free chelate in solution (depending on the field strength) and as much as six to seven times that of memsomes encapsulating similar chelates. However, increasing the size of the vesicles did not result in an increase in relaxivity, since any further gain due to increased molecular size is offset by the rate of diffusion of the paramagnetic chelate across the membrane. That is, if the attachment of the paramagnetic chelate to the membrane is not rigid, variation in the size of the vesicle has no bearing on the relaxivity of the memsome.[318] To this end, Storrs and co-workers reported the synthesis of paramagnetic polymerized liposomes (PPLs), in which the alkyl chains of the liposome are photochemically cross-linked. Though the relaxivity of this system was measured to be three times that of Gd^{3+}-DTPA (under the same field strength), it was found to depend not so much on particle size but on the length of the linker used.[319] Gløgård and co-workers also described a memsome in which the Gd^{3+} chelate was conjugated to the liposome via a disulfide bond susceptible to radical-induced cleavage. In the presence of dithiothreitol, the chelates were cleaved from the liposome, reducing the measured relaxivity by half.[320] The aggregation behavior of amphiphilic Gd^{3+}-chelates has also been shown to be pH dependent. Vaccaro and co-workers reported the synthesis of a Gd^{3+}-DTPA derivative incorporating two C18 alkyl chains which self-assembles into micelles at neutral pH but which redistributes into liposomes as the pH is decreased,[321] suggesting a design for pH-responsive MR contrast agents which switch between aggregation states. However, since the acetate arms of DTPA are conjugated to the long-chain alkyl groups, this structural change will have a direct impact on the stability of the resulting Gd^{3+} chelates and may result in toxicity issues due to possible decomplexation *in vivo*.

10.1.3. Micelles

Amphiphilic Gd^{3+}-chelates have also been shown to self-assemble into micelles of low critical micelle concentration (CMC). In a study involving a series of amphiphilic Gd^{3+}-chelates of increasing alkyl chain length, only those chelates with 10 carbons or more exhibited micelle formation, as evidenced by the measured relaxivities dependent on the CMC.[322] ^{17}O NMR measurements of micelles constituted of a Gd^{3+}-DOTA derivative linked to a C12 alkyl chain demonstrate that since the Gd^{3+}-chelates face outward toward the solvent, the exchange rate k_{ex} of water between the bulk solvent and the inner-coordination sphere of the chelate is conserved, i.e. identical to that of the free chelate. That is, similar to the case of memsomes, the relaxivity of micelles is not limited by access of solvent to the paramagnetic center, the chief limitation of ensomes. In addition, the supramolecular assembly as a whole exhibits a high rotational correlation time τ_R, which results in a relaxivity comparable to that of lower generation dendrimers or Gd^{3+} chelates with noncovalent protein binding.[323] Furthermore, incorporation of cholesterol into the hydrophobic interior of the micelle resulted in a more rigid structure and a 10% increase in relaxivity. To circumvent the limitation of rapid diffusion of metal chelate across the micellar surface, improvements would have to come in the form of using chelates with better properties. For example, Hovland and co-workers found that micelles formed from an amphiphilic Gd^{3+}-chelate based on a derivative of 3,6,9,15-tetraazabicyclo[9.3.1]pentadeca-1(15),11,13-triene-3,6,9-triacetate (PCTA-[12]) had improved relaxivities due to a faster water exchange rate k_{ex} relative to analogous chelates such as Gd^{3+}-DO3A.[324] Micellar structures whose relaxivities and aggregation states are responsive to pH have also been reported,[325] as well as micelles based on Gd^{3+}-chelates conjugated to biodegradable polymers proposed as potential platforms for drug-delivery systems.[326]

10.1.4. LipoCEST Agents

More recently, an innovative approach to liposome-based MR imaging takes advantage of the chemical exchange saturation transfer (CEST) effect. Saturation transfer occurs when protons of the contrast agent undergoing exchange with the bulk solvent are selectively irradiated at their absorption frequency, resulting in a decrease in intensity of the bulk signal. The effect was first demonstrated by Balaban and co-workers and applied to naturally occurring metabolites.[327] The idea was soon extended to ensomes incorporating non-Gd^{3+} lanthanide chelates. The first example of a lipoCEST agent was reported by Aime and co-workers, in which a Tm^{3+} complex was encapsulated within a liposome. Two different water resonances were observed: an intense signal corresponding to the bulk solvent and a less intense peak shifted downfield by 3.1 ppm, corresponding to intraliposomal water in slow exchange with the bulk through the lipid membrane. Irradiation at this frequency resulted in saturation transfer detectable at liposomal concentrations as low as 90 pM.[328] Zhao and co-workers demonstrated that the lipoCEST effect is also dependent on the size of the liposome and that increased lipoCEST contrast is observed in smaller ensomes due to their larger surface-to-volume ratio and faster exchange of water across the lipid membrane.[329]

Even more interestingly, an ensome containing Gd^{3+}-HPDO3A was osmotically shrunk by increasing the ionic strength of the extra-liposomal solvent, resulting in the contraction of the liposomes from spheres to oblate vesicles. The shrinking of the vesicles resulted in an increase in relaxivity relative to the spherically shaped liposome; however, the change in shape was also accompanied by a downfield shift of the intraliposomal water resonance from the bulk by 7 ppm.[330] Indeed, even greater increases in the paramagnetic-induced shift were observed in osmotically shrunken ensomes containing polymetallic Tm^{3+} chelates, as large as 28.2 ppm downfield in an ensome containing a trinuclear Tm^{3+} complex, due to contributions from both dipolar and magnetic susceptibility effects.[331] Similar large shifts were observed in osmotically shrunken liposomes incorporating Tm^{3+} chelates in both the liposomal interior and the lipid membrane (as it were, a combined ensome−memsome system).[332] Mixed-metal systems involving Dy^{3+}- and Tm^{3+}-chelates extended the window of irradiation frequencies from $\delta = \pm 4$ ppm (for spherical lipoCEST agents) to $+30 < \delta < -45$ ppm, with the shift direction determined by the magnetic anisotropy of the membrane-incorporated chelate.[333,334] Taking advantage of the large frequency separation between intraliposomal water resonances for spherical and osmotically shrunken liposomes (3 ppm and 15 ppm downfield from the bulk solvent, respectively, in systems containing Tm^{3+} chelates), multiple CEST visualization of these two agents was demonstrated on bovine muscle tissue with no interference.[335] More recently, Langereis and co-workers described a temperature sensitive lipoCEST agent incorporating both a Tm^{3+} chelate, as a CEST reporter, and NH_4PF_6, as a ^{19}F-NMR probe: below

the melting temperature T_M of the liposome, the CEST effect is observed due to the presence of the paramagnetic chelate. However, above T_M, the contents of the liposome leak out of the vesicle, switching off the CEST effect but switching on the ^{19}F resonance.[336]

10.2. Biodistribution

10.2.1. Passive Distribution

The high aqueous solubility and low molecular weight of early Gd^{3+}-based MR contrast agents results in their rapid clearance. Though sufficient for visualizing renal vasculature, longer circular times are required for contrast agent to accumulate in other organs of interest. Simple ensomes and memsomes incorporating paramagnetic species have invariably been reported to accumulate in the liver and spleen by a passive targeting mechanism.[308,315−317,337−339] Indeed, early on, an ensome encapsulating Gd^{3+}-DTPA was shown to enhance contrast between normal and tumor liver tissue, with the smallest liposomes under study producing the greatest contrast enhancement.[340] Simple ensomes have been tested in hyperthermia protocols to monitor contrast agent and/or drug delivery to liver tissue upon heating beyond the T_M of the liposomal preparation.[341,342] More recently, Gd^{3+}-DTPA-lipid derivatives were found to accumulate in atherosclerotic plaques.[343−345]

The relatively large molecular weight of liposomes also increases their circulation in blood. However, Gd^{3+} chelates have been shown to undergo decomplexation *in vivo* if retained in the body for extended periods,[346] and structural modifications were performed to establish control over clearance rates. Kabalka and co-workers synthesized a series of liposomes composed of Gd^{3+}-DTPA-stearyl derivatives conjugated through a variety of linkages, and they found that the stearylamide derivative was completely retained in the liver for over 11 days, while half of the stearyl ester derivative had cleared in the same time period. In addition, the liver clearance half-life of the stearylthiol derivative was only two days. However, the reverse trend was observed with respect to serum stability.[317] Another derivative, Gd^{3+}-DTPA conjugated to phosphatidylethanolamine, was found to have a liver clearance half-life of 24 h.[337,338] Paramagnetic polymerized liposomes were found to recirculate in the body without immediate clearance by either the kidneys or the liver,[347] and liposomes conjugated with polyethylene glyocol (PEG) exhibited long blood circulation times, permitting longer acquisition times for the visualization of fine vasculature.[348,349] Furthermore, biotinylation of PEG-coated liposomes also permits controlled avidin-mediated blood clearance.[350]

10.2.2. Targeted Delivery and Cell Labeling

The design of liposomes conjugated with targeting vectors extends the utility of these agents for visualizing a greater number of histological types by monitoring known physiological responses. Several "mixed micelles" have been reported in the literature incorporating amphiphilic Gd^{3+}-chelates and a bioactive peptide conjugated to an alkyl chain.[351−353] However, their use *in vivo* has yet to be demonstrated. Larger constructs involve liposomes conjugated with antibodies, which also take advantage of emergent multimodal imaging protocols. Mulder and co-workers described the preparation of PEGylated paramagnetic and fluorescent immunoliposomes to monitor the overexpression of E-selectin in human umbilical endothelial cells (HUVEC) when treated with tumor necrosis factor α (TNFα).[354] Erdogan and co-workers also described the use of a similar system exhibiting specificity for nucleosomes on cancer cell surfaces in *in vivo* murine experiments.[355] These examples illustrate the combined advantage of using targeting moieties of high specificity in tandem with PEG-functionalization, which permits blood circulation times sufficiently long enough for the contrast agent to accumulate in the tissue of interest.

Finally, novel liposomal formulations are designed to deliver paramagnetic and fluorescent reporters directly into cells. Together with the increasing interest in cell-based therapies is the need to develop noninvasive methods for monitoring the fate of transplanted cells and their tissue biodistribution *in vivo*. Though incubation of a paramagnetic and fluorescent PPL with T47D breast cancer cell lines demonstrated cellular uptake of agent,[356] a novel lipid formulation containing 40 mol % *N*′-cholesteryloxycarbonyl-3,7-diazanonane-1,9,-diamine (CDAN), 30 mol % dioleoylphosphatidylethanolamine (DOPE), and 30 mol % Gd^{3+}-DOTA-cholesterol conjugate, coined as "MAGfect", has shown better cell transfection properties for both contrast agent and the delivery of plasmid DNA.[357,358] Also, a cationic liposome conjugated with hyaluronic acid has also been shown to efficiently label cells via a CD44 receptor-mediated uptake mechanism.[359]

11. Viral Particles

Viral capsids are natural biological vectors, but only when control was established over their chemical properties were they considered in depth as potential platforms for paramagnetic reporters (Figure 16). Douglas and co-workers first established a methodology for encapsulating polyoxometallate species within a virion—the cowpea chlorotic mottle virus (CCMV)—by pH modulation.[360] In addition, work by Wang,[361] Raja,[362] and co-workers demonstrated that the covalent labeling of cowpea mosaic virus (CPMV) did not compromise the integrity of the viral particle; both the interior of the virion through cysteine residues and the exterior through lysine residues were conjugated with fluorescent reporter dyes. The same groups also managed to covalently modify the surface of the virion with PEG in order to reduce its immunogenicity.

Based on these encouraging results, Allen and co-workers investigated the uptake of Gd^{3+} ions in CCMV through Ca^{2+} binding sites on the protein components of the virion.[363] They achieved a loading of 140 Gd^{3+} ions per viral particle, and the assembly was measured to have a longitudinal ion relaxivity r_1 of 202 mM^{-1} s^{-1}, a value five times higher than that of MS-325 bound to albumin[206] and ten times that even of Gd^{3+}-labeled higher generation PAMAM dendrimers.[90] However, spectrophotometric measurements showed that the Gd^{3+}-labeled particle had a $K_D = 31$ μM, disqualifying it for biological applications. To avoid the danger of possible "leakage" of free Gd^{3+} *in vivo*, Anderson and co-workers used a stronger chelator and covalently labeled bacteriophage MS2 viral particles with Gd^{3+}-DTPA, achieving a bioconjugate containing 514 Gd^{3+}-DTPA moieties and exhibiting a total relaxivity of 7200 mM^{-1} s^{-1} per particle and an ion relaxivity of 14.0 mM^{-1} s^{-1} (1.5 T).[364] Similarly, Prasuhn and co-workers covalently labeled CPMV particles using "click chemistry"; lysine residues on CPMV were first

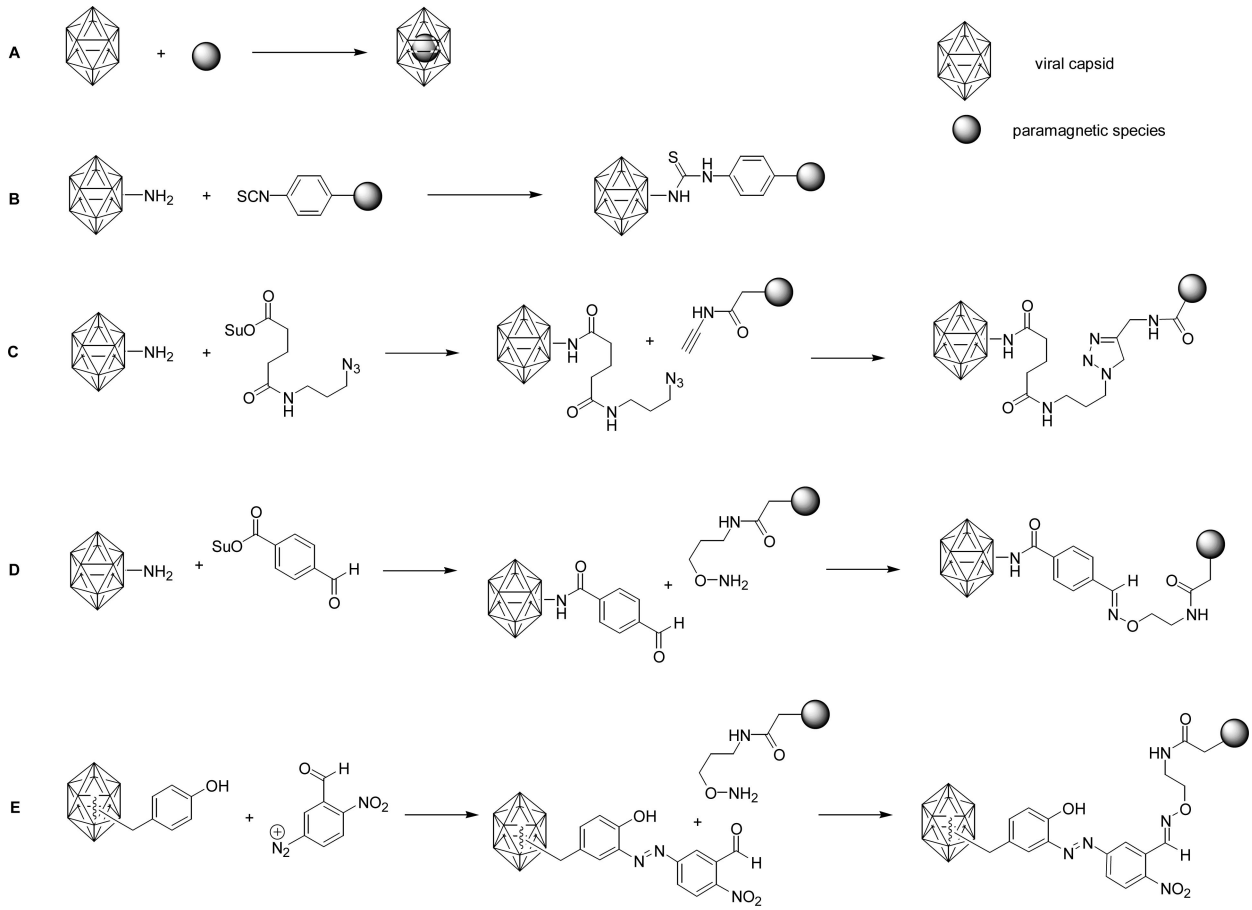

Figure 16. Labeling strategies of viral particles: (A) direct encapsulation; (B) conjugation via external lysines; (C) "click" chemsitry; (D) functionalization of external lysines; (E) functionalization of internal tyrosines.

derivatized with azides, which were then reacted with alkyne-functionalized DOTA. Reaction with Gd^{3+} resulted in 80 ± 20 Gd^{3+} ions per virion.[365] Also, Hooker,[366] Datta,[367] and co-workers labeled the bacteriophage MS2 with bis(HOPO)-TAM, either at the interior of the capsid through tyrosine residues or at the exterior through lysine residues, by functionalization of these residues with an aldehyde, followed by conjugation with the ligand via oxime condensation. The externally modified virion was measured to have an ion relaxivity of 30.7 mM^{-1} s^{-1}, while that of the internally modified virion was 41.6 mM^{-1} s^{-1}, which are among the highest values reported so far for viral-based macromolecular contrast agents. Finally, Vasalatiy and co-workers reported the labeling of adenovirus particles (AdCMVLuc) with Tm^{3+} and $^{177}Lu^{3+}$ chelates of 1,4,7,10-tetraazacyclododecane-1,4,7,10-tetra(methylcarbonylamide) (DTMA), the former a PARACEST agent and the latter a radioactive reporter, while retaining the capability of the virus to infect cells and express luciferase.[368] Though between 630 and 1960 ligands could be loaded onto the adenovirus, a limit of ~800 attached ligands was determined to maintain a 75−80% bioactivity.

12. Gadofullerenes and Gadonanotubes

Efforts to develop fullerenes as a platform for MR contrast agents began after the successful encapsulation of Gd^{3+} into the endohedral fullerene C_{82} was first described.[369] This endohedral metallofullerene was designated as Gd@C_{82}, with "@" indicating the incorporation of Gd^{3+} into the interior of the fullerene. Synthesis of Gd@C_{82} was achieved through a modification of the traditional arc synthesis by using Gd_2O_3-impregnated graphite rods. However, this species was highly insoluble in water, and Mikawa and co-workers attempted to increase its hydrophilicity by hydroxylating the exterior of the fullerene to produce Gd@$C_{82}(OH)_n$, the first example of what are now called Gd-fullerenols and which was also found to have an *in vitro* relaxivity 20 times higher than that of Gd^{3+}-DTPA when measured at 1 T.[370] This high relaxivity is a surprising observation considering that there is no direct interaction between bulk solvent water molecules and the gadolinium ion. However, electron energy loss spectroscopy (EELS) experiments show that this is due to the paramagnetic electronic structure of the metallofullerene itself, a result of a 3-electron transfer from gadolinium to the fullerene cage,[371,372] and hence, the protons of many water molecules H-bonded across the metallofullerene surface undergo relaxation simultaneously.

Soon after, the synthesis of a whole series of lanthanide-based fullerenols incorporating La^{3+}, Ce^{3+}, Dy^{3+}, and Er^{3+} in addition to the previously established Gd-fullerenol was reported.[373] To further improve water-solubility and provide sites for bioconjugation, Shu and co-workers modified the surface of Gd@$C_{82}(OH)_n$ with β-alanine residues, to yield the compound Gd@$C_{82}O_6(OH)_{16}(NHCH_2CH_2COOH)_8$.[374] The synthesis of endohedral trimetallic fullerenes has also been reported,[375] the Gd^{3+} analogue of which has been modified with PEG groups on the surface, Gd_3N@C_{80}-[DiPEG5000$(OH)_n$], to further improve water solubility.[376]

However, higher yields of material were made available for study when Bolskar and co-workers developed a strategy for separating Gd@C_{60}, a major component of the arc

synthesis sublimate, by first extracting out $Gd@C_{82}$ (a minor product) with *o*-dichlorobenzene, followed by successive reductive and oxidative treatment of the remaining endohedral material to separate the majority $Gd@C_{60}$ fraction.[377] Further improvements to this synthetic procedure have recently been reported.[378] The surface of $Gd@C_{60}$ has also been modified with hydroxyl and carboxylic acid groups, yielding $Gd@C_{60}(OH)_n$ and $Gd@C_{60}[C(COOH)_2]_{10}$, and these derivatives were observed to form aggregates as the pH of the solution is decreased from 9 to 7, resulting in large increases in relaxivity,[377,379,380] as the formation of aggregates results in an increase in rotational correlation time, τ_R. Indeed, similar pH-dependent aggregation was also observed with the larger metallofullerene $Gd@C_{82}O_6(OH)_{16}(NHCH_2CH_2COOH)_8$.[381] However, when relaxivity measurements of these metallofullerenes were taken in phosphate-buffered saline (PBS) solution, the presence of salt, in particular phosphate, disrupted the aggregation, leading to a reduction in relaxivity.[382] Variable-temperature and multiple-field ^{17}O and ^{1}H NMR studies have shown that, in the aggregated form, the major contribution to relaxivity enhancement was due to outer-sphere effects caused by water molecules within the interstitial spaces of the aggregates in exchange with the bulk solvent, whereas, in the nonaggregate form, inner-sphere relaxation predominates as a result of proton exchange between the bulk and protonated OH or COOH sites.[383] $Gd@C_{60}[C(COOH)_2]_{10}$ was also found to label mammalian cells with close to 100% efficiency without the use of a transfecting agent, suggesting its use as an *in vivo* probe for tracking mammalian cells.[384] Future perspectives on the use of gadofullerene MRI contrast agents in a clinical setting have been discussed in more detail in a recent review.[385]

Investigations into using carbon nanotubes impregnated with Gd^{3+}, now referred to as gadonanotubes, are still in their infancy, the basic synthesis of which involves the chemical "cutting" of singe-wall carbon nanotubes (SWNTs) into ultrasmall (US) tubes, followed by sonication with aqueous $GdCl_3$.[386] These gadonanotubes were found to have relaxivities nearly 40 times larger than those of current contrast agents measured at field strengths employed in a clinical setting (20−60 MHz).[387] And similar to the case of gadofullerenes, their relaxivity was found to be pH-dependent, exhibiting a dramatic increase when pH is decreased from 7.4 to 7.0, suggesting their use as highly sensitive probes for monitoring small changes in pH under physiological conditions.[388] Indeed, surface chemistry has been performed on these agents, and water-soluble derivatives functionalized with a variety of amino acids and even cyclic RGD peptide have been reported toward the development of these gadonanotubes as targeted bioconjugate MR agents.[389]

At this time, only a few gadofullerenes have been tested *in vivo*. $Gd@C_{82}(OH)_{40}$ was found to selectively accumulate in the reticular-endothelial system (RES) and was retained in liver and spleen 24 h postinjection,[370] but $Gd@C_{60}[C(COOH)_2]_{10}$ showed enhanced renal uptake as opposed to liver, and excretion via the bladder within 1 h postinjection in a mouse.[377] Furthermore, $Gd_3N@C_{80}[DiPEG5000(OH)_n]$ was used to visualize infusions into rat brain.[376] Hence, too few examples exist at present to definitely state how safe these agents are in a clinical setting.

13. Superparamagnetic Iron Oxide

Thus far we have described T_1 positive contrast agents. A discussion of MR nanomaterials would be incomplete without mentioning superparamagnetic iron oxide nanoparticles (SPIOs), a category of T_2 MR agents which provide negative contrast for *in vitro* and *in vivo* cellular and molecular imaging. SPIOs present an important advantage in their huge magnetic moments, which can increase proton relaxivities 10-fold.[390] The typical SPIO agent has a T_2 relaxivity of 100 mM^{-1} s^{-1} and a T_1 relaxivity of 30 mM^{-1} s^{-1}, substantially larger than Gd^{3+}-DTPA's T_2 relaxivity of 6 mM^{-1} s^{-1} and T_1 relaxivity of 4 mM^{-1} s^{-1}.[391]

SPIO agents were recently reviewed in exhaustive depth in this journal,[392] and so their synthesis and applications, such as hyperthermia and drug delivery, will not be repeated here, but rather, we focus on comparing them to T_1 macromolecular agents. SPIO particles are crystalline structures with the general formula of $Fe^{3+}{}_2O_3M^{2+}O$, wherein M^{2+} is a divalent metal ion such as iron, manganese, nickel, cobalt, or magnesium. Because of the ubiquitous presence of iron in living tissue, the ferrous ion Fe^{2+} is the most common divalent ion used in SPIOs to make magnetite (Fe_3O_4 or $Fe^{3+}[Fe^{2+}Fe^{3+}]O_4$). Indeed, magnetite is particularly suitable for manipulation in MR, as it has been isolated from certain birds, fish, and bacteria, in which its interaction with the magnetic field of the earth has been found to play a critical role in navigation.[393] Maghemite (γ-Fe_2O_3 or $Fe^{3+}[Fe^{3+}_{5/3}V_{1/3}]O_4$) forms from the oxidation of magnetite and is similar, but it possesses cation vacancies. Both magnetite and maghemite have practically identical magnetic and relaxation properties. In fact, rarely will a pure magnetite sample be found, particularly in the relevant biomedical applications. Maghemite/magnetite particles have face-centered cubic packing (aka cubic close packed) of oxygen that allows fast electron hopping or continuous exchange of electrons between iron ions occupying interstitial tetrahedral (surrounded by 4 oxygen atoms) and octahedral (surrounded by 8 oxygen atoms) sites (Figure 17A). All tetrahedral holes are filled by Fe^{3+} ions, and octahedral sites are filled by the remaining Fe^{3+} and Fe^{2+} (or vacancies).[394] The magnetic properties of this material arise from the ferrimagnetic alignment of the iron ions. The tetrahedral Fe^{3+} ions are aligned in one direction, and all the octahedral ions are aligned in the opposite direction (Figure 17B). In magnetite, the octahedral and tetrahedral Fe^{3+} ions cancel each other and the magnetic moment is due to uncompensated octahedral Fe^{2+} ions. In maghemite, the moment arises from uncompensated octahedral Fe^{3+} ions. Compared to single

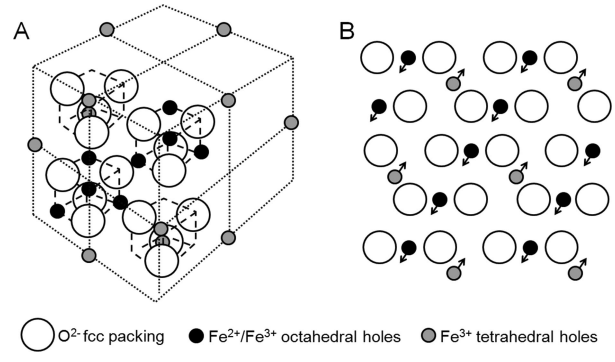

Figure 17. (A) Crystalline structure of magnetite. (B) Ferrimagnetic alignment observed from the [1,1,1] plane.

paramagnetic ions, each vectorized SPIO particle has a huge magnetic moment, one of its advantages for MR applications.

13.1. Understanding Superparamagnetism

The magnetic moment of magnetite/maghemite preferentially aligns on what are known as easy directions or anisotropy axes. For large materials, Weiss domains of uniformly oriented magnetic momenta can be observed between which the alignments are different (Figure 18A).[395] The diameters of SPIO-based particles used for MRI are well within the size of a Weiss domain and are thus single-domain with a unique magnetic moment. Even while under ambient field conditions, superparamagnets are almost fully saturated along the anisotropy axis. However, the magnetic moment of the entire crystal very rapidly jumps from one axis direction to another, time-averaging to a net zero magnetization. These fluctuations in magnetization that have a characteristic Néel relaxation time occur because the thermal energy is sufficient to overcome the magnetic anisotropy energy barrier.[396]

In the absence of an external magnetic field, the effective magnetic anisotropy energy E_α serves as an energy barrier for blocking the flips of magnetic moments and can be approximated by

$$E_\alpha = K_{\text{eff}}V \tag{26}$$

where K_{eff} is the effective magnetic anisotropy energy constant per unit volume and V is the volume of magnetic nanocrystal. As this relation implies, a larger particle radius very rapidly increases the anisotropy energy. Thermal activation overcomes the anisotropy energy barrier when E_α is comparable with the thermal activation energy:[397,398]

$$K_{\text{eff}}V = \beta k_{\text{B}}T_{\text{B}} \tag{27}$$

Here, k_{B} is the Boltzmann constant, T_{B} is the critical blocking temperature, and the constant β, which typically varies between 25 and 34,[398] represents the ratio between anisotropy and thermal energy when the relaxation time of a given particle is similar to the characteristic measuring time of the experiment. At temperatures below T_{B}, thermal fluctuations do not dominate and the magnetic moments "freeze" in random orientations, while above T_{B} a stable bulk magnetization cannot be established and the material demonstrates superparamagnetism.[396]

Thus, in the absence of an applied magnetic field, the direction of crystallite magnetization is free to rotate with thermal motion and randomly orient to average a net zero magnetization. The material behaves similarly to a paramagnet, except that, instead of each individual atom being independently influenced by an external magnetic field, the magnetic moment of the entire crystallite tends to align with the applied field. Furthermore, the resultant magnetic moment after an external field is applied is much greater for a superparamagnet than for a paramagnet.[399,400] When removed from the applied field, the magnetic orientation again randomizes, with no hysteresis from the previous alignment (Figure 18B). This behavior applies up to the Néel and Curie temperatures, and above them, the material exhibits normal paramagnetic behavior.

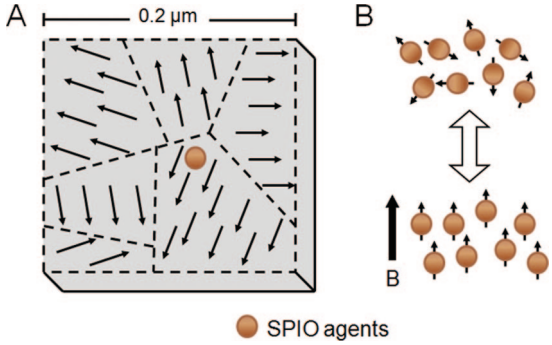

Figure 18. (A) Weiss domains in a large magnetite crystal in comparison to a typical SPIO agent. (B) Magnetic alignment of SPIO particles in the absence and presence of an external magnetic field.

13.2. Superparamagnetic Relaxation

In the previous sections, relaxation by paramagnetic ions, such as Gd^{3+}-based agents, was described, where the primary focus was on the inner-sphere contribution and how macromolecular complexes enhance relaxivity by increasing the rotational correlation time, τ_{R}. A key difference between those agents and superparamagnetic particles is that for the latter the inner-sphere contribution is minor, if not negligible, when compared to the dominant outer-sphere relaxation. SPIO relaxation is also based on the theory described in section 2, with relaxation due to the fluctuating dipole−dipole interaction between the water proton's nuclear magnetic spins and the superparamagnet's global magnetic moment. The key differences that we will discuss, however, relate to the electronic relaxation of the agent itself and its subsequent effect on proton relaxation.

The global *electronic* relaxation of superparamagnetic particles occurs by two mechanisms: (1) internal magnetic dipole Néel relaxation and (2) bulk Brownian relaxation (Figure 20A). The external magnetic field supplies energy to overcome the anisotropic energy barrier and allows internal magnetic moments to rotate away from the anisotropy axis. The energy is then dissipated when the particle moment relaxes to its equilibrium orientation and is known as Néel relaxation. It is characterized by the Arrhenius law:

$$\tau_{\text{N}} = \tau_0 e^{E_\alpha/(k_{\text{B}}T)} \tag{28}$$

where T is the absolute temperature and the pre-exponential factor τ_0 is also an expression of the anisotropy energy.[401] The second type of relaxation is due to bulk rotational Brownian motion within a carrier liquid. With the energy barrier defined by viscous rotational friction in the surrounding liquid, the magnetic particle rotates as a whole because of the torque exerted on the magnetic moment by the external magnetic field. The Brown relaxation time τ_{B} is

$$\tau_{\text{B}} = \frac{3V\eta}{k_{\text{B}}T} \tag{29}$$

where η is the viscosity of the surrounding liquid and V the hydrodynamic volume of the particle.[402] Thus, the global magnetic relaxation rate of the colloid τ_{eff} is

$$\frac{1}{\tau_{\text{eff}}} = \frac{1}{\tau_{\text{N}}} + \frac{1}{\tau_{\text{B}}} \tag{30}$$

For large particles ($r > 7.5$ nm), τ_{B} is shorter than τ_{N} because of their direct versus exponential dependence on volume. Thus, the viscous rotation of the particle becomes the dominant mechanism determining the global relaxation. For smaller particles, the primary process becomes Néel relaxation (Figure 19). These two mechanisms refer to the

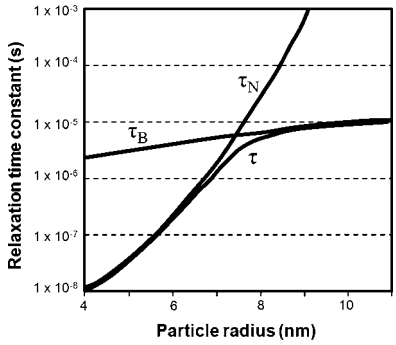

Figure 19. Effects of Neel and Brownian relaxation in relation to magnetite crystal radius (according to Rosensweig[403]).

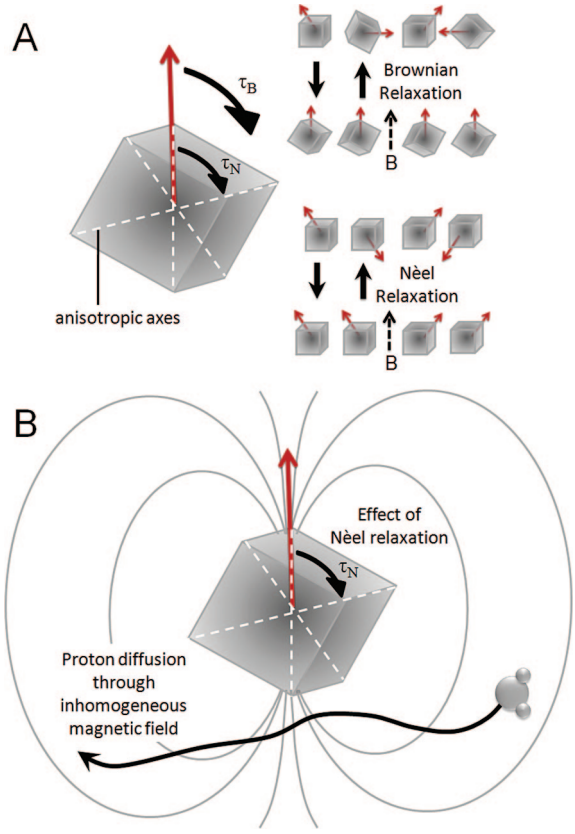

Figure 20. (A) Neel and Brownian components of electronic relaxation, and (B) effects of Neel and Curie spin relaxation on proton nuclear relaxation.

relaxation of the *electronic* moments of the crystal and not the *nuclear* relaxation of water protons.

The superparamagnetic agent's effect on proton *nuclear* relaxation occurs by two mechanisms (Figure 20B). The first is by the electronic moment fluctuations as a result of Néel relaxation. The second results from diffusion into the inhomogeneous *nonfluctuating* magnetic field created by the mean crystal moment. As described by Gueron[404] and Vega and Fiat,[405] the thermal average of an electron spin (the molecular susceptibility or Curie spin) that is aligned along the applied magnetic field B_0 relaxes protons with an effect that increases quadratically with the external field and is proportional to the square of the magnetic moment of the molecule.[406] Curie spin relaxation is primarily a T_2 effect found at high fields and is modulated by reorientation and exchange but not by the fluctuations of the electron magnetic moment.

For large particles in low fields, both water diffusion and Néel relaxation effects are significant, and so superparamagnetic relaxation is generally governed by Freed's equations with $\tau_{S1} = \tau_N$. At high fields, the magnetic moment of large particles is locked onto the external magnetic field direction and Néel relaxation is no longer possible. Thus, τ_N drops out and nuclear relaxation is reduced to Ayant equations, where τ_D is the primary correlation time. At intermediate fields, both the mean and the fluctuating magnetic moments contribute to the induced nuclear relaxation and a combination of Freed and Ayant equations is used to model the relaxation. For further discussion on these equations, please refer to the previously mentioned review article.[392]

For very small particles, crystal anisotropy energy is low and so particle magnetic moment locking on anisotropy axes is reduced. This results in the observation of low field dispersion in the NMRD profile of ultrasmall SPIOs, whereas there is no dispersion for larger SPIOs. Various models that account for anisotropy energy differently have been used to describe this occurrence.[392]

Aggregated particles have very different relaxation properties in terms of both the agglomeration's magnetic field distribution on its surrounding environment and the internal moments of the crystal itself. Transverse relaxivity appears to increase initially to a maximum and then decrease, while longitudinal relaxivity continuously decreases with increasing aggregate size.[407] Furthermore, compartmentalization of the particles within cells[408−410] and the type of cell play key roles in relaxivity.[411] With transverse relaxivity of superparamagnetic particles dropping 2−3-fold when in cells, the effect must be accounted for when analyzing the agents by MRI.

13.3. Current SPIOs

In order to stabilize colloidal ferrofluids, it is necessary to functionalize the iron oxide surface.[392] Particularly in the physiological pH range, uncoated USPIOs do not have a strong enough surface charge to maintain electrostatic repulsion and thus will flocculate in suspension, forming large aggregates.[412] Surface functionalization can provide a strong negative ζ potential, allowing the particles to both remain in stable colloidal suspension as well as mimic the surface charge of typical biomolecules. Monomeric stabilizers such as carboxylates, phosphates, and sulfates can be used to form electrostatic layers.[392] Thicker layers of material also provide steric hindrance to prevent particle−particle interaction. Silica[392,412−414] and gold[392,415,416] are the two inorganic materials that have been used to coat iron oxide particles. The most commonly used, however, are organic materials which include polymeric structures such as dextran, carboxymethylated dextran, carboxydextran, polyvinyl alcohol, polyethylene glycol, alginate, starch, arabinogalactan, glycosaminoglycan, sulfonated styrene−divinylbenzene, chitosan, poloxamers, and polyoxamines.[392]

Superparamagnetic iron oxide contrast agents with their full functionalization are loosely categorized into two groups classed by size (inclusive of coatings):

(1) SPIOs: >60 nm
   (a) large oral SPIOs: 300 nm to 3.5 μm
   (b) standard SPIOs (SSPIO): 60−150 nm
(2) ultrasmall SPIOs (USPIO): <40 nm
   (a) monocrystalline iron oxide nanoparticles (MION)
      (i) cross-linked iron oxide (CLIO).

Table 4 provides a list of commercially available SPIOs and their properties.

Table 4. Commercial Superparamagnetic Iron Oxide Particles[392,432−435]

agent	particle size	classification	surface coating	relaxivity (mM^{-1} s^{-1}) (37 °C, 0.47 T)	target organs	dose[a]	mode of admin	generic name	trade name	developing company	status
OMP	3.5 μm	oral SPIO	polystyrene		GI lumen	0.5 g/L, 400−600 mL	p.o.	Ferristene	Abdoscan	Amersham/GE Healthcare	discontinued
AMI-121	300 nm	oral SPIO	siloxane		GI lumen	52.5 mg of Fe (= 0.94 mmol of Fe)	p.o.	Ferumoxsil	Lumirem Gastromark	Guerbet Advanced Magnetics/ AMAG Pharmaceuticals	approved in U.S. and Europe
AMI-25	80−150 nm	SSPIO	dextran	$r_1 = 20.2$; $r_2 = 101$	liver/spleen, perfusion, MRA	15 μmol of Fe/kg	slow infusion	Ferumoxide	Endorem Feridex IV	Guerbet Advanced Magnetics/ AMAG Pharmaceuticals	approved in U.S. and Europe, discontinued
SHU 555A	62 nm	SSPIO	carboxy-dextran	$r_1 = 23.6$; $r_2 = 179$	liver	<60 kg = 0.45 mmol of Fe, >60 kg = 0.7 mmol of Fe	bolus injection	Ferrixan, Ferucarbotran	Resovist	Bayer Schering Pharma	approved in Europe, Australia, Japan
SHU 555C	21 nm	USPIO	carboxy-dextran	$r_1 = 24$; $r_2 = 60$	MRA				Supravist	Bayer Schering Pharma	phase III complete
AMI-227	20−40 nm	USPIO	dextran	$r_1 = 23.3$; $r_2 = 65$	lymph nodes, MRA	14−45 μmol of Fe/kg	slow infusion	Ferumoxtran	Sinerem Combidex	Guerbet Advanced Magnetics/ AMAG Pharmaceuticals	not approved in U.S. or Europe, discontinued
AMI-228	30 nm	USPIO	semisynthetic carbohydrate	$r_1 = 38$; $r_2 = 83$	iron replacement	2 doses of 510 mg of Fe	bolus injection	Ferumoxytol	Feraheme	Advanced Magnetics/ AMAG Pharmaceuticals	approved in U.S. (for iron therapy)
NC100150	20 nm	USPIO	PEG	$r_1 = 21.8$; $r_2 = 35.3$	perfusion, MRA	7−100 μmol of Fe/kg	bolus injection	Feruglose	Clariscan	Amersham/GE Healthcare	completed phase II, discontinued

[a] Doses may vary with imaging sequences and target organs.

Oral SPIO preparations used for contrast enhancement of the abdomen typically contain larger particles and are coated with a nonbiodegradable and insoluble matrix to reduce aggregation. They are suspended in viscosity-increasing agents based on ordinary food additives such as starch and cellulose that prevent ingested iron absorption and particle aggregation to allow homogeneous contrast distribution throughout the bowel. These suspensions are well-tolerated by the patients, and the intestinal mucosal membrane is not irritated.[417,418]

Standard superparamagnetic iron oxide agents are easily sequestered by reticuloendothelial system (RES) cells in the liver and spleen upon intravenous administration with minimal lymph node uptake. AMI-25 (Endorem or Feridex) consists of iron oxide crystals coated by dextran with a final diameter of 80−150 nm. The T_2 and T_1 relaxivities respectively are 98.3 and 23.9 mL^{-1} s^{-1}.[419] With a blood half-life of 6 min, AMI-25 quickly accumulates in the liver (~80% of the injected dose) and spleen (5−10% of the injected dose) within minutes of injection. Peak concentrations of iron are found in the liver and spleen after 2 and 4 h with half-lives of 3 and 4 days, respectively.[419] The preparation is usually not administered in a bolus injection because of cardiovascular side effects and lumbar pain. The recommended mode of administration is a dose of 15 μmol of Fe/kg in 100 mL of 5% glucose with a biphasic infusion (2 mL/min over 10 min and 4 mL/min over 20 min). SHU 555A (Resovist) is a carbodextran SSPIO with 4.2 nm iron crystals and a hydrodynamic diameter of 62 nm. Its T_2 and T_1 relaxivities are 151.0 and 25.4 mM^{-1} s^{-1}, respectively. This particle shows no side effects after rapid intravenous injection and a dose of 8 μmol of Fe/kg can be scanned within 30 min after administration.[420] Due to smaller size and higher T_1 relaxation, SHU 555A has also been used for MRA and dynamic T_1-weighted MR imaging, similar to gadolinium chelates.[421]

USPIOs typically have iron crystals of 5−12 nm and prolonged blood half-life that affords them the opportunity to eventually cross capillary walls and have more widespread tissue distribution. They can be delivered to the interstitium by nonspecific vesicular transport and through transendothelial channels. Once in the interstitium, draining lymphatic vessels transport them to lymph nodes, thus making them suitable agents for MR lymphography (MRL). At low concentrations, these agents can be used for T_1-weighted MRA, though high concentrations will lead to signal loss due to T_2-shortening effects. AMI-227 (Sinerem or Combidex) is a 20−40 nm dextran-coated USPIO with a human blood pool half-life of more than 24 h.[422] It can be used as an MRA agent during the early phase of intravenous administration[423−425] and as an MRL agent during the late phase.[426,427] To avoid hypotensive reactions or acute lumbar pain, AMI-227 is infused slowly over a period of 30 min. NC100150 (Clariscan), a PEGylated USPIO, and HU 555C (Resovist) are bolus-injectable agents developed for MRA and perfusion studies.[428] NC100150 has been tested as a brain T_2*-weight perfusion agent at a dose of 7 μmol Fe/kg,[429] but because of some adverse events and improvements in MRI units allowing better MRA with low molecular weight contrast agents, the sponsor (GE Healthcare) discontinued development of this product. Monocrystalline iron oxide nanoparticles (MIONs) are a subclass of USPIOs that differ from other SPIOs in their monocrystallinity. Their small iron oxide diameter, typically 2−9 nm, allows them to pass through the capillary endothelium while retaining their

superparamagnetism. *In vivo* detection of the agent is feasible with MRI at concentrations as low as 1 μg of Fe/g of tissue.[430,431] CLIOs are a specific form of MIONs stabilized by a cross-linked aminated dextran coating. The USPIO size affords them great potential for receptor-directed and magnetically labeled cell probe MRI.

13.4. Applications

SPIO agents are endocytosed and metabolized by RES cells and thereafter incorporated into the normal metabolic iron pool.[436] Eventually they are secreted as the body iron stores turn over. Smaller particles degrade faster into paramagnetic forms of iron. When injected at an appropriate rate, the toxicity of SPIO agents is low, and animal studies have disclosed no acute toxicity or chronic injury at doses more than 100 times the clinical effective dose.[429] The amount of iron oxide required for clinical MRI is small when compared with actual physiological iron stores.[417,420] The diameter of superparamagnetic agents greatly affects their localization *in vivo*, even without targeting ligands on the surface. Particles ranging in size from 60 to 150 nm rapidly appear in the liver and spleen,[437] while USPIOs are optimal for prolonged blood circulation, can cross capillary walls, and are often extensively taken up by lymph nodes and bone marrow.[437]

Pharmacokinetic behavior of SPIOs is generally comparable in animals and humans.[419,438−441] Hepatic RES Kupffer cells account for 80% of the uptake of the injected dose of AMI-25 (Feridex).[419,438−441] After intravenous injection, the agent has a blood half-life of 10 min and accumulates in the liver and spleen. The first clinical trials with SPIOs were for hepatic imaging,[439,441−443] where particle uptake by Kupffer cells in healthy liver tissue darkened the normal liver. The cancerous lesions appeared bright against the dark background, as they did not take up the SPIOs. Similar studies followed where USPIOs were used to detect cancer metastasis in lymph nodes and bone marrow.[427,444−446] USPIOs have also been successfully used to visualize inflammation in the brain after stroke,[447] surrounding atherosclerotic plaques,[448−450] and from transplant rejection[451−454] when macrophages that have phagocytosed particles enter the regions. Another application of SPIOs that has not yet reached the clinic is specific cell tracking where nonphagocytotic cells are loaded with particles *in vitro* using cell-permeable peptides[455−457] and transfection agents in combination with the negatively charged surface of magnetic nanoparticles.[136,458−460] Such a method has allowed the noninvasive tracking of stem cells,[455] neural transplants,[461] white blood cells,[462] T-cells,[463−465] and monocytes[466] in animal studies.

While the above-mentioned applications have used untargeted superparamagnetic agents, recent developments have been directed toward molecular imaging. Targeting agents that have been conjugated include antibodies, antibody fragments, oligosaccharides, proteins, peptides, peptidomimetics, and other small ligands. Laurent et al.[392] have provided an excellent table that describes these targeting studies. The field has advanced incredibly, where it is now possible to use iron oxide to detect down to single cells *in vivo*.[467]

14. Manganese-Based Agents

The first contrast agent for MRI was in fact not Gd^{3+} based but instead centered on the use of Mn^{2+}. With an administration of manganese salt, Lauterbur et al.[468] found T_1 enhancement, particularly in liver, kidney, and heart.[469] Mn^{2+} is dominated by a dipole−dipole contribution to T_1 and a strong scalar contribution to T_2.[8] Manganese chloride ($MnCl_2$) can be administrated orally at a dosage of 0.8−1.6 g per patient,[470] where it reaches from the gastrointestinal tract to the liver through the portal system. However, interest in Mn-based agents has been sporadic and the development was significantly less than that of Gd^{3+}-based agents because of concerns over free Mn^{2+} toxicity. Parkinsonism-like symptoms occur when the ion blocked normal calcium fluxes in the heart.[469,471] To avoid cardiotoxicity, two strategies were considered: (1) administration in combination with Ca^{2+} ions[472,473] to competitively reduce binding of Mn^{2+} to Ca^{2+} channels and (2) chelation[474−476] to control or modulate the concentration of free Mn^{2+}; both approaches reduced toxicity.

The most well-known Mn^{2+} chelate is Mn-dipyridoxyldiphosphate (MnDPDP, Mangafodipir, or Teslascan, manufactured by GE Healthcare) (Figure 21). Whereas, following oral intake, manganese accumulates only in the liver and bile,[470] after intravenous injection, it is also found in the pancreas, kidneys, and cardiac muscle.[477] T_1 liver enhancement after intravenous infusion begins early, 1−2 min postinjection, maximizes within 5−10 min, and persists for several hours, allowing flexibility for patient scheduling when compared to Gd^{3+} chelates. No longer on the market, for human clinical imaging to detect hepatic lesions, the approved dosage of Mn-DPDP was 5 μmol/kg,[478] and approximately 15% was eliminated in the urine by 24 h postinjection and 59% in the feces by 5 days.[30] In a European phase III clinical trial, adverse events, such as nausea, headache, and pruritus, were observed in 7% of the 624 patients.[478,479] Transient decreases in alkaline phosphatase levels and sensations of heat and flushing with high injection rates most likely related to peripheral vasodilatation have also been reported.

Given the theme of this specific review, what is most relevant is the use of Mn^{2+} in macromolecular structures. As with relaxation by Gd^{3+}, increasing the rotational correlation time τ_R also increases the relaxivity of Mn^{2+}. T_1 relaxation of MnDPDP has been shown to increase by intracellular protein binding. In the rat myocardium, intracellular relaxivity by Mn^{2+} ions was 8 times and 36 times higher than that by Mn^{2+} aqua ions and MnDPDP *in vitro* ($r_1 = 56\ mM^{-1}\ s^{-1}$ at 0.47 T).[480] Later, Mn^{2+} complexes derivatized with benzyloxymethyl (BOM) substituents were synthesized to promote noncovalent interaction with human serum albumin (HSA).[481] The two EDTA-based agents contained one coordinated water molecule and the third no directly coordinated molecules. They displayed relaxivity values smaller than that of Gd^{3+}-DTPA (Table 5); however, the exchange rates of the coordinated water were 1 order of magnitude higher than those reported for Gd^{3+} complexes with octadentate ligands. The relaxivity of the agents increased up to 15 times when bound to HSA.[481] Building on this work, Troughton et al.[482] synthesized an EDTA complex with a diphenylcyclohexyl moiety, such as gadolinium-based MS-325, to again promote binding to serum albumin. MnL1 was also found to bind well to HSA and had double the water exchange rate (Table 5).

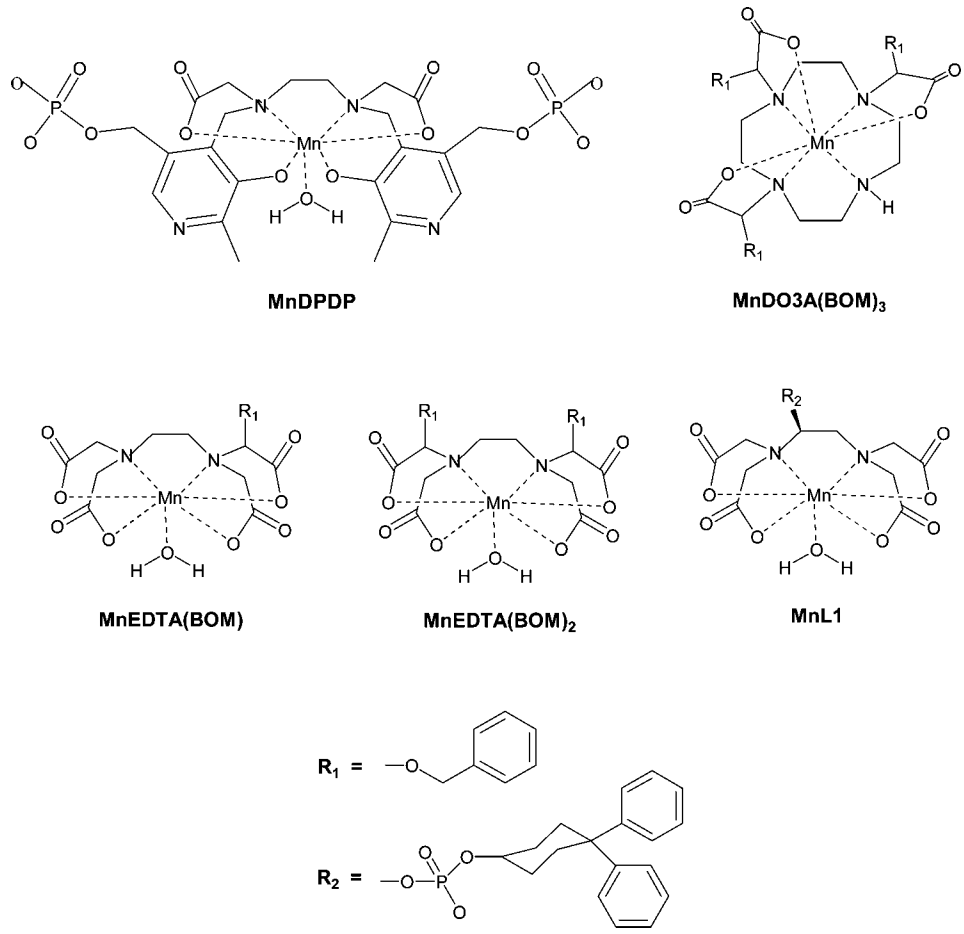

Figure 21. Manganese chelates.

Table 5. Manganese Chelate Properties—Effect on Relaxivity Due to Binding of Mn^{2+} Complexes to HAS[481,482]

	relaxivity (mM^{-1} s^{-1}) (20 MHz, 298 K, pH 7.4)		
	unbound	bound to HSA	k_{ex}^{298} (s^{-1}) at 298 K
EDTA(BOM)	3.6 ± 0.2	55.3 ± 2.5	0.93×10^8
$EDTA(BOM)_2$	4.3 ± 0.2	48.0 ± 2.3	1.3×10^8
$DO3A(BOM)_3$	1.6 ± 0.1	8.1 ± 0.4	no coordinated water
L1	5.8 (37 °C)	48 (37 °C)	$(2.3 \pm 0.9) \times 10^8$

These chelating agents were useful in providing MR contrast; however, work with them was mostly abandoned in favor of Gd^{3+}-based agents, partially due to the significantly larger doses needed for nonhepatic imaging applications. Searches of the literature will find a handful of macromolecular structures synthesized to sequester manganese. In the mid-1980s, Mn^{2+}-DTPA and Mn^{2+}-citrate were entrapped in multilamellar liposomes[308,483] and accumulation compared to free Mn^{2+}-DTPA was dramatically increased in spleen and liver while relatively reduced in the heart and kidney. The work was then followed by encapsulation of Mn^{2+}-labeled HSA in liposomes as MRI contrast agents.[484] Enclosure in the liposome did not affect the relaxivity of the HSA−Mn^{2+} complex. More recently, Mn^{2+} has been incorporated in SPIO agents to increase magnetic moment and relaxivity and has now been used to target tumors by conjugating the monoclonal antibody trastuzumab to the surface.[485] Larger manganese structures currently being developed for MR that will release Mn^{2+} ions over time are metal−organic frameworks with trimesic acid (BTC) bridging ligands.[486] $Mn_3(BTC)_2(H_2O)_6$ nanoparticles adopted a spiral rod morphology with diameters of 50−100 nm and lengths of 1−2 μm. They were further labeled with Rhodamine B dye for fluorescence imaging and c(RGDfK) peptide to target angiogenic cancers. The relaxivity of this particulate on a per Mn basis was $r_1 = 4.0$ and $r_2 = 112.8$ mM^{-1} s^{-1} at 9.4T, but the hope is that T_1 enhancement will increase as Mn^{2+} leaches out of the structure. Initial *in vitro* and *in vivo* studies have begun, but much work must be done to further characterize this agent.

15. Conclusions

A decade after an excellent review by Caravan and coworkers was published in this same journal on Gd^{3+}-based MR contrast agents,[4] we have seen a tremendous amount of growth in the field. New macromolecular constructs have been added to the arsenal of already well-studied macromolecular and supramolecular platforms. These, in addition to maximizing the benefits of large rotational correlation times, optimal water residency times, and retention in blood plasma, also employ "smart" drug delivery strategies which improve pharmacokinetics and report on selective physiological phenomena.

While throughout this article the advantages of macromolecular agents have been highlighted, one observation that is clear at this point is that bigger is not necessarily better. The chemist would do well to keep in mind the real biological limits in designing macromolecular constructs for MR applications. Attempts to push rotational correlation times to their theoretical maximum by increasing molecular weight are all too often compromised either by nonoptimal water residency times, poor solubility in water, or lack of

realistic usefulness in the actual intended or hypothesized application. Attempts to maximize Gd^{3+}-loading onto targeted agents such as antibodies can result in reduced target affinity and selectivity. Furthermore, the pharmacokinetic behavior of these agents remains a challenge and is determined on a case-by-case basis. Yet, the creation of assemblies that exist to just contain remarkably large numbers of Gd^{3+} continues to be pursued despite an apparent lack of acceptance that the accompanying sizes of such assemblies are truly limiting to their usefulness. Improvements in MR technology have certainly enhanced the sensitivity of the technique. While the lure of novel materials such as fullerenes and carbon nanotubes and advances of the chemistry to append additional functionality are readily available, the value added of using such platforms solely as platforms for the novelty is unclear. The toxicity of SWNTs and fullerenes, whole body clearance, and retention of the Gd^{3+} *in vivo* are issues that have barely begun to be addressed. The appending of functionality to the exterior of such structures fundamentally has to disrupt their exquisite structural stability so that again the issue of long-term *in vivo* stability remains to be addressed.

Much of these limitations apply across the agents discussed herein. The use of dendrimers as a core platform for the assembly of MRI contrast agents has been studied for less than 20 years. The number of types of dendrimers that have been reported for this application is less than 10. The potential diversity of the core, the repeating units, and the internal and exterior functionality that might be applied to the creation of dendrimers is, for practical purposes, near infinite. These variations may be the subject of ongoing investigations, but standardized methods for comparison across the board have not been established, and so systematically investigating what advantages might be gained through manipulating the possibilities remains an unknown. By and large, the existing studies have been based upon commercially available or previously reported dendrimers, which does provide a basis to begin some comparisons. In parallel, a similar condition and assessment of how little is really known and how vast the remaining opportunities are for dendrimers can be extended directly to most of the other platforms for assembling novel and potentially useful clinical agents. Equally challenging, however, are a host of issues that regulatory agencies face, such as consistent characterization, reproducibility in production of clinical use materials, long-term toxicity, and the metrics for assessing these agents; those available for low molecular weight agents all too frequently simply do not apply. Thus, to state that this field remains in its infancy is probably conservative.

While the future is still bright for Gd^{3+}-based contrast agents, new roads have been paved toward the development of alternatives which depend on different detection protocols, as is the case with lipoCEST agents, SPIOs, and other agents. The ranges of these possible MR agents are continuously expanding, and while there remains more than adequate room for more interesting chemistry, we are now also faced with the challenge of determining which agents are most suitable for particular medical protocols.

16. Acknowledgments

This work was supported by the Intramural Research Program of the NIH, National Cancer Institute, Center for Cancer Research.

17. References

(1) Andrä, W.; Nowak, H. *Magnetism in Medicine: A Handbook*; Wiley-VCH: Berlin, 2006.
(2) Bernard, V. *Australas. Radiol.* **1989**, *33*, 390.
(3) Lauffer, R. B. *Chem. Rev.* **1987**, *87*, 901.
(4) Caravan, P.; Ellison, J. J.; McMurry, T. J.; Lauffer, R. B. *Chem. Rev.* **1999**, *99*, 2293.
(5) Shellock, F. G.; Kanal, E. *J. Magn. Reson. Imaging* **1999**, *10*, 477.
(6) Banci, L.; Bertini, I.; Luchinat, C. *Nuclear and Electron Relaxation*; VCH: Weinheim, 1991.
(7) Kowalewski, J.; Nordenskiold, L.; Benetis, N.; Westlund, P. O. *Prog. Nucl. Magn. Reson. Spectrosc.* **1985**, *17*, 145.
(8) Bertini, I.; Luchinat, C. *Coord. Chem. Rev.* **1996**, *150*, 1.
(9) Luz, Z.; Meiboom, S. *J. Chem. Phys.* **1964**, *40*, 2686.
(10) Swift, T. J.; Connick, R. E. *J. Chem. Phys.* **1962**, *37*, 307.
(11) Bloembergen, N.; Morgen, L. O. *J. Chem. Phys.* **1961**, *34*, 842.
(12) Strandberg, E.; Westlund, P.-O. *J. Magn. Reson. A* **1996**, *122*, 179.
(13) Abernathy, S. M.; Sharp, R. R. *J. Chem. Phys.* **1997**, *106*, 9032.
(14) Abernathy, S. M.; Miller, J. C.; Lohr, L. L.; Sharp, R. R. *J. Chem. Phys.* **1998**, *109*, 4035.
(15) Sharp, R.; Abernathy, S. M.; Lohr, L. L. *J. Chem. Phys.* **1997**, *107*, 7620.
(16) Sharp, R. R. *J. Chem. Phys.* **1993**, *98*, 912.
(17) Sharp, R. R. *J. Chem. Phys.* **1993**, *98*, 2507.
(18) Sharp, R. R. *J. Chem. Phys.* **1993**, *98*, 6092.
(19) Westlund, P.-O. *J. Chem. Phys.* **1998**, *108*, 4945.
(20) Banci, L.; Bertini, I.; Briganti, F.; Luchinat, C. *J. Magn. Reson.* **1986**, *66*, 58.
(21) Lipari, G.; Szabo, A. *J. Am. Chem. Soc.* **1982**, *104*, 4546.
(22) Bennett, H. F.; Brown, R. D.; Koenig, S. H.; Swartz, H. M. *Magn. Reson. Med.* **1987**, *4*, 93.
(23) Freed, J. H. *J. Chem. Phys.* **1978**, *68*, 4034.
(24) Hwang, L.-P.; Freed, J. H. *J. Chem. Phys.* **1975**, *63*, 4017.
(25) Geraldes, C. F. G. C.; Sherry, A. D.; Cacheris, W. P.; Kuan, K. T.; Brown, R. D.; Koenic, S. H.; Spillers, M. *Magn. Reson. Med.* **1988**, *8*, 191.
(26) Geraldes, C. F. G. C.; Urbano, A. M.; Alpoim, M. C.; Sherry, A. D.; Kuan, K. T.; Rajagopalan, R.; Maton, F.; Muller, R. N. *Magn. Reson. Imaging* **1995**, *13*, 401.
(27) Vega, A. J.; Fiat, D. *Mol. Phys.* **1976**, *31*, 347.
(28) Kellar, K. E.; Fossheim, S. L.; Koenig, S. H. *Invest. Radiol.* **1998**, *33*, 835.
(29) Evans, C. *Biochemistry of the Lanthanides*; Plenum Press: New York, 1990.
(30) Bellin, M.-F. *Eur. J. Radiol.* **2006**, *60*, 314.
(31) Ersoy, H.; Rybicki, F. J. *J. Magn. Reson. Imaging* **2007**, *26*, 1190.
(32) Chang, C. *Invest. Radiol.* **1993**, *28*, 521.
(33) Zhang, Z.; Nair, S. A.; McMurry, T. J. *Curr. Med. Chem.* **2005**, *12*, 751.
(34) Wiener, E.; Narayanan, V. V. In *Advances in Dendritic Macromolecules*; Newkome, G. R., Ed.; Elsevier: Oxford, 2002; Vol. 5.
(35) Adzamli, K.; Periasamy, M. P.; Spiller, M.; Koenig, S. H. *Invest. Radiol.* **1999**, *34*, 410.
(36) de Graaf, R. A.; Brown, P. B.; McIntyre, S.; Nixon, T. W.; Behar, K. L.; Rothman, D. L. *Magn. Reson. Med.* **2006**, *56*, 386.
(37) Kirchin, M. A.; Runge, V. M. *Top. Magn. Reson. Imaging* **2003**, *14*, 426.
(38) Laurent, S.; Botteman, F.; Elst, L. V.; Muller, R. N. *Eur. J. Inorg. Chem.* **2004**, *3*, 463.
(39) Laurent, S.; Elst, L. V.; Muller, R. N. *Contrast Media Mol. Imaging* **2006**, *1*, 128.
(40) Vander, E. L.; Maton, F.; Laurent, S.; Seghi, F.; Chapelle, F.; Muller, R. N. *Magn. Reson. Imaging* **1997**, *38*, 604.
(41) Oksendal, A. N.; Hals, P. A. *J. Magn. Reson. Imaging* **1993**, *3*, 157.
(42) Tweedle, M. F.; Wedeking, P.; Kumar, K. *Invest. Radiol.* **1995**, *30*, 372.
(43) Wiener, E.; Brechbiel, M. W.; Brothers, H.; Magin, R. L.; Gansow, O. A.; Tomalia, D. A.; Lauterbur, P. C. *Magn. Reson. Med.* **1994**, *31*, 1.
(44) Kirchin, M. A.; Pirovano, G.; Venetianer, C.; Spinazzi, A. *J. Magn. Reson. Imaging* **2001**, *14*, 281.
(45) Xu, J.; Franklin, S. J.; Whisenhunt, D. W.; Raymond, K. N. *J. Am. Chem. Soc.* **1995**, *117*, 7245.
(46) Werner, E. J.; Avedano, S.; Botta, M.; Hay, B. P.; Moore, E. G.; Aime, S.; Raymond, K. N. *J. Am. Chem. Soc.* **2007**, *129*, 1870.
(47) Thompson, M. K.; Misselwitz, B.; Tso, L. S.; Doble, D. M. J.; Schmitt-Willich, H.; Raymond, K. N. *J. Med. Chem.* **2005**, *48*, 3874.
(48) Seitz, M.; Pluth, M. D.; Raymond, K. N. *Inorg. Chem.* **2007**, *46*, 351.
(49) Webb, J. A. W.; Thomsen, H. S.; Morcos, S. K. *Eur. Radiol.* **2005**, *15*, 1234.

(50) Kubik-Huch, R. A.; Gottstein-Aalame, N. M.; Frenzel, T.; Seifert, B.; Puchert, E.; Wittek, S.; Debatin, J. F. *Radiology* **2000**, *216*, 555.
(51) Thomsen, H. S.; Morcos, S. K.; Dawson, P. *Clin. Radiol.* **2006**, *61*, 905.
(52) Cowper, S.; Boyer, P. *Curr. Rheumatol. Rep.* **2006**, *8*, 151.
(53) Knopp, E. A.; Cowper, S. E. *Semin. Dial.* **2008**, *21*, 123.
(54) Chewning, R. H.; Murphy, K. J. *J. Vasc. Interv. Radiol.* **2007**, *18*, 331.
(55) Grobner, T. *Nephrol. Dial. Transplant.* **2006**, *21*, 1104.
(56) Agarwal, R.; Brunelli, S. M.; Williams, K.; Mitchell, M. D.; Feldman, H. I.; Umscheid, C. A. *Nephrol. Dial. Transplant.* **2009**, *24*, 856.
(57) Boyd, A. S.; Zic, J. A.; Abraham, J. L. *J. Am. Acad. Dermatol.* **2007**, *56*, 27.
(58) Peak, A. S.; Sheller, A. *Ann. Pharmacother.* **2007**, *41*, 1481.
(59) Issa, N.; Poggio, E. D.; Fatica, R. A.; Patel, R.; Ruggieri, P. M.; Heyka, R. J. *Cleveland Clin. J. Med.* **2008**, *75*, 95.
(60) Information for Healthcare Professionals Gadolinium-Based Contrast Agents for Magnetic Resonance Imaging (marketed as Magnevist, MultiHance, Omniscan, OptiMARK, ProHance). http://www.fda.gov/Drugs/DrugSafety/PostmarketDrugSafetyInformationforPatientsandProviders/ucm142884.htm (accessed October 1, 2009).
(61) Kanal, E.; Barkovich, A. J.; Bell, C.; Borgstede, J. P.; Bradley, W. G., Jr.; Froelich, J. W.; Gilk, T.; Gimbel, J. R.; Gosbee, J.; Kuhni-Kaminski, E.; Lester, J. W., Jr.; Nyenhuis, J.; Parag, Y.; Schaefer, D. J.; Sebek-Scoumis, E. A.; Weinreb, J.; Zaremba, L. A.; Wilcox, P.; Lucey, L.; Sass, N. *Am. J. Roentgenol.* **2007**, *188*, 1447.
(62) Sessler, J. L.; Murai, T.; Lynch, V.; Cyr, M. *J. Am. Chem. Soc.* **1988**, *110*, 5586.
(63) Magda, D.; Miller, R. A. *Semin. Cancer Biol.* **2006**, *16*, 466.
(64) Bohmer, R. M.; Morstyn, G. *Cancer Res.* **1985**, *45*, 5328.
(65) Mehta, M.; Gervais, R.; Chabot, P.; Shapiro, W. R.; Patchell, R. A.; Glantz, M. J.; Recht, L.; Phan, S.; Smith, J. A.; Renschler, M. F. *J. Clin. Oncol.* **2006**, *24*, 7014; Meeting Abstracts.
(66) Rosenthal, D. I.; Nurenberg, P.; Becerra, C. R.; Frenkel, E. P.; Carbone, D. P.; Lum, B. L.; Miller, R.; Engel, J.; Young, S.; Miles, D.; Renschler, M. F. *Clin. Cancer Res.* **1999**, *5*, 739.
(67) Maeda, H. *Adv. Enzyme Regul.* **2001**, *41*, 189.
(68) Wang, D.; Miller, S. C.; Sima, M.; Parker, D.; Buswell, H.; Goodrich, K. C.; Kopeckova, P.; Kopecek, J. *Pharm. Res.* **2004**, *21*, 1741.
(69) Venditto, V. J.; Regino, C. A. S.; Brechbiel, M. W. *Mol. Pharmacol.* **2005**, *2*, 302.
(70) Fischer, M.; Vögtle, F. *Angew. Chem., Int. Ed.* **1999**, *38*, 884.
(71) Langereis, S.; Dirksen, A.; Hackeng, T. M.; van Genderen, M. H. P.; Meijer, E. W. *New J. Chem.* **2007**, *31*, 1152.
(72) Stiriba, S.-E.; Frey, H.; Haag, R. *Angew. Chem., Int. Ed. Engl.* **2002**, *41*, 1329.
(73) Tomalia, D. A.; Baker, H.; Dewald, J.; Hall, M.; Kallos, G.; Martin, S.; Roeck, J.; Ryder, J.; Smith, P. *Polym. J.* **1985**, *17*, 117.
(74) Frechet, J. M. *Science* **1994**, *263*, 1710.
(75) Newkome, G. R.; Moorefield, C. N.; Vogtle, F. *Dendrimers and Dendrons: Concepts, Syntheses, Applications*; Wiley-VCH: Weinheim, 2001.
(76) Tomalia, D. A.; Naylor, A. M.; Goddard, W. A., III. *Angew. Chem., Int. Ed. Engl.* **1990**, *29*, 138.
(77) Hawker, C.; Frechet, J. M. J. *J. Chem. Soc., Chem. Commun.* **1990**, *15*, 1010.
(78) Jayaraman, M.; Frechet, J. M. J. *J. Am. Chem. Soc.* **1998**, *120*, 12996.
(79) Buhleier, E.; Wehner, W.; Vögtle, F. *Synthesis* **1978**, *1978*, 155.
(80) Newkome, G. R.; Yao, Z.; Baker, G. R.; Gupta, V. K. *J. Org. Chem.* **1985**, *50*, 2003.
(81) Tomalia, D. A.; Baker, H.; Dewald, J.; Hall, M.; Kallos, G.; Martin, S.; Roeck, J.; Ryder, J.; Smith, P. *Polym. J.* **1985**, *17*, 117.
(82) Maiti, P. K.; Cagin, T.; Wang, G.; Goddard, W. A. *Macromolecules* **2004**, *37*, 6236.
(83) de Brabander-van den Berg, E. M. M.; Meijer, E. W. *Angew. Chem., Int. Ed. Engl.* **1993**, *32*, 1308.
(84) Wörner, C.; Mülhaupt, R. *Angew. Chem., Int. Ed. Engl.* **1993**, *32*, 1306.
(85) Hummelen, J. C.; Van Dongen, J. L. J.; Meijer, E. W. *Chem.—Eur. J.* **1997**, *3*, 1489.
(86) Tomalia, D. A.; Huang, B.; Swanson, D. R.; Brothers, H. M.; Klimash, J. W. *Tetrahedron* **2003**, *59*, 3799.
(87) Xu, H.; Regino, C. A. S.; Bernardo, M.; Koyama, Y.; Kobayashi, H.; Choyke, P. L.; Brechbiel, M. W. *J. Med. Chem.* **2007**, *50*, 3185.
(88) Langereis, S.; de Lussanet, Q. G.; van Genderen, M. H. P.; Backes, W. H.; Meijer, E. W. *Macromolecules* **2004**, *37*, 3084.
(89) Margerum, L. D.; Campion, B. K.; Koo, M.; Shargill, N.; Lai, J.-J.; Marumoto, A.; Sontum, P. C. *J. Alloys Compd.* **1997**, *249*, 185.
(90) Bryant, L. H. J.; Brechbiel, M. W.; Wu, C.; Bulte, J. W. M.; Herynek, V.; Frank, J. A. *J. Magn. Reson. Imaging* **1999**, *9*, 348.
(91) Tóth, E.; Pubanz, D.; Vauthey, S.; Helm, L.; Merbach, A. E. *Chem.—Eur. J.* **1996**, *2*, 1607.
(92) Laus, S.; Sour, A.; Ruloff, R.; Tóth, E.; Merbach, A. E. *Chem.—Eur. J.* **2005**, *11*, 3064.
(93) Laus, S.; Ruloff, R.; Tóth, E.; Merbach, A. E. *Chem.—Eur. J.* **2003**, *9*, 3555.
(94) Rudovsky, J.; Botta, M.; Hermann, P.; Hardcastle, K. I.; Lukes, I.; Aime, S. *Bioconjugate Chem.* **2006**, *17*, 975.
(95) Rudovsky, J.; Hermann, P.; Botta, M.; Aime, S.; Lukes, I. *Chem. Commun.* **2005**, *18*, 2390.
(96) Rudovsky, J.; Kotek, J.; Hermann, P.; Lukes, I.; Mainero, V.; Aime, S. *Org. Biomol. Chem.* **2005**, *3*, 112.
(97) Lebduskova, P.; Sour, A.; Helm, L.; Toth, E.; Kotek, J.; Lukes, I.; Merbach, A. E. *Dalton Trans.* **2006**, *28*, 3399.
(98) Ali, M. M.; Woods, M.; Caravan, P.; Opina, A. C. L.; Spiller, M.; Fettinger, J. C.; Sherry, A. D. *Chem.—Eur. J.* **2008**, *14*, 7250.
(99) Pikkemaat, J. A.; Wegh, R. T.; Lamerichs, R.; van de Molengraaf, R. A.; Langereis, S.; Burdinski, D.; Raymond, A. Y. F.; Janssen, H. M.; de Waal, B. F. M.; Willard, N. P.; Meijer, E. W.; Grüll, H. *Contrast Media Mol. Imaging* **2007**, *2*, 229.
(100) Aime, S.; Carrera, C.; Delli Castelli, D.; Crich, S. G.; Terreno, E. *Angew. Chem., Int. Ed.* **2005**, *44*, 1813.
(101) Fulton, D. A.; O'Halloran, M.; Parker, D.; Senanayake, K.; Botta, M.; Aime, S. *Chem. Commun.* **2005**, *4*, 474.
(102) *The Chemistry of Contrast Agents in Medical Magnetic Resonance Imaging*; Merbach, A. E., Toth, E., Eds.; Wiley: Chichester, 2001.
(103) Bourne, M. W.; Margerun, L.; Hylton, N.; Campion, B.; Lai, J.-J.; Derugin, N.; Higgins, C. B. *J. Magn. Reson. Imaging* **1996**, *6*, 305.
(104) Weinmann, H. J.; Ebert, W.; Wagner, S.; Taupitz, M.; Misselwitz, M.; Schmitt-Wilich, H. Proceedings of the IX International Workshop on Magnetic Resonance Angiography, Valencia, 1997; p 355.
(105) Adam, G.; Neuerburg, J.; Spüntrup, E.; Mühler, A.; Scherer, K.; Günther, R. W. *J. Magn. Reson. Imaging* **1994**, *4*, 462.
(106) Roberts, H. C.; Saeed, M.; Roberts, T. P. L.; Mühler, A.; Shames, D. M.; Mann, J. S.; Stiskal, M.; Demsar, F.; Brasch, R. C. *J. Magn. Reson. Imaging* **1997**, *7*, 331.
(107) Tacke, J.; Adam, G.; Claβen, H.; Mühler, A.; Prescher, A.; Günther, R. W. *J. Magn. Reson. Imaging* **1997**, *7*, 678.
(108) Su, M.-Y.; Mühler, A.; Lao, X.; Nalcioglu, O. *Magn. Reson. Imaging* **1998**, *39*, 259.
(109) Roberts, H. C.; Saeed, M.; Roberts, T. P. L.; Mühler, A.; Brasch, R. C. *J. Magn. Reson. Imaging* **1999**, *9*, 204.
(110) Kobayashi, H.; Sato, N.; Kawamoto, S.; Saga, T.; Hiraga, A.; Ishimori, T.; Konishi, J.; Togashi, K.; Brechbiel, M. W. *Magn. Reson. Med.* **2001**, *46*, 579.
(111) Dong, Q.; Hurst, D. R.; Weinmann, H. J.; Chevenert, T. L.; Londy, F. J.; Prince, M. R. *Invest. Radiol.* **1998**, *33*, 699.
(112) Sato, N.; Kobayashi, H.; Hiraga, A.; Saga, T.; Togashi, K.; Konishi, J.; Brechbiel, M. W. *Magn. Reson. Med.* **2001**, *46*, 1169.
(113) Kobayashi, H.; Kawamoto, S.; Star, R. A.; Waldmann, T. A.; Brechbiel, M. W.; Choyke, P. L. *Bioconjugate Chem.* **2003**, *14*, 1044.
(114) Kobayashi, H.; Kawamoto, S.; Star, R. A.; Waldmann, T. A.; Tagaya, Y.; Brechbiel, M. W. *Cancer Res.* **2003**, *63*, 271.
(115) Yordanov, A.; Kobayashi, H.; English, S. J.; Reijnders, K.; Milenic, D.; Krishna, M. C.; Mitchell, J. B.; Brechbiel, M. W. *J. Mater. Chem.* **2003**, *13*, 1523.
(116) Langereis, S.; de Lussanet, Q. G.; van Genderen, M. H. P.; Meijer, E. W.; Beets-Tan, R. G. H.; Griffioen, A. W.; van Engelshoven, J. M. A.; Backes, W. H. *NMR Biomed.* **2006**, *19*, 133.
(117) Kobayashi, H.; Sato, N.; Kawamoto, S.; Saga, T.; Hiraga, A.; Laz Haque, T.; Ishimori, T.; Konishi, J.; Togashi, K.; Brechbiel, M. W. *Bioconjugate Chem.* **2001**, *12*, 100.
(118) Kobayashi, H.; Kawamoto, S.; Saga, T.; Sato, N.; Hiraga, A.; Ishimori, T.; Akita, Y.; Mamede, M. H.; Konishi, J.; Togashi, K.; Brechbiel, M. W. *Magn. Reson. Med.* **2001**, *46*, 795.
(119) Kobayashi, H.; Saga, T.; Kawamoto, S.; Sato, N.; Hiraga, A.; Ishimori, T.; Konishi, J.; Togashi, K.; Brechbiel, M. W. *Cancer Res.* **2001**, *61*, 4966.
(120) Kobayashi, H.; Kawamoto, S.; Jo, S.; Bryant, L. H.; Brechbiel, M. W.; Star, R. A. *Bioconjugate Chem.* **2003**, *14*, 388.
(121) Kobayashi, H.; Jo, S.-K.; Kawamoto, S.; Yasuda, H.; Hu, X.; Knopp, M. V.; Brechbiel, M. W.; Choyke, P. L.; Star, R. A. *J. Magn. Reson. Imaging* **2004**, *20*, 512.
(122) Kobayashi, H.; Kawamoto, S.; Saga, T.; Sato, N.; Hiraga, A.; Ishimori, T.; Konishi, J.; Togashi, K.; Brechbiel, M. W. *Magn. Reson. Med.* **2001**, *46*, 781.
(123) Kobayashi, H.; Sato, N.; Kawamoto, S.; Saga, T.; Hiraga, A.; Ishimori, T.; Konishi, J.; Togashi, K.; Brechbiel, M. W. *Magn. Reson. Med.* **2001**, *46*, 457.
(124) Kobayashi, H.; Kawamoto, S.; Star, R. A.; Waldmann, T. A.; Brechbiel, M. W.; Choyke, P. L. *Bioconjugate Chem.* **2003**, *14*, 1044.
(125) Kobayashi, H.; Kawamoto, S.; Choyke, P. L.; Sato, N.; Knopp, M. V.; Star, R. A.; Waldmann, T. A.; Tagaya, Y.; Brechbiel, M. W. *Magn. Reson. Med.* **2003**, *50*, 758.

(126) Koyama, Y.; Talanov, V. S.; Bernardo, M.; Hama, Y.; Regino, C. A. S.; Brechbiel, M. W.; Choyke, P. L.; Kobayashi, H. *J. Magn. Reson. Imaging* **2007**, *25*, 866.
(127) Talanov, V. S.; Regino, C. A. S.; Kobayashi, H.; Bernardo, M.; Choyke, P. L.; Brechbiel, M. W. *Nano Lett.* **2006**, *6*, 1459.
(128) Regino, C. A. S.; Walbridge, S.; Bernardo, M.; Wong, K. J.; Johnson, D.; Lonser, R.; Oldfield, E. H.; Choyke, P. L.; Brechbiel, M. W. *Contrast Media Mol. Imaging* **2008**, *3*, 2.
(129) Wu, C.; Brechbiel, M. W.; Kozak, R. W.; Gansow, O. A. *Bioorg. Med. Chem.* **1994**, *4*, 449.
(130) Kobayashi, H.; Sato, N.; Saga, T.; Nakamoto, Y.; Ishimori, T.; Toyama, S.; Tagashi, K.; Konishi, J.; Brechbiel, M. W. *Eur. J. Nucl. Med.* **2000**, *27*, 1334.
(131) Konda, S.; Aref, M.; Brechbiel, M. W.; Wiener, E. C. *Invest. Radiol.* **2000**, *35*, 50.
(132) Konda, S. D.; Aref, A.; Wang, S.; Brechbiel, M. W.; Wiener, E. C. *Magn. Reson. Mater. Phys., Biol. Med.* **2001**, *12*, 104.
(133) Konda, S. D.; Wang, S.; Brechbiel, M. W.; Weiner, E. C. *Invest. Radiol.* **2002**, *37*, 199.
(134) Wiener, E. C.; Konda, S.; Shadron, A.; Brechbiel, M.; Gansow, O. *Invest. Radiol.* **1997**, *32*, 748.
(135) Boswell, C. A.; Eck, P. K.; Regino, C. A. S.; Bernardo, M.; Wong, K. J.; Milenic, D. E.; Choyke, P. L.; Brechbiel, M. W. *Mol. Pharmacol.* **2008**, *5*, 527.
(136) Kalish, H.; Arbab, A. S.; Miller, B. R.; Lewis, B. K.; Zywicke, H. A.; Bulte, J. W. M.; Bryant, L. H., Jr.; Frank, J. A. *Magn. Reson. Med.* **2003**, *50*, 275.
(137) Kobayashi, H.; Kawamoto, S.; Saga, T.; Sato, N.; Ishimori, T.; Konishi, J.; Ono, K.; Togashi, K.; Brechbiel, M. W. *Bioconjugate Chem.* **2001**, *12*, 587.
(138) Zhu, W.; Okollie, B.; Bhujwalla, Z. M.; Artemov, D. *Magn. Reson. Med.* **2008**, *59*, 679.
(139) Xu, H.; Regino, C. A. S.; Koyama, Y.; Hama, Y.; Gunn, A. J.; Bernardo, M.; Kobayashi, H.; Choyke, P. L.; Brechbiel, M. W. *Bioconjugate Chem.* **2007**, *18*, 1474.
(140) Spanoghe, M.; Lanens, D.; Dommisse, R.; Van der Linden, A.; Alderweireldt, F. *Magn. Reson. Imaging* **1992**, *10*, 913.
(141) Sieving, P. F.; Watson, A. D.; Rocklage, S. M. *Bioconjugate Chem.* **1990**, *1*, 65.
(142) Schuhmann-Giampieri, G.; Schmitt-Wilich, H.; Frenzel, T.; Press, W. R.; Weinmann, H. J. *Invest. Radiol.* **1991**, *26*, 969.
(143) Van Hecke, P.; Marchal, G.; Bosmans, H.; Johannik, K.; Jiang, Y.; Vogler, H.; Van Ongeval, C.; Baert, A. L.; Speck, U. *Magn. Reson. Imaging* **1991**, *9*, 313.
(144) Vexler, V. S.; Clément, O.; Schmitt-Willich, H.; Brasch, R. C. *J. Magn. Reson. Imaging* **1994**, *4*, 381.
(145) Marchal, G.; Bosmans, H.; Van Hecke, P.; Speck, U.; Aerts, P.; Vanhoenacker, P.; Baert, A. L. *Am. J. Roentgenol.* **1990**, *155*, 407.
(146) Lim, T. H.; Lee, D. H.; Kim, Y. H.; Park, S. W.; Park, P. H.; Seo, D. M.; Kim, S. T.; Lee, T. K.; Mun, C. W. *Radiology* **1993**, *189*, 765.
(147) Berthezene, Y.; Vexler, V.; Jerome, H.; Sievers, R.; Moseley, M. E.; Brasch, R. C. *Radiology* **1991**, *181*, 773.
(148) Berthezene, Y.; Vexler, V.; Price, D.; Wisner-Dupon, J.; Moseley, M. E.; Aicher, K. P.; Brasch, R. C. *Invest. Radiol.* **1992**, *27*, 346.
(149) Berthezene, Y.; Vexler, V.; Kuwatsuru, R.; Rosenau, W.; Muhler, A.; Clement, O.; Price, D. C.; Brasch, R. C. *Radiology* **1992**, *185*, 97.
(150) Opsahl, L. R.; Uzgiris, E. E.; Vera, D. R. *Acad. Radiol.* **1995**, *2*, 762.
(151) Zalipsky, S. *Adv. Drug Delivery Rev.* **1995**, *16*, 157.
(152) Abuchowski, A.; van Es, T.; Palczuk, N. C.; Davis, F. F. *J. Biol. Chem.* **1977**, *252*, 3578.
(153) Tóth, E.; van Uffelen, I.; Helm, L.; Merbach, A. E.; Ladd, D.; Briley-Sæbø, K.; Kellar, K. E. *Magn. Reson. Chem.* **1998**, *36*, S125.
(154) Desser, T. S.; Rubin, D. L.; Muller, H. H.; Qing, F.; Khodor, S.; Zanazzi, G.; Young, S. W.; Ladd, D. L.; Wellons, J. A.; Kellar, K. E.; Toner, J. L.; Snow, R. A. *J. Magn. Reson. Imaging* **1994**, *4*, 467.
(155) Bogdanov, A. A., Jr.; Weissleder, R.; Frank, H. W.; Bogdanova, A. V.; Nossif, N.; Schaffer, B. K.; Tsai, E.; Papisov, M. I.; Brady, T. J. *Radiology* **1993**, *187*, 701.
(156) Fu, Y.; Raatschen, H.-J.; Nitecki, D. E.; Wendland, M. F.; Novikov, V.; Fournier, L. S.; Cyran, C.; Rogut, V.; Shames, D. M.; Brasch, R. C. *Biomacromolecules* **2007**, *8*, 1519.
(157) Cyran, C. C.; Fu, Y.; Raatschen, H.-J.; Rogut, V.; Chaopathomkul, B.; Shames, D. M.; Wendland, M. F.; Yeh, B. M.; Brasch, R. C. *J. Magn. Reson. Imaging* **2008**, *27*, 581.
(158) Cavagna, F.; Luchinat, C.; Scozzafava, A.; Xia, Z. *Magn. Reson. Med.* **1994**, *31*, 58.
(159) Allen, M. J.; Raines, R. T.; Kiessling, L. L. *J. Am. Chem. Soc.* **2006**, *128*, 6534.
(160) Lucas, R. L.; Benjamin, M.; Reineke, T. M. *Bioconjugate Chem.* **2008**, *19*, 24.
(161) Kellar, K. E.; Henrichs, P. M.; Hollister, R.; Koenig, S. H.; Eck, J.; Wei, D. *Magn. Reson. Med.* **1997**, *38*, 712.
(162) Tóth, E.; Helm, L.; Kellar, K. E.; Merbach, A. E. *Chem.—Eur. J.* **1999**, *5*, 1202.
(163) Lee, H. Y.; Jee, H. W.; Seo, S. M.; Kwak, B. K.; Khang, G.; Cho, S. H. *Bioconjugate Chem.* **2006**, *17*, 700.
(164) Ladd, D. L.; Hollister, R.; Peng, X.; Wei, D.; Wu, G.; Delecki, D.; Snow, R. A.; Toner, J. L.; Kellar, K.; Eck, J.; Desai, V. C.; Raymond, G.; Kinter, L. B.; Desser, T. S.; Rubin, M. D. D. L. *Bioconjugate Chem.* **1999**, *10*, 361.
(165) Yan, G.-P.; Liu, M.-L.; Li, L.-Y. *Bioconjugate Chem.* **2005**, *16*, 967.
(166) Zarabi, B.; Nan, A.; Zhuo, J.; Gullapalli, R.; Ghandehari, H. *Mol. Pharmacol.* **2006**, *3*, 550.
(167) Amirkhanov, N. V.; Dimitrov, I.; Opitz, A. W.; Zhang, K.; Lackey, J. P.; Cardi, C. A.; Lai, S.; Wagner, N. J.; Thakur, M. L.; Wickstrom, E. *Biopolymers* **2008**, *89*, 1061.
(168) Bogdanov, A. A., Jr.; Matuszewski, L.; Bremer, C.; Petrovsky, A.; Weissleder, R. *Mol. Imaging* **2002**, *1*, 16.
(169) Lu, Z.-R.; Wang, X.; Parker, D. L.; Goodrich, K. C.; Buswell, H. R. *Bioconjugate Chem.* **2003**, *14*, 715.
(170) Wen, X.; Jackson, E. F.; Price, R. E.; Kim, E. E.; Wu, Q.; Wallace, S.; Charnsangavej, C.; Gelovani, J. G.; Li, C. *Bioconjugate Chem.* **2004**, *15*, 1408.
(171) Ye, F.; Ke, T.; Jeong, E.-K.; Wang, X.; Sun, Y.; Johnson, M.; Lu, Z.-R. *Mol. Pharmacol.* **2006**, *3*, 507.
(172) Mohs, A. M.; Wang, X.; Goodrich, K. C.; Zong, Y.; Parker, D. L.; Lu, Z. R. *Bioconjugate Chem.* **2004**, *15*, 1424.
(173) Mohs, A. M.; Zong, Y.; Guo, J.; Parker, D. L.; Lu, Z.-R. *Biomacromolecules* **2005**, *6*, 2305.
(174) Mikawa, M.; Miwa, N.; Bräutigam, M.; Akaike, T.; Maruyama, A. *J. Biomed. Mater. Res.* **2000**, *49*, 390.
(175) Wu, Y.; Zhou, Y.; Ouari, O.; Woods, M.; Zhao, P.; Soesbe, T. C.; Kiefer, G. E.; Sherry, A. D. *J. Am. Chem. Soc.* **2008**, *130*, 13854.
(176) Strich, G.; Hagan, P. L.; Gerber, K. H.; Slutsky, R. A. *Radiology* **1985**, *154*, 723.
(177) Schmiedl, U.; Ogan, M. D.; Moseley, M. E.; Brasch, R. C. *Am. J. Roentgenol.* **1986**, *147*, 1263.
(178) Lauffer, R. B.; Brady, T. J. *Magn. Reson. Imaging* **1985**, *3*, 11.
(179) Schmiedl, U.; Ogan, M.; Paajanen, H.; Marotti, M.; Crooks, L. E.; Brito, A. C.; Brasch, R. C. *Radiology* **1987**, *162*, 205.
(180) Ogan, M. D.; Schmiedl, U.; Moseley, M. E.; Grodd, W.; Paajanen, H.; Brasch, R. C. *Invest. Radiol.* **1987**, *22*, 665.
(181) Paajanen, H.; Reisto, T.; Hemmila, I.; Komu, M.; Niemi, P.; Kormano, M. *Magn. Reson. Med.* **1990**, *13*, 38.
(182) Sherry, A. D.; Cacheris, W. P.; Kuan, K.-T. *Magn. Reson. Imaging* **1988**, *8*, 180.
(183) Kuwatsuru, R.; Shames, D. M.; Mühler, A.; Mintorovitch, J.; Vexler, V.; Mann, J. S.; Cohn, F.; Price, D.; Huberty, J.; Brasch, R. C. *Magn. Reson. Med.* **1993**, *30*, 76.
(184) Shames, D. M.; Kuwatsuru, R.; Vexler, V.; Mühler, A.; Brasch, R. C. *Magn. Reson. Imaging* **1993**, *29*, 616.
(185) Vexler, V. S.; Berthezene, Y.; Wolfe, C. L.; Sievers, R.; Dupon, J. W.; Aicher, K.; Moseley, M. E.; Brasch, R. C. *Invest. Radiol.* **1992**, *27*, 935.
(186) Moseley, M. E.; Chew, W. M.; White, D. L.; Kucharczyk, J.; Litt, L.; Derugin, N.; Dupon, J.; Brasch, R. B.; Norman, D. *Magn. Reson. Med.* **1992**, *23*, 21.
(187) van Dijke, C. F.; Kirk, B. A.; Peterfy, C. G.; Genant, H. K.; Brasch, R. C.; Kapila, S. *Radiology* **1997**, *204*, 825.
(188) Vexler, V. S.; Berthèzene, Y.; Clément, O.; Mühler, A.; Rosenau, W.; Moseley, M. E.; Brasch, R. C. *J. Magn. Reson. Imaging* **1992**, *2*, 311.
(189) Schmiedl, U.; Sievers, R. E.; Brasch, R. C.; Wolfe, C. L.; Chew, W. M.; Ogan, M. D.; Engeseth, H.; Lipton, M. J.; Moseley, M. E. *Radiology* **1989**, *170*, 351.
(190) Sievers, R. E.; Schmiedl, U.; Wolfe, C. L.; Moseley, M. E.; Parmley, W. W.; Brasch, R. C.; Lipton, M. J. *Magn. Reson. Imaging* **1989**, *10*, 172.
(191) Wolfe, C. L.; Moseley, M. E.; Wikstrom, M. G.; Sievers, R. E.; Wendland, M. F.; Dupon, J. W.; Finkbeiner, W. E.; Lipton, M. J.; Parmley, W. W.; Brasch, R. C. *Circulation* **1989**, *80*, 969.
(192) Bremerich, J.; Wendland, M. F.; Arheden, H.; Wyttenbach, R.; Gao, D. W.; Huberty, J. P.; Dae, M. W.; Higgins, C. B.; Saeed, M. *J. Am. Coll. Cardiol.* **1998**, *32*, 787.
(193) Wikstrom, M. G.; Moseley, M. E.; White, D. L.; Dupon, J.; Winkelhake, J. L.; Kopplin, J.; Brasch, R. C. *Invest. Radiol.* **1989**, *24*, 609.
(194) Daldrup, H.; Shames, D. M.; Wendland, M.; Okuhata, Y.; Link, T. M.; Rosenau, W.; Lu, Y.; Brasch, R. C. *Am. J. Roentgenol.* **1998**, *171*, 941.
(195) Gossmann, A.; Okuhata, Y.; Shames, D. M.; Helbich, T. H.; Roberts, T. P. L.; Wendland, M. F.; Huber, S.; Brasch, R. C. *Radiology* **1999**, *213*, 265.
(196) van Dijke, C. F.; Brasch, R. C.; Roberts, T. P.; Weidner, N.; Mathur, A.; Shames, D. M.; Mann, J. S.; Demsar, F.; Lang, P.; Schwickert, H. C. *Radiology* **1996**, *198*, 813.

(197) Turetschek, K.; Huber, S.; Floyd, E.; Helbich, T.; Roberts, T. P. L.; Shames, D. M.; Tarlo, K. S.; Wendland, M. F.; Brasch, R. C. *Radiology* **2001**, *218*, 562.
(198) Brasch, R.; Pham, P.; Shames, D.; Roberts, T.; van Dijke, K.; van Bruggen, N.; Mann, J.; Ostrowitzki, S.; Melnyk, O. *J. Magn. Reson. Imaging* **1997**, *7*, 68.
(199) Aicher, K. P.; Dupon, J. W.; White, D. L.; Aukerman, S. L.; Moseley, M. E.; Juster, R.; Rosenau, W.; Winkelhake, J. L.; Brasch, R. C. *Cancer Res.* **1990**, *50*, 7376.
(200) Schwickert, H. C.; Stiskal, M.; Roberts, T. P.; van Dijke, C. F.; Mann, J.; Muhler, A.; Shames, D. M.; Demsar, F.; Disston, A.; Brasch, R. C. *Radiology* **1996**, *198*, 893.
(201) Murad, G. J. A.; Walbridge, S.; Morrison, P. F.; Garmestani, K.; Degen, J. W.; Brechbiel, M. W.; Oldfield, E. H.; Lonser, R. R. *Clin. Cancer Res.* **2006**, *12*, 3145.
(202) Barrett, T.; Kobayashi, H.; Brechbiel, M.; Choyke, P. L. *Eur. J. Radiol.* **2006**, *60*, 353.
(203) Tyeklar, Z.; Dunham, S. U.; Midelfort, K.; Scott, D. M.; Sajiki, H.; Ong, K.; Lauffer, R. B.; Caravan, P.; McMurry, T. J. *Inorg. Chem.* **2007**, *46*, 6621.
(204) Caravan, P.; Comuzzi, C.; Crooks, W.; McMurry, T. J.; Choppin, G. R.; Woulfe, S. R. *Inorg. Chem.* **2001**, *40*, 2170.
(205) Muller, R. N.; Radüchel, B.; Laurent, S.; Platzek, J.; Piérart, C.; Mareski, P.; Elst, L. V. *Eur. J. Inorg. Chem.* **1999**, *11*, 1949.
(206) Caravan, P.; Cloutier, N. J.; Greenfield, M. T.; McDermid, S. A.; Dunham, S. U.; Bulte, J. W.; Amedio, J. C.; Looby, R. J.; Supkowski, R. M.; Horrocks, W. D.; McMurry, T. J.; Lauffer, R. B. *J. Am. Chem. Soc.* **2002**, *124*, 3152.
(207) Caravan, P.; Parigi, G.; Chasse, J. M.; Cloutier, N. J.; Ellison, J. J.; Lauffer, R. B.; Luchinat, C.; McDermid, S. A.; Spiller, M.; McMurry, T. J. *Inorg. Chem.* **2007**, *46*, 6632.
(208) Zech, S. G.; Eldredge, H. B.; Lowe, M. P.; Caravan, P. *Inorg. Chem.* **2007**, *46*, 3576.
(209) McMurry, T. J.; Parmelee, D. J.; Sajiki, H.; Scott, D. M.; Ouellet, H. S.; Walovitch, R. C.; Tyeklar, Z.; Dumas, S.; Bernard, P.; Nadler, S.; Midelfort, K.; Greenfield, M.; Troughton, J.; Lauffer, R. B. *J. Med. Chem.* **2002**, *45*, 3465.
(210) Lauffer, R. B.; Parmelee, D. J.; Ouellet, H. S.; Dolan, R. P.; Sajiki, H.; Scott, D. M.; Bernard, P. J.; Buchanan, E. M.; Ong, K. Y.; Tyeklár, Z.; Midelfort, K. S.; McMurry, T. J.; Walovitch, R. C. *Acad. Radiol.* **1996**, *3*, S356.
(211) Corot, C.; Violas, J.; Robert, P.; Gagneur, G.; Port, M. *Invest. Radiol.* **2003**, *38*, 311.
(212) Lauffer, R. B.; Parmelee, D. J.; Dunham, S. U.; Ouellet, H. S.; Dolan, R. P.; Witte, S.; McMurry, T. J.; Walovitch, R. C. *Radiology* **1998**, *207*, 529.
(213) Grist, T. M.; Korosec, F. R.; Peters, D. C.; Witte, S.; Walovitch, R. C.; Dolan, R. P.; Bridson, W. E.; Yucel, E. K.; Mistretta, C. A. *Radiology* **1998**, *207*, 539.
(214) Bluemke, D. A.; Stillman, A. E.; Bis, K. G.; Grist, T. M.; Baum, R. A.; D'Agostino, R.; Malden, E. S.; Pierro, J. A.; Yucel, E. K. *Radiology* **2001**, *219*, 114.
(215) Perreault, P.; Edelman, M. A.; Baum, R. A.; Yucel, E. K.; Weisskoff, R. M.; Shamsi, K.; Mohler, E. R. *Radiology* **2003**, *229*, 811.
(216) Rapp, J. H.; Wolff, S. D.; Quinn, S. F.; Soto, J. A.; Meranze, S. G.; Muluk, S.; Blebea, J.; Johnson, S. P.; Rofsky, N. M.; Duerinckx, A.; Foster, G. S.; Kent, K. C.; Moneta, G.; Middlebrook, M. R.; Narra, V. R.; Toombs, B. D.; Pollak, J.; Yucel, E. K.; Shamsi, K.; Weisskoff, R. M. *Radiology* **2005**, *236*, 71.
(217) Goyen, M.; Edelman, M. A.; Perreault, P.; O'Riordan, E.; Bertoni, H.; Taylor, J.; Siragusa, D.; Sharafuddin, M.; Mohler, E. R., III.; Breger, R.; Yucel, E. K.; Shamsi, K.; Weisskoff, R. M. *Radiology* **2005**, *236*, 825.
(218) Zhang, Y.; Choyke, P. L.; Lu, H.; Takahashi, H.; Mannon, R. B.; Zhang, X.; Marcos, H.; Li, K. C. P.; Kopp, J. B. *J. Am. Soc. Nephrol.* **2005**, *16*, 1752.
(219) Turetschek, K.; Floyd, E.; Helbich, T.; Roberts, T. P. L.; Shames, D. M.; Wendland, M. F.; Carter, W. O.; Brasch, R. C. *J. Magn. Reson. Imaging* **2001**, *14*, 237.
(220) Uggeri, F.; Aime, S.; Anelli, P. L.; Botta, M.; Brocchetta, M.; de Haeen, C.; Ermondi, G.; Grandi, M.; Paoli, P. *Inorg. Chem.* **1995**, *34*, 633.
(221) Cavagna, F. M.; Maggioni, F.; Castelli, P. M.; Dapra, M.; Imperatori, L. G.; Lorusso, V.; Jenkins, B. G. *Invest. Radiol.* **1997**, *32*, 780.
(222) Prokop, M.; Schneider, G.; Vanzulli, A.; Goyen, M.; Ruehm, S. G.; Douek, P.; Dapra, M.; Pirovano, G.; Kirchin, M. A.; Spinazzi, A. *Radiology* **2005**, *234*, 399.
(223) Aime, S.; Botta, M.; Fasano, M.; Crich, S. G.; Terreno, E. *J. Biol. Inorg. Chem.* **1996**, *1*, 312.
(224) Aime, S.; Chiaussa, M.; Digilio, G.; Gianolo, E.; Terreno, E. *J. Biol. Inorg. Chem.* **1999**, *4*, 766.
(225) Aime, S.; Botta, M.; Crich, S. G.; Giovenzana, G. B.; Pagliarin, R.; Piccinini, M.; Sisti, M.; Terreno, E. *J. Biol. Inorg. Chem.* **1997**, *2*, 470.
(226) Botta, M.; Quici, S.; Pozzi, G.; Marzanni, G.; Pagliarin, R.; Barra, S.; Crich, S. G. *Org. Biomol. Chem.* **2004**, *2*, 570.
(227) Wallace, R. A.; Haar, J. P. J.; Miller, D. B.; Woulfe, S. R.; Polta, J. A.; Galen, K. P.; Hynes, M. R.; Adzamli, K. *Magn. Reson. Med.* **1998**, *40*, 733.
(228) Tóth, E.; Connac, F.; Helm, L.; Adzamli, K.; Merbach, A. E. *J. Biol. Inorg. Chem.* **1998**, *3*, 606.
(229) Ou, M.-H.; Chen, Y.-M.; Chang, Y.-H.; Lu, W.-K.; Liu, G.-C.; Wang, Y.-M. *Dalton Trans.* **2007**, *26*, 2749.
(230) Schuhmann-Giampieri, G.; Schmitt-Willich, H.; Press, W. R.; Negishi, C.; Weinmann, H. J.; Speck, U. *Radiology* **1992**, *183*, 59.
(231) Reimer, P.; Rummeny, E. J.; Shamsi, K.; Balzer, T.; Daldrup, H. E.; Tombach, B.; Hesse, T.; Berns, T.; Peters, P. E. *Radiology* **1996**, *199*, 177.
(232) Elst, L. V.; Maton, F.; Laurent, S.; Seghi, F.; Chapelle, F.; Muller, R. N. *Magn. Reson. Med.* **1997**, *38*, 604.
(233) Elst, L. V.; Chapelle, F.; Laurent, S.; Muller, R. N. *J. Biol. Inorg. Chem.* **2001**, *6*, 196.
(234) Martin, V. V.; Ralston, W. H.; Hynes, M. R.; Keana, J. F. W. *Bioconjugate Chem.* **1995**, *6*, 616.
(235) Parac-Vogt, T. N.; Kimpe, K.; Laurent, S.; Elst, L. V.; Burtea, C.; Chen, F.; Muller, R. N.; Ni, Y.; Verbruggen, A.; Binnemans, K. *Chem.—Eur. J.* **2005**, *11*, 3077.
(236) Nivorozhkin, A. L.; Kolodziej, A. F.; Caravan, P.; Greenfield, M. T.; Lauffer, R. B.; McMurry, T. J. *Angew. Chem., Int. Ed.* **2001**, *40*, 2903.
(237) Hanaoka, K.; Kikuchi, K.; Terai, T.; Komatsu, T.; Nagano, T. *Chem.—Eur. J.* **2008**, *14*, 987.
(238) Anelli, P. L.; Bertini, I.; Fragai, M.; Lattuada, L.; Luchinat, C.; Parigi, G. *Eur. J. Inorg. Chem.* **2000**, *4*, 625.
(239) Tomaselli, S.; Zanzoni, S.; Ragona, L.; Gianolio, E.; Aime, S.; Assfalg, M.; Molinari, H. *J. Med. Chem.* **2008**, *51*, 6782.
(240) De Leon-Rodriguez, L. M.; Ortiz, A.; Weiner, A. L.; Zhang, S.; Kovacs, Z.; Kodadek, T.; Sherry, A. D. *J. Am. Chem. Soc.* **2002**, *124*, 3514.
(241) Botnar, R. M.; Perez, A. S.; Witte, S.; Wiethoff, A. J.; Laredo, J.; Hamilton, J.; Quist, W.; Parsons, E. C., Jr.; Vaidya, A.; Kolodziej, A. F.; Barrett, J. A.; Graham, P. B.; Weisskoff, R. M.; Manning, W. J.; Johnstone, M. T. *Circulation* **2004**, *109*, 2023.
(242) Overoye-Chan, K.; Koerner, S.; Looby, R. J.; Kolodziej, A. F.; Zech, S. G.; Deng, Q.; Chasse, J. M.; McMurry, T. J.; Caravan, P. *J. Am. Chem. Soc.* **2008**, *130*, 6025.
(243) De Leon-Rodriguez, L. M.; Kovacs, Z. *Bioconjugate Chem.* **2008**, *19*, 391.
(244) Aime, S.; Frullano, L.; Crich, S. G. *Angew. Chem., Int. Ed.* **2002**, *41*, 1017.
(245) Karfeld, L. S.; Bull, S. R.; Davis, N. E.; Meade, T. J.; Barron, A. E. *Bioconjugate Chem.* **2007**, *18*, 1697.
(246) Yang, J. J.; Yang, J.; Wei, L.; Zurkiya, O.; Yang, W.; Li, S.; Zou, J.; Zhou, Y.; Maniccia, A. L. W.; Mao, H.; Zhao, F.; Malchow, R.; Zhao, S.; Johnson, J.; Hu, X.; Krogstad, E.; Liu, Z.-R. *J. Am. Chem. Soc.* **2008**, *130*, 9260.
(247) Gustafsson, B.; Youens, S.; Louie, A. Y. *Bioconjugate Chem.* **2006**, *17*, 538.
(248) Langereis, S.; Kooistra, H.-A. T.; Genderen, M. H. P. v.; Meijer, E. W. *Org. Biomol. Chem.* **2004**, *2*, 1271.
(249) Dirksen, A.; Langereis, S.; Waal, B. F. M. d.; Genderen, M. H. P. v.; Hackeng, T. M.; Meijer, E. W. *Chem. Commun.* **2005**, *22*, 2811.
(250) Jung, H.-i.; Kettunen, M. I.; Davletov, B.; Brindle, K. M. *Bioconjugate Chem.* **2004**, *15*, 983.
(251) Neves, A. A.; Krishnan, A. S.; Kettunen, M. I.; Hu, D.; de Backer, M. M.; Davletov, B.; Brindle, K. M. *Nano Lett.* **2007**, *7*, 1419.
(252) Krishnan, A. S.; Neves, A. A.; de Backer, M. M.; Hu, D.-E.; Davletov, B.; Kettunen, M. I.; Brindle, K. M. *Radiology* **2008**, *246*, 854.
(253) Hnatowich, D. J.; Layne, W. W.; Childs, R. L.; Lanteigne, D.; Davis, M. A.; Griffin, T. W.; Doherty, P. W. *Science* **1983**, *220*, 613.
(254) Paik, C. H.; Ebbert, M. A.; Murphy, P. R.; Lassman, C. R.; Reba, R. C.; Eckelman, W. C.; Pak, K. Y.; Powe, J.; Steplewski, Z.; Koprowski, H. *J. Nucl. Med.* **1983**, *24*, 1158.
(255) Unger, E. C.; Totty, W. G.; Neufeld, D. M.; Otsuka, F. L.; Murphy, W. A.; Welch, M. S.; Connett, J. M.; Philpott, G. W. *Invest. Radiol.* **1985**, *20*, 693.
(256) Anderson-Berg, W. T.; Strand, M.; Lempert, T. E.; Rosenbaum, A. E.; Joseph, P. M. *J. Nucl. Med.* **1986**, *27*, 829.
(257) Shahbazi-Gahrouei, D.; Williams, M.; Rizvi, S.; Allen, B. J. *J. Magn. Reson. Imaging* **2001**, *14*, 169.
(258) Kuriu, Y.; Otsuji, E.; Kin, S.; Nakase, Y.; Fukuda, K.-I.; Okamoto, K.; Hagiwara, A.; Yamagishi, H. *J. Surg. Oncol.* **2006**, *94*, 144.
(259) Curtet, C.; Tellier, C.; Bohy, J.; Conti, M. L.; Saccavini, J. C.; Thedrez, P.; Douillard, J. Y.; Chatal, J. F.; Koprowski, H. *Proc. Natl. Acad. Sci.* **1986**, *83*, 4277.

(260) Curtet, C.; Bourgoin, C.; Bohy, J.; Saccavini, J.-C.; Thédrez, P.; Akoka, S.; Tellier, C.; Chatal, J.-F. *Int. J. Cancer* **1988**, *41*, 126.
(261) Shreve, P.; Aisen, A. M. *Magn. Reson. Imaging* **1986**, *3*, 336.
(262) Manabe, Y.; Longley, C.; Furmanski, P. *Biochim. Biophys. Acta* **1986**, *883*, 460.
(263) Göhr-Rosenthal, S.; Schmitt-Wilich, H.; Ebert, W.; Conrad, J. *Invest. Radiol.* **1993**, *28*, 789.
(264) Artemov, D.; Mori, N.; Ravi, R.; Bhujwalla, Z. M. *Cancer Res.* **2003**, *63*, 2723.
(265) Fagnani, R.; Hagan, M. S.; Bartholomew, R. *Cancer Res.* **1990**, *50*, 3638.
(266) Fagnani, R.; Halpern, S.; Hagan, M. S. *Nucl. Med. Commun.* **1995**, *16*, 362.
(267) Mehvar, R. *J. Controlled Release* **2000**, *69*, 1.
(268) Gibby, W. A.; Bogdan, A.; Ovitt, T. W. *Invest. Radiol.* **1989**, *24*, 302.
(269) Armitage, F. E.; Richardson, D. E.; Li, K. C. P. *Bioconjugate Chem.* **1990**, *1*, 365.
(270) Rongved, P.; Klaveness, J. *Carbohydr. Res.* **1991**, *214*, 315.
(271) Bligh, S. W. A.; Harding, C. T.; Sadler, P. J.; Bulman, R. A.; Bydder, G. M.; Pennock, J. M.; Kelly, J. D.; Clatham, I. A.; Marriott, J. A. *Magn. Reson. Med.* **1991**, *17*, 516.
(272) Mann, J. S.; Huang, J. C.; Keana, J. F. W. *Bioconjugate Chem.* **1992**, *3*, 154.
(273) Chu, W.-J.; Elgavish, G. A. *NMR Biomed.* **1995**, *8*, 159.
(274) Meyer, D.; Schaefer, M.; Chambon, C.; Beaute, S. *Invest. Radiol.* **1994**, *29*, S90.
(275) Rebizak, R.; Schaefer, M.; Dellacherie, E. *Bioconjugate Chem.* **1997**, *8*, 605.
(276) Rebizak, R.; Schaefer, M.; Dellacherie, E. *Bioconjugate Chem.* **1998**, *9*, 94.
(277) Helbich, T. H.; Gossman, A.; Mareski, P. A.; Radüchel, B.; Roberts, T. P. L.; Shames, D. M.; Mühler, M.; Turetschek, K.; Brasch, R. C. *J. Magn. Reson. Imaging* **2000**, *11*, 694.
(278) Corsi, D. M.; Elst, L. V.; Muller, R. N.; van Bekkum, H.; Peters, J. A. *Chem.—Eur. J.* **2001**, *7*, 64.
(279) Lebduskova, P.; Kotek, J.; Hermann, P.; VanderElst, L.; Muller, R. N.; Lukes, I.; Peters, J. A. *Bioconjugate Chem.* **2004**, *15*, 881.
(280) Gibby, W. A.; Billings, J.; Hall, J.; Ovitt, T. W. *Invest. Radiol.* **1990**, *25*, 164.
(281) Wang, S. C.; Wikstrom, M. G.; White, D. L. *Radiology* **1990**, *175*, 483.
(282) Wikstrom, M.; Martinussen, H. J.; Wikstrom, G.; Ericsson, A.; Nyman, R.; Waldenstrom, A.; Hemmingsson, A. *Acta Radiol.* **1992**, *33*, 301.
(283) Sirlin, C. B.; Vera, D. R.; Corbeil, J. A.; Caballero, M. B.; Buxton, R. B.; Mattrey, R. F. *Acad. Radiol.* **2004**, *11*, 1361.
(284) Loubeyre, P.; Canet, E.; Zhao, S.; Benderbous, S.; Amiel, M.; Revel, D. *Invest. Radiol.* **1996**, *31*, 288.
(285) Casali, C.; Canet, E.; Obadia, F. J.; Benderbous, S.; Desenfant, A.; Revel, D.; Janier, M. *Acad. Radiol.* **1998**, *5*, S214.
(286) Kroft, L. J. M.; Doornbos, J.; Benderbous, S.; De Roos, A. *J. Magn. Reson. Imaging* **1999**, *9*, 777.
(287) Jacobs, R. E.; Fraser, S. E. *Science* **1994**, *263*, 681.
(288) Huber, M. M.; Staubli, A. B.; Kustedjo, K.; Gray, M. H. B.; Shih, J.; Fraser, S. E.; Jacobs, R. E.; Meade, T. J. *Bioconjugate Chem.* **1998**, *9*, 242.
(289) Modo, M.; Cash, D.; Mellodew, K.; Williams, S. C. R.; Fraser, S. E.; Meade, T. J.; Price, J.; Hodges, H. *Neuroimage* **2002**, *17*, 803.
(290) Takahashi, M.; Hara, Y.; Aoshima, K.; Kurihara, H.; Oshikawa, T.; Yamashita, M. *Tetrahedron Lett.* **2000**, *41*, 8485.
(291) Fulton, D. A.; Elemento, E. M.; Aime, S.; Chaabane, L.; Botta, M.; Parker, D. *Chem. Commun.* **2006**, *10*, 1064.
(292) Tanaka, H.; Ando, Y.; Wada, M.; Takahashi, T. *Org. Biomol. Chem.* **2005**, *3*, 3311.
(293) Bammer, R.; de Crespigny, A. J.; Howard, D.; Seri, S.; Hashiguchi, Y.; Nakatani, A.; Moseley, M. E. *Magn. Reson. Imaging* **2004**, *22*, 619.
(294) de Crespigny, A. J.; Howard, D.; D'Arceuil, H.; Muller, H.; Agoston, A. T.; Seri, S.; Hashiguchi, Y.; Fujimoto, C.; Nakatani, A.; Moseley, M. E. *Magn. Reson. Imaging* **1999**, *17*, 1297.
(295) Vera, D. R.; Buonocore, M. H.; Wisner, E. R.; Katzberg, R. W.; Stadalnik, R. C. *Acad. Radiol.* **1995**, *2*, 497.
(296) André, J. P.; Geraldes, C. F. G. C.; Martins, J. A.; Merbach, A. E.; Prata, M. I. M.; Santos, A. C.; de Lima, J. J. P.; Tóth, E. *Chem.—Eur. J.* **2004**, *10*, 5804.
(297) Baía, P.; André, J. P.; Geraldes, C. F. G. C.; Martins, J. A.; Merbach, A. E.; Tóth, E. *Eur. J. Inorg. Chem.* **2005**, *11*, 2110.
(298) Prata, M. I. M.; Santos, A. C.; Torres, S.; André, J. P.; Martins, J. A.; Neves, M.; García-Martín, M. L.; Rodrigues, T. B.; López-Larrubia, P.; Cerdán, S.; Geraldes, C. F. G. C. *Contrast Media Mol. Imaging* **2006**, *1*, 246.
(299) Unger, E. C.; Shen, D.-K.; Fritz, T. A. *J. Magn. Reson. Imaging* **1993**, *3*, 195.
(300) Unger, E.; Fritz, T.; Wu, G.; Shen, D.; Kulik, B.; New, T.; Crowell, M.; Wilke, N. *J. Liposome Res.* **1994**, *4*, 811.
(301) Krause, W.; Klopp, R.; Leike, J.; Sachse, A.; Schuhmann-Giampieri, G. *J. Liposome Res.* **1995**, *5*, 1.
(302) Torchilin, V. P. *Mol. Med. Today* **1996**, *2*, 242.
(303) Mulder, W. J. M.; Strijkers, G. J.; van Tilborg, G. A. F.; Griffioen, A. W.; Nicolay, K. *NMR Biomed.* **2006**, *19*, 142.
(304) Terreno, E.; Delli Castelli, D.; Cabella, C.; Dastrù, W.; Sanino, A.; Stancanello, J.; Tei, L.; Aime, S. *Chem. Biodiversity* **2008**, *5*, 1901.
(305) Barsky, D.; Pütz, B.; Schulten, K.; Magin, R. L. *Magn. Reson. Med.* **1992**, *24*, 1.
(306) Pütz, B.; Barsky, D.; Schulten, K. *J. Liposome Res.* **1994**, *4*, 771.
(307) Bacic, G.; Niesman, M. R.; Bennett, H. F.; Magin, R. L.; Swartz, H. M. *Magn. Reson. Med.* **1988**, *6*, 445.
(308) Caride, V. J.; Sostman, H. D.; Winchell, R. J.; Gore, J. C. *Magn. Reson. Imaging* **1984**, *2*, 107.
(309) Navon, G.; Panigel, R.; Valensin, G. *Magn. Reson. Med.* **1986**, *3*, 876.
(310) Tilcock, C.; Unger, E.; Cullis, P.; MacDougall, P. *Radiology* **1989**, *171*, 77.
(311) Fossheim, S. L.; Fahlvik, A. K.; Klaveness, J.; Muller, R. N. *Magn. Reson. Imaging* **1999**, *17*, 83.
(312) Løkling, K.-E.; Fossheim, S. L.; Skurtveit, R.; Bjørnerud, A.; Klaveness, J. *Magn. Reson. Imaging* **2001**, *19*, 731.
(313) Løkling, J.-E.; Skurtveit, R.; Bjørnerud, A.; Fossheim, S. L. *Magn. Reson. Med.* **2004**, *51*, 688.
(314) Wang, T.; Hossann, M.; Reinl, H. M.; Peller, M.; Eibl, H.; Reiser, M.; Issels, R. D.; Lindner, L. H. *Contrast Media Mol. Imaging* **2008**, *3*, 19.
(315) Kabalka, G.; Buonocore, E.; Hubner, K.; Moss, T.; Norley, N.; Huang, L. *Radiology* **1987**, *163*, 255.
(316) Kabalka, G. W.; Buonocore, E.; Hubner, K.; Davis, M.; Huang, L. *Magn. Reson. Med.* **1988**, *8*, 89.
(317) Kabalka, G. W.; Davis, M. A.; Moss, T. H.; Buonocore, E.; Hubner, K.; Holmberg, E.; Maruyama, K.; Huang, L. *Magn. Reson. Med.* **1991**, *19*, 406.
(318) Tilcock, C.; Ahkong, Q. F.; Koenig, S. H.; Brown, R. D.; Davis, M.; Kabalka, G. *Magn. Reson. Imaging* **1992**, *27*, 44.
(319) Storrs, R. W.; Tropper, F. D.; Li, H. Y.; Song, C. K.; Kuniyoshi, J. K.; Sipkins, D. A.; Li, K. C. P.; Bednarski, M. D. *J. Am. Chem. Soc.* **1995**, *117*, 7301.
(320) Gløgård, C.; Stensrud, G.; Aime, S. *Magn. Reson. Chem.* **2003**, *41*, 585.
(321) Vaccaro, M.; Accardo, A.; Tesauro, D.; Mangiapia, G.; Lof, D.; Schillen, K.; Soderman, O.; Morelli, G.; Paduano, L. *Langmuir* **2006**, *22*, 6635.
(322) Glogard, C.; Hovland, R.; Fossheim, S. L.; Aasen, A. J.; Klaveness, J. *J. Chem. Soc., Perkin Trans. 2* **2000**, *5*, 1047.
(323) André, J. P.; Tóth, E.; Fischer, H.; Seelig, A.; Mäcke, H. R.; Merbach, A. E. *Chem.—Eur. J.* **1999**, *5*, 2977.
(324) Hovland, R.; Glogard, C.; Aasen, A. J.; Klaveness, J. *Org. Biomol. Chem.* **2003**, *1*, 644.
(325) Hovland, R.; Glogard, C.; Aasen, A. J.; Klaveness, J. *J. Chem. Soc., Perkin Trans. 2* **2001**, *6*, 929.
(326) Zhang, G.; Zhang, R.; Wen, X.; Li, L.; Li, C. *Biomacromolecules* **2008**, *9*, 36.
(327) Ward, K. M.; Aletras, A. H.; Balaban, R. S. *J. Magn. Reson. Imaging* **2000**, *143*, 79.
(328) Aime, S.; Delli Castelli, D.; Terreno, E. *Angew. Chem., Int. Ed.* **2005**, *44*, 5513.
(329) Zhao, J. M.; Har-el, Y.; McMahon, M. T.; Zhou, J.; Sherry, A. D.; Sgouros, G.; Bulte, J. W. M.; van Zijl, P. C. M. *J. Am. Chem. Soc.* **2008**, *130*, 5178.
(330) Aime, S.; Delli Castelli, D.; Lawson, D.; Terreno, E. *J. Am. Chem. Soc.* **2007**, *129*, 2430.
(331) Terreno, E.; Barge, A.; Beltrami, L.; Cravotto, G.; Delli Castelli, D.; Fedeli, F.; Jebasingh, B.; Aime, S. *Chem. Commun.* **2008**, *5*, 600.
(332) Terreno, E.; Delli Castelli, D.; Violante, E.; Sanders, H. M. H. F.; Sommerdijk, A. J. M.; Aime, S. *Chem.—Eur. J.* **2009**, *15*, 1440.
(333) Terreno, E.; Cabella, C.; Carrera, C.; Delli Castelli, D.; Mazzon, R.; Rollet, S.; Stancanello, J.; Visigalli, M.; Aime, S. *Angew. Chem., Int. Ed.* **2007**, *46*, 966.
(334) Delli Castelli, D.; Terreno, E.; Carrera, C.; Giovenzana, G. B.; Mazzon, R.; Rollet, S.; Visigalli, M.; Aime, S. *Inorg. Chem.* **2008**, *47*, 2928.
(335) Terreno, E.; Delli Castelli, D.; Milone, L.; Rollet, S.; Stancanello, J.; Violante, E.; Aime, S. *Contrast Media Mol. Imaging* **2008**, *3*, 38.
(336) Langereis, S.; Keupp, J.; van Velthoven, J. L. J.; de Roos, I. H. C.; Burdinski, D.; Pikkemaat, J. A.; Grull, H. *J. Am. Chem. Soc.* **2009**, *131*, 1380.

(337) Grant, C. W. M.; Karlik, S.; Florio, E. *Magn. Reson. Med.* **1989**, *11*, 236.
(338) Karlik, S.; Florio, E.; Grant, C. W. M. *Magn. Reson. Med.* **1991**, *19*, 56.
(339) Unger, E.; Shen, D.-K.; Wu, G.; Fritz, T. *Magn. Reson. Imaging* **1991**, *22*, 304.
(340) Unger, E. C.; Winokur, T.; MacDougall, P.; Rosenblum, J.; Clair, M.; Gatenby, R.; Tilcock, C. *Radiology* **1989**, *171*, 81.
(341) Frich, L.; Bjørnerud, A.; Fossheim, S.; Tillung, T.; Gladhaug, I. *Magn. Reson. Med.* **2004**, *52*, 1302.
(342) Viglianti, B. L.; Abraham, S. A.; Michelich, C. R.; Yarmolenko, P. S.; MacFall, J. R.; Bally, M. B.; Dewhirst, M. W. *Magn. Reson. Med.* **2004**, *51*, 1153.
(343) Frias, J. C.; Williams, K. J.; Fisher, E. A.; Fayad, Z. A. *J. Am. Chem. Soc.* **2004**, *126*, 16316.
(344) Mulder, W. J. M.; Douma, K.; Koning, G. A.; van Zandvoort, M. A.; Lutgens, E.; Daemen, M. J.; Nicolay, K.; Strijkers, G. J. *Magn. Reson. Med.* **2006**, *55*, 1170.
(345) Chen, W.; Vucic, E.; Leupold, E.; Mulder, W. J. M.; Cormode, D. P.; Briley-Saebo, K. C.; Barazza, A.; Fisher, E. A.; Dathe, M.; Fayad, Z. A. *Contrast Media Mol. Imaging* **2008**, *3*, 233.
(346) Unger, E. C.; Fritz, T. A.; Tilcock, C.; New, T. E. *J. Magn. Reson. Imaging* **1991**, *1*, 689.
(347) Storrs, R. W.; Tropper, F. D.; Li, H. Y.; Song, C. K.; Sipkins, D. A.; Kuniyoshi, J. K.; Bednarski, M. D.; Strauss, H. W.; Li, K. C. P. *J. Magn. Reson. Imaging* **1995**, *5*, 719.
(348) Bertini, I.; Bianchini, F.; Calorini, L.; Colagrande, S.; Fragai, M.; Franchi, A.; Gallo, O.; Gavazzi, C.; Luchinat, C. *Magn. Reson. Med.* **2004**, *52*, 669.
(349) Ayyagari, A. L.; Zhang, X.; Ghaghada, K. B.; Annapragada, A.; Hu, X.; Bellamkonda, R. V. *Magn. Reson. Imaging* **2006**, *55*, 1023.
(350) van Tilborg, G. A. F.; Strijkers, G. J.; Pouget, E. M.; Reutelingsperger, C. P. M.; Sommerdijk, N. A. J. M.; Nicolay, K.; Mulder, W. J. M. *Magn. Reson. Imaging* **2008**, *60*, 1444.
(351) Accardo, A.; Tesauro, D.; Roscigno, P.; Gianolio, E.; Paduano, L.; D'Errico, G.; Pedone, C.; Morelli, G. *J. Am. Chem. Soc.* **2004**, *126*, 3097.
(352) Mangiapia, G.; Accardo, A.; Lo Celso, F.; Tesauro, D.; Morelli, G.; Radulescu, A.; Paduano, L. *J. Phys. Chem. B* **2004**, *108*, 17611.
(353) Morisco, A.; Accardo, A.; Gianolio, E.; Tesauro, D.; Benedetti, E.; Morelli, G. *J. Pept. Sci.* **2009**, *15*, 242.
(354) Mulder, W. J. M.; Strijkers, G. J.; Griffioen, A. W.; van Bloois, L.; Molema, G.; Storm, G.; Koning, G. A.; Nicolay, K. *Bioconjugate Chem.* **2004**, *15*, 799.
(355) Erdogan, S.; Medarova, Z. O.; Roby, A.; Moore, A.; Torchilin, V. P. *J. Magn. Reson. Imaging* **2008**, *27*, 574.
(356) Vuu, K.; Xie, J.; McDonald, M. A.; Bernardo, M.; Hunter, F.; Zhang, Y.; Li, K.; Bednarski, M.; Guccione, S. *Bioconjugate Chem.* **2005**, *16*, 995.
(357) Oliver, M.; Ahmad, A.; Kamaly, N.; Perouzel, E.; Caussin, A.; Keller, M.; Herlihy, A.; Bell, J.; Miller, A. D.; Jorgensen, M. R. *Org. Biomol. Chem.* **2006**, *4*, 3489.
(358) Kamaly, N.; Kalber, T.; Ahmad, A.; Oliver, M. H.; So, P.-W.; Herlihy, A. H.; Bell, J. D.; Jorgensen, M. R.; Miller, A. D. *Bioconjugate Chem.* **2008**, *19*, 118.
(359) Esposito, G.; Crich, S. G.; Aime, S. *ChemMedChem* **2008**, *3*, 1858.
(360) Douglas, T.; Young, M. *Nature* **1998**, *393*, 152.
(361) Wang, Q.; Lin, T.; Tang, L.; Johnson, J. E.; Finn, M. G. *Angew. Chem., Int. Ed.* **2002**, *41*, 459.
(362) Raja, K. S.; Wang, Q.; Gonzalez, M. J.; Manchester, M.; Johnson, J. E.; Finn, M. G. *Biomacromolecules* **2003**, *4*, 472.
(363) Allen, M.; Bulte, J. W. M.; Liepold, L.; Basu, G.; Zywicke, H. A.; Frank, J. A.; Young, M.; Douglas, T. *Magn. Reson. Imaging* **2005**, *54*, 807.
(364) Anderson, E. A.; Isaacman, S.; Peabody, D. S.; Wang, E. Y.; Canary, J. W.; Kirshenbaum, K. *Nano Lett.* **2006**, *6*, 1160.
(365) Prasuhn, D. E. J.; Yeh, R. M.; Obenaus, A.; Manchester, M.; Finn, M. G. *Chem. Commun.* **2007**, *12*, 1269.
(366) Hooker, J. M.; Datta, A.; Botta, M.; Raymond, K. N.; Francis, M. B. *Nano Lett.* **2007**, *7*, 2207.
(367) Datta, A.; Hooker, J. M.; Botta, M.; Francis, M. B.; Aime, S.; Raymond, K. N. *J. Am. Chem. Soc.* **2008**, *130*, 2546.
(368) Vasalatiy, O.; Gerard, R. D.; Zhao, P.; Sun, X.; Sherry, A. D. *Bioconjugate Chem.* **2008**, *19*, 598.
(369) Wilson, L. J. *Electrochem. Soc. Interface* **1999**, *8*, 24.
(370) Mikawa, M.; Kato, H.; Okumura, M.; Narazaki, M.; Kanazawa, Y.; Miwa, N.; Shinohara, H. *Bioconjugate Chem.* **2001**, *12*, 510.
(371) Funasaka, H.; Sakurai, K.; Oda, Y.; Yamamoto, K.; Takahashi, T. *Chem. Phys. Lett.* **1995**, *232*, 273.
(372) Kato, H.; Suenaga, K.; Mikawa, M.; Okumura, M.; Miwa, N.; Yashiro, A.; Fujimura, H.; Mizuno, A.; Nishida, Y.; Kobayaashi, K.; Shinohara, H. *Chem. Phys. Lett.* **2000**, *324*, 255.
(373) Kato, H.; Kanazawa, Y.; Okumura, M.; Taninaka, A.; Yokawa, T.; Shinohara, H. *J. Am. Chem. Soc.* **2003**, *125*, 4391.
(374) Shu, C.-Y.; Gan, L.-H.; Wang, C.-R.; Pei, X.-L.; Han, H.-B. *Carbon* **2006**, *44*, 496.
(375) Ge, Z.; Duchamp, J. C.; Cai, T.; Gibson, H. W.; Dorn, H. C. *J. Am. Chem. Soc.* **2005**, *127*, 16292.
(376) Fatouros, P. P.; Corwin, F. D.; Chen, Z.-J.; Broaddus, W. C.; Tatum, J. L.; Kettenmann, B.; Ge, Z.; Gibson, H. W.; Russ, J. L.; Leonard, A. P.; Duchamp, J. C.; Dorn, H. C. *Radiology* **2006**, *240*, 756.
(377) Bolskar, R. D.; Benedetto, A. F.; Husebo, L. O.; Price, R. E.; Jackson, E. F.; Wallace, S.; Wilson, L. J.; Alford, J. M. *J. Am. Chem. Soc.* **2003**, *125*, 5471.
(378) Raebiger, J. W.; Bolskar, R. D. *J. Phys. Chem. C* **2008**, *112*, 6605.
(379) Toth, E.; Bolskar, R. D.; Borel, A.; Gonzalez, G.; Helm, L.; Merbach, A. E.; Sitharaman, B.; Wilson, L. J. *J. Am. Chem. Soc.* **2005**, *127*, 799.
(380) Sitharaman, B.; Bolskar, R. D.; Rusakova, I.; Wilson, L. J. *Nano Lett.* **2004**, *4*, 2373.
(381) Shu, C.-Y.; Zhang, E.-Y.; Xiang, J.-F.; Zhu, C.-F.; Wang, C.-R.; Pei, X.-L.; Han, H.-B. *J. Phys. Chem. B* **2006**, *110*, 15597.
(382) Laus, S.; Sitharaman, B.; Toth, E.; Bolskar, R. D.; Helm, L.; Asokan, S.; Wong, M. S.; Wilson, L. J.; Merbach, A. E. *J. Am. Chem. Soc.* **2005**, *127*, 9368.
(383) Laus, S.; Sitharaman, B.; Toth, E.; Bolskar, R. D.; Helm, L.; Wilson, L. J.; Merbach, A. E. *J. Phys. Chem. C* **2007**, *111*, 5633.
(384) Sitharaman, B.; Tran, L. A.; Pham, Q. P.; Bolskar, R. D.; Muthupillai, R.; Flamm, S. D.; Mikos, A. G.; Wilson, L. J. *Contrast Media Mol. Imaging* **2007**, *2*, 139.
(385) Bolskar, R. D. *Nanomedicine* **2008**, *3*, 201.
(386) Sitharaman, B.; Kissell, K. R.; Hartman, K. B.; Tran, L. A.; Baikalov, A.; Rusakova, I.; Sun, Y.; Khant, H. A.; Ludtke, S. J.; Chiu, W.; Laus, S.; Toth, E.; Helm, L.; Merbach, A. E.; Wilson, L. J. *Chem. Commun.* **2005**, *31*, 3915.
(387) Sitharaman, B.; Wilson, L. J. *Int. J. Nanomedicine* **2006**, *1*, 291.
(388) Hartman, K. B.; Laus, S.; Bolskar, R. D.; Muthupillai, R.; Helm, L.; Toth, E.; Merbach, A. E.; Wilson, L. J. *Nano Lett.* **2008**, *8*, 415.
(389) Mackeyev, Y.; Hartman, K. B.; Ananta, J. S.; Lee, A. V.; Wilson, L. J. *J. Am. Chem. Soc.* **2009**, *131*, 8342.
(390) Coroiu, I. *J. Magn. Magn. Mater.* **1999**, *201*, 449.
(391) Jung, C. W.; Jacobs, P. *Magn. Reson. Imaging* **1995**, *13*, 661.
(392) Laurent, S.; Forge, D.; Port, M.; Roch, A.; Robic, C.; Vander Elst, L.; Muller, R. N. *Chem. Rev.* **2008**, *108*, 2064.
(393) Blakemore, R. P.; Frankel, R. *Sci. Am.* **1981**, *246*, 58.
(394) Fleet, M. *Acta Crystallogr., B* **1981**, *37*, 917.
(395) Weiss, P. *J. Phys. (Paris)* **1907**, *6*, 661.
(396) Neel, L. *Ann. Geophys.* **1949**, *5*, 99.
(397) Kumar, D.; Narayan, J.; Kvit, A. V.; Sharma, A. K.; Sankar, J. *J. Magn. Magn. Mater.* **2001**, *232*, 161.
(398) Martinez, B.; Roig, A.; Obradors, X.; Molins, E.; Rouanet, A.; Monty, C. *J. Appl. Phys.* **1996**, *79*, 2580.
(399) Bean, C. P. *J. Appl. Physiol.* **1995**, *26*, 1381.
(400) Bean, C. P.; Livingston, J. D. *J. Appl. Physiol.* **1959**, *30*, 120S.
(401) Dormann, J. L.; Spinu, L.; Tronc, E.; Jolivet, J. P.; Lucari, F.; D'Orazio, F.; Fiorani, D. *J. Magn. Magn. Mater.* **1998**, *183*, L255.
(402) Zeng, P.; Kline, T. L.; Wang, J.-p.; Wiedmann, T. S. *J. Magn. Magn. Mater.* **2009**, *321*, 373.
(403) Rosensweig, R. E. *J. Magn. Magn. Mater.* **2002**, *252*, 370.
(404) Gueron, M. *J. Magn. Reson.* **1975**, *19*, 58.
(405) Vega, A. J.; Fiat, D. *Mol. Phys.* **1976**, *31*, 347.
(406) Caravan, P.; Greenfield, M. T.; Bulte, J. W. M. *Magn. Reson. Med.* **2001**, *46*, 917.
(407) Roch, A.; Gossuin, Y.; Muller, R. N.; Gillis, P. *J. Magn. Magn. Mater.* **2005**, *293*, 532.
(408) Bowen, C. V.; Zhang, X.; Saab, G.; Gareau, P. J.; Rutt, B. K. *Magn. Reson. Med.* **2002**, *48*, 52.
(409) Hartung, A.; Lisy, M. R.; Herrmann, K.-H.; Hilger, I.; Schüler, D.; Lang, C.; Bellemann, M. E.; Kaiser, W. A.; Reichenbach, J. R. *J. Magn. Magn. Mater.* **2007**, *311*, 454.
(410) Simon, G.; Bauer, J.; Saborovski, O.; Fu, Y.; Corot, C.; Wendland, M.; Daldrup-Link, H. *Eur. Radiol.* **2006**, *16*, 738.
(411) Rad, A. M.; Arbab, A. S.; Iskander, A. S. M.; Jiang, Q.; Soltanian-Zadeh, H. *J. Magn. Reson. Imaging* **2007**, *26*, 366.
(412) Bumb, A.; Brechbiel, M. W.; Choyke, P. L.; Fugger, L.; Eggeman, A.; Prabhakaran, D.; Hutchinson, J.; Dobson, P. J. *Nanotechnology* **2008**, *19*, 335601.
(413) Alcalá, M. D.; Real, C. *Solid State Ionics* **2006**, *177*, 955.
(414) Woo, K.; Hong, J.; Ahn, J.-P. *J. Magn. Magn. Mater.* **2005**, *293*, 177.
(415) Lyon, J. L.; Fleming, D. A.; Stone, M. B.; Schiffer, P.; Williams, M. E. *Nano Lett.* **2004**, *4*, 719.
(416) Lin, J.; Zhou, W.; Kumbhar, A.; Wiemann, J.; Fang, J.; Carpenter, E. E.; O'Connor, C. J. *J. Solid State Chem.* **2001**, *159*, 26.
(417) Bach-Gansmo, T. *Acta Radiol.* **1993**, *387*, 1.

(418) Hahn, P. F.; Stark, D. D.; Lewis, J. M.; Saini, S.; Elizondo, G.; Weissleder, R.; Fretz, C. J.; Ferrucci, J. T. *Radiology* **1990**, *175*, 695.
(419) Weissleder, R.; Stark, D. D.; Engelstad, B. L.; Bacon, B. R.; Compton, C. C.; White, D. L.; Jacobs, P.; Lewis, J. *Am. J. Roentgenol.* **1989**, *152*, 167.
(420) Reimer, P.; Rummeny, E. J.; Daldrup, H. E.; Balzer, T.; Tombach, B.; Berns, T.; Peters, P. E. *Radiology* **1995**, *195*, 489.
(421) Reimer, P.; Tombach, B. *Eur. Radiol.* **1998**, *8*, 1198.
(422) McLachlan, S. J.; Morris, M. R.; Lucas, M. A.; Fisco, R. A.; Eakins, M. N.; Fowler, D. R.; Scheetz, R. B.; Olukotun, A. Y. *J. Magn. Reson. Imaging* **1994**, *4*, 301.
(423) Stillman, A. E.; Wilke, N.; Li, D.; Haacke, M.; McLachlan, S. *J. Comput. Assist. Tomogr.* **1996**, *20*, 51.
(424) Stillman, A. E.; Wilke, N.; Jerosch-Herold, M. *J. Magn. Reson. Imaging* **1997**, *7*, 765.
(425) Mayo-Smith, W. W.; Saini, S.; Slater, G.; Kaufman, J. A.; Sharma, P.; Hahn, P. F. *Am. J. Roentgenol.* **1996**, *166*, 73.
(426) Anzai, Y.; Brunberg, J. A.; Lufkin, R. B. *J. Magn. Reson. Imaging* **1997**, *7*, 774.
(427) Anzai, Y.; Blackwell, K. E.; Hirschowitz, S. L.; Rogers, J. W.; Sato, Y.; Yuh, W. T.; Runge, V. M.; Morris, M. R.; McLachlan, S. J.; Lufkin, R. B. *Radiology* **1994**, *192*, 709.
(428) Saeed, M.; Wendland, M. F.; Engelbrecht, M.; Sakuma, H.; Higgins, C. B. *Eur. Radiol.* **1998**, *8*, 1047.
(429) Simonsen, C. Z.; Ostergaard, L.; Vestergaard-Poulsen, P.; Rohl, L.; Bjornerud, A.; Gyldensted, C. *J. Magn. Reson. Imaging* **1999**, *9*, 342.
(430) Weissleder, R.; Lee, A. S.; Khaw, B. A.; Shen, T.; Brady, T. J. *Radiology* **1992**, *182*, 381.
(431) Weissleder, R.; Lee, A. S.; Fischman, A. J.; Reimer, P.; Shen, T.; Wilkinson, R.; Callahan, R. J.; Brady, T. J. *Radiology* **1991**, *181*, 245.
(432) Wang, Y. X.; Hussain, S. M.; Krestin, G. P. *Eur. Radiol.* **2001**, *11*, 2319.
(433) Magnetic Resonance—Technology Information Portal. http://www.mr-tip.com (accessed November 3, 2009).
(434) Ferumoxytol (Feraheme) Injection. http://www.fda.gov/AboutFDA/CentersOffices/CDER/ucm170316.htm (accessed November 3, 2009).
(435) Corot, C.; Port, M.; Guilbert, I.; Robert, P.; Raynal, I.; Robic, C.; Raynand, J. S.; Prigent, P.; Dencausse, A.; Idee, J. M. In *Molecular and Cellular MR Imaging*; Modo, M. M. J., Bulte, J. W. M., Eds.; Taylor & Francis Group, LLC: Boca Raton, FL, 2007.
(436) Andrews, N. C. *N. Engl. J. Med.* **1999**, *341*, 1986.
(437) LaConte, L.; Nitin, N.; Bao, G. *Mater. Today* **2005**, *8*, 32.
(438) Bacon, B. R.; Stark, D. D.; Park, C. H.; Saini, S.; Groman, E. V.; Hahn, P. F.; Compton, C. C.; Ferrucci, J. T. *J. Lab. Clin. Med.* **1987**, *110*, 164.
(439) Stark, D. D.; Weissleder, R.; Elizondo, G.; Hahn, P. F.; Saini, S.; Todd, L. E.; Wittenberg, J.; Ferrucci, J. T. *Radiology* **1988**, *168*, 297.
(440) Saini, S.; Stark, D. D.; Hahn, P. F.; Wittenberg, J.; Brady, T. J.; Ferrucci, J. T. *Radiology* **1987**, *162*, 211.
(441) Weissleder, R. *Radiology* **1994**, *193*, 593.
(442) Pouliquen, D.; Lucet, I.; Chouly, C.; Perdrisot, R.; Le Jeune, J. J.; Jallet, P. *Magn. Reson. Imaging* **1993**, *11*, 219.
(443) Pouliquen, D.; Perdrisot, R.; Ermias, A.; Akoka, S.; Jallet, P.; Le Jeune, J. J. *Magn. Reson. Imaging* **1989**, *7*, 619.
(444) Anzai, Y.; McLachlan, S.; Morris, M.; Saxton, R.; Lufkin, R. B. *Am. J. Neuroradiol.* **1994**, *15*, 87.
(445) Deserno, W. M. L. L. G.; Harisinghani, M. G.; Taupitz, M.; Jager, G. J.; Witjes, J. A.; Mulders, P. F.; Hulsbergen van de Kaa, C. A.; Kaufmann, D.; Barentsz, J. O. *Radiology* **2004**, *233*, 449.
(446) Vassallo, P.; Matei, C.; Heston, W. D.; McLachlan, S. J.; Koutcher, J. A.; Castellino, R. A. *Invest. Radiol.* **1995**, *30*, 706.
(447) Saleh, A.; Schroeter, M.; Jonkmanns, C.; Hartung, H.-P.; Modder, U.; Jander, S. *Brain* **2004**, *127*, 1670.
(448) Kool, M. E.; Cappendijk, V. C.; Cleutjens, K. B. J. M.; Kessels, A. G. H.; Kitslaar, P. J. E. H. M.; Borgers, M.; Frederik, P. M.; Daemen, M. J. A. P.; Van Engelshoven, J. M. A. *Circulation* **2003**, *107*, 2453.
(449) Ruehm, S. G.; Corot, C.; Vogt, P.; Cristina, H.; Debatin, J. F. *Acad. Radiol.* **2002**, *9*, S143.
(450) Schmitz, S. A.; Taupitz, M.; Wagner, S.; Wolf, K. J.; Beyersdorff, D.; Hamm, B. *J. Magn. Reson. Imaging* **2001**, *14*, 355.
(451) Beckmann, N.; Cannet, C.; Fringeli-Tanner, M.; Baumann, D.; Pally, C.; Bruns, C.; Zerwes, H. G.; Andriambeloson, E.; Bigaud, M. *Magn. Reson. Med.* **2003**, *49*, 459.
(452) Kanno, S.; Lee, P. C.; Dodd, S. J.; Williams, M.; Griffith, B. P.; Ho, C.; Mentzer, S. J.; Egan, T. M.; DeCamp, M. M. *J. Thorac. Cardiovasc. Surg.* **2000**, *120*, 923.
(453) Kanno, S.; Yi-Jen Lin, W.; Lee, P. C.; Dodd, S. J.; Williams, M.; Griffith, B. P.; Ho, C. *Circulation* **2001**, *104*, 934.
(454) Zhang, Y.; Dodd, S. J.; Hendrich, K. S.; Williams, M.; Ho, C. *Kidney Int.* **2000**, *58*, 1300.
(455) Bulte, J. W. M.; Douglas, T.; Witwer, B.; Zhang, S. C.; Strable, E.; Lewis, B. K.; Zywicke, H.; Miller, B.; Van Gelderen, P.; Moskowitz, B. M.; Duncan, I. D.; Frank, J. A. *Nat. Biotechnol.* **2001**, *19*, 1141.
(456) Josephson, L.; Tung, C. H.; Moore, A.; Weissleder, R. *Bioconjugate Chem.* **1999**, *10*, 186.
(457) Lewin, M.; Carlesso, N.; Tung, C. H.; Tang, X. W.; Cory, D.; Scadden, D. T.; Weissleder, R. *Nat. Biotechnol.* **2000**, *18*, 410.
(458) Arbab, A. S.; Bashaw, L. A.; Miller, B. R.; Jordan, E. K.; Lewis, B. K.; Kalish, H.; Frank, J. A. *Radiology* **2003**, *229*, 838.
(459) Arbab, A. S.; Yocum, G. T.; Kalish, H.; Jordan, E. K.; Anderson, S. A.; Khakoo, A. Y.; Read, E. J.; Frank, J. A. *Blood* **2004**, *104*, 1217.
(460) Frank, J. A.; Miller, B. R.; Arbab, A. S.; Zywicke, H. A.; Jordan, E. K.; Lewis, B. K.; Bryant, L. H., Jr.; Bulte, J. W. M. *Radiology* **2003**, *228*, 480.
(461) Hawrylak, N.; Ghosh, P.; Broadus, J.; Schlueter, C.; Greenough, W. T.; Lauterbur, P. C. *Exp. Neurol.* **1993**, *121*, 181.
(462) Bulte, J. W. M.; Ma, L. D.; Magin, R. L.; Kamman, R. L.; Hulstaert, C. E.; Go, K. G.; The, T. H.; De Leij, L. *Magn. Reson. Med.* **1993**, *29*, 32.
(463) Anderson, S. A.; Shukaliak-Quandt, J.; Jordan, E. K.; Arbab, A. S.; Martin, R.; McFarland, H.; Frank, J. A. *Ann. Neurol.* **2004**, *55*, 654.
(464) Sundstrom, J. B.; Mao, H.; Santoianni, R.; Villinger, F.; Little, D. M.; Huynh, T. T.; Mayne, A. E.; Hao, E.; Ansari, A. A. *J. Acquired Immune Defic. Syndr.* **2004**, *35*, 9.
(465) Yeh, T. C.; Zhang, W.; Ildstad, S. T.; Ho, C. *Magn. Reson. Med.* **1993**, *30*, 617.
(466) Zelivyanskaya, M. L.; Nelson, J. A.; Poluektova, L.; Uberti, M.; Mellon, M.; Gendelman, H. E.; Boskal, M. D. *J. Neurosci. Res.* **2003**, *73*, 284.
(467) Shapiro, E. M.; Sharer, K.; Skrtic, S.; Koretsky, A. P. *Magn. Reson. Med.* **2006**, *55*, 242.
(468) Lauterbur, P. C.; Dias, M. H. M.; Rudin, A. M. In *Frontiers of Biological Energetics*; Dutton, P. L., Leigh, J. S., Scarpa, A., Eds.; Academic Press: New York, 1978.
(469) Mendonca-Dias, M. H.; Gaggelli, E.; Lauterbur, P. C. *Semin. Nucl. Med.* **1983**, *13*, 364.
(470) Thomsen, H. S.; Loegager, V.; Noerrgaard, H.; Chabanova, E.; Moller, J.; Sonne, J. *Acad. Radiol.* **2005**, *12*, S21.
(471) Wolf, G. L.; Baum, L. *Am. J. Roentgenol.* **1983**, *141*, 193.
(472) Schaefer, S.; Lange, R. A.; Kulkarni, P. V.; Katz, J.; Parkey, R. W.; Willerson, J. T.; Peshock, R. M. *J. Am. Coll. Cardiol.* **1989**, *14*, 472.
(473) Schaefer, S.; Lange, R. A.; Gutekunst, D. P.; Parkey, R. W.; Willerson, J. T.; Peshock, R. M. *Invest. Radiol.* **1991**, *26*, 551.
(474) Pflugfelder, P. W.; Wendland, M. F.; Holt, W. W.; Quay, S. C.; Worah, D.; Derugin, N.; Higgins, C. B. *Radiology* **1988**, *167*, 129.
(475) Pomeroy, O. H.; Wendland, M.; Wagner, S.; Derugin, N.; Holt, W. W.; Rocklage, S. M.; Quay, S.; Higgins, C. B. *Invest. Radiol.* **1989**, *24*, 531.
(476) Saeed, M.; Wagner, S.; Wendland, M. F.; Derugin, N.; Finkbeiner, W. E.; Higgins, C. B. *Radiology* **1989**, *172*, 59.
(477) Hustvedt, S. O.; Grant, D.; Southon, T. E.; Zech, K. *Acta Radiol.* **1997**, *38*, 690.
(478) Torres, C. G.; Lundby, B.; Tufte Sterud, A.; McGill, S.; Gordon, P. B.; Strand Bjerknes, H. *Acta Radiol.* **1997**, *38*, 631.
(479) Federle, M.; Chezmar, J.; Rubin, D. L.; Weinreb, J.; Freeny, P.; Schmiedl, U. P.; Brown, J. J.; Borrello, J. A.; Lee, J. K. T.; Semelka, R. C.; Mattrey, R.; Dachman, A. H.; Saini, S.; Harms, S. E.; Mitchell, D. G.; Anderson, M. W.; Halford, H. H., III; Bennett, W. F.; Young, S. W.; Rifkin, M.; Gay, S. B.; Ballerini, R.; Sherwin, P. F.; Robison, R. O. *J. Magn. Reson. Imaging* **2000**, *12*, 689.
(480) Nordhøy, W.; Anthonsen, H. W.; Bruvold, M.; Brurok, H.; Skarra, S.; Krane, J.; Jynge, P. *Magn. Reson. Med.* **2004**, *52*, 506.
(481) Aime, S.; Anelli, P.; Botta, M.; Brocchetta, M.; Canton, S.; Fedeli, F.; Gianolio, E.; Terreno, E. *J. Biol. Inorg. Chem.* **2002**, *7*, 58.
(482) Troughton, J. S.; Greenfield, M. T.; Greenwood, J. M.; Dumas, S.; Wiethoff, A. J.; Wang, J.; Spiller, M.; McMurry, T. J.; Caravan, P. *Inorg. Chem.* **2004**, *43*, 6313.
(483) Parasassi, T.; Bombieri, G.; Conti, F.; Croatto, U. *Inorg. Chim. Acta* **1985**, *106*, 135.
(484) Navon, G.; Panigel, R.; Valensin, G. *Magn. Reson. Med.* **1986**, *3*, 876.
(485) Lee, J.-H.; Huh, Y.-M.; Jun, Y.-W.; Seo, J.-W.; Jang, J.-T.; Song, H.-T.; Kim, S.; Cho, E.-J.; Yoon, H.-G.; Suh, J.-S.; Cheon, J. *Nat. Med.* **2007**, *13*, 95.
(486) Taylor, K. M. L.; Rieter, W. J.; Lin, W. *J. Am. Chem. Soc.* **2008**, *130*, 14358.

CR900232T